Title
STUDY OF THE REACTION K- + p->A+ n+ + n- FROM 1.2 TO 1.7 BeV/c

Author
Huwe, Darrell O.

Publication Date
1964-07-09

University of California

Ernest O. Lawrence Radiation Laboratory

Berkeley, California

DISCLAIMER

UCRL-11291
cy 2

UNIVERSITY OF CALIFORNIA
Lawrence Radiation Laboratory
Berkeley, California

AEC Contract No. W-7405-eng-48

STUDY OF THE REACTION $K^- + p \rightarrow \Lambda + \pi^+ + \pi^-$ FROM 1.2 TO 1.7 BeV/c

Darrell O. Huwe

(Ph. D. Thesis)

July 9, 1964

STUDY OF THE REACTION $K^- + p \rightarrow \Lambda + \pi^+ + \pi^-$ FROM 1.2 TO 1.7 BeV/c

Contents

STUDY OF THE REACTION $K^- + p \rightarrow \Lambda + \pi^+ + \pi^-$ FROM 1.2 TO 1.7 BeV/c

Darrell O. Huwe

Lawrence Radiation Laboratory
University of California
Berkeley, California

July 9, 1964

ABSTRACT

A sample of events of the reaction $K^- + p \rightarrow \Lambda + \pi^+ + \pi^-$ was selected from an exposure of the Laboratory's 72 inch hydrogen bubble chamber to a separated K^- beam of the Bevatron. Laboratory momentum of the K^- in this sample was set at six values, ranging from 1.22 to 1.69 BeV/c. A sample at lower energy was also used in part of the analysis. Dalitz plots and effective-mass distributions show that the Λ-π resonance, $Y_1^*(1385)$, is the dominant final state; the π-π resonance, $\rho(750)$, also important, has a maximum cross section at 1.5 BeV/c; and $Y_1^*(1660)$ is produced weakly. A peak in the π-π distribution can be interpreted as the electromagnetic decay, $\omega \rightarrow \pi^+\pi^-$, but possible interference of this state with the ρ^0 precludes a unique assignment of the branching ratio of this mode to the three-pion mode. We can set a lower limit of $(0.6 \pm 0.2)\%$ for this ratio, and thus establish the existence of the mode. There is also evidence of an enhancement in the π-π spectrum at very low energy. We studied the angular correlations of the decay products of the $Y_1^*(1385)$ and determined that the spin parity of this resonance is $P_{3/2}$, with a slight chance that it is $D_{5/2}$. With this spin-parity assignment, all of the observed properties of the $Y_1^*(1385)$ are consistent with assignment to a decuplet in the eightfold-way theory. There is evidence of initiation of peripheral production of $Y_1^*(1385)$ above 1.5 BeV/c, but this process is not yet dominant at 1.7 BeV/c.

I. INTRODUCTION

Margaret Alston and collaborators reported in 1960 the discovery of a resonance between the Λ hyperon and the π meson, the $Y_1^*(1385)$.[1] The reaction studied was the one of concern to this paper:

$$K^- + p \rightarrow \Lambda + \pi^+ + \pi^- . \qquad (1)$$

In the 3 years since (as pointed out by R. H. Dalitz in his recent review article on strange-particle resonant states[2]) many more such states have been discovered. However, not all of the interesting properties of these resonances have been found. Any theory of particles and resonances that claims to be complete must take these properties into account. Consequently, though pressing forward into new areas in search of still more states of matter may be fruitful for some time to come, more concentrated study of the particles already known does have its own merit.

The work of Alston et al. was done in a hydrogen bubble chamber at 1.15 BeV/c.[1] Other workers have studied reaction (1) (in hydrogen bubble chamber unless otherwise noted) at 300 to 850 MeV/c,[3,4] at 1.11 BeV/c in a propane chamber,[5] at 1.45 BeV/c,[6] and at 2.24 BeV/c.[7] Reports have also been published on parts of the data that we studied and that are reported on in this paper.[8-12] All of these papers report that $Y_1^*(1385)$ dominates this reaction, though two of them, references 10 and 12, concern less dominant features. A review of early work in strange-particle resonances was written by Alston and Ferro-Luzzi,[13] and Dalitz' recent review article covers all work to date.[2]

The title of this report covers a wide scope, so that a more careful delineation of subject matter to be covered is in order. The major emphasis of this report is on final-state interactions, and little attention is given to the production process. The reasons for this

choice are twofold: (a) study of final-state interactions could be initiated while the data were being accumulated, and enough interesting problems were found to warrant a follow-through study at depth of these interactions by themselves; and (b) a study of all channels simultaneously is more likely to be fruitful for production analysis than is the study of one channel, especially a three-body channel, by itself. (M. L. Stevenson is currently developing a general program for such an analysis.) The philosophy of this paper, then, is to embrace a large sample of data at a wide range of energy and to find and study all final-state interactions that appear to be present. The sample is large enough to minimize statistical fluctuations, and the energy region covered has not been studied in a bubble chamber experiment before, except for the experiment at 1.45 BeV/c.[6]

The dominant interaction in this range of energy, K^- laboratory momentum of about 1.2 to about 1.7 BeV/c, is still the $Y_1^*(1385)$, so that the major part of the paper is devoted to determining the properties of this resonance, especially the spin and parity, which have not yet been definitely established. With the increase of energy, however, less and less of the kinematically allowed region is influenced by this resonance, so that other effects, especially in the pion-pion system, can also be looked at.

Section II of this paper reviews the theory of final-state interactions with reference to reaction (1), sketches briefly predictions about the properties of the Y_1^* based upon dynamics and/or group theory, describes the theoretical dependence of the angular correlations of the particles in the final state of reaction (1) upon the spin and parity of the Y_1^* state, discusses the theory of the decay mode $\omega \to \pi^+\pi^-$, and sketches briefly the theory of peripheral production in reaction (1).

Section III describes (a) the setup of the experimental apparatus, (b) the general procedure followed in analysis of the data, (c) development of the criteria for separating events of reaction (1) from

competing reactions, (d) effective-mass distribution of each pair of particles in the reaction, (e) the branching ratio of the ω meson into two pions, (f) angular correlations among the particles from Y_1^* production and decay, (g) a comparison of this reaction with others in order to look at the branching ratio of the Y_1^*, and (h) a determination of the excitation function of this reaction into its various final states.

Section IV takes the experimental findings of the previous section, and those of other workers who have studied similar final states, and relates them to the theoretical discussion of Sec. II, in order to make possible as many physical conclusions as are warranted.

II. THEORY

A. Watson's Theorem

One experiment that would shed a great deal of light on interactions within the Λ-π system would involve a study of the reaction

$$\pi + \Lambda \rightarrow \pi + \Lambda \,. \qquad (2)$$

This experiment, however, is not physically realizable. Watson has pointed out that, under the proper circumstances, reaction (1), which is physically realizable, can be viewed as being followed immediately by a scattering between the Λ hyperon and one of the pions after the manner of (2).[14] He calls "final-state interactions" those instances when particles produced interact among themselves so strongly that they influence appreciably the properties of the reaction cross section. The conditions needed to insure the validity of a two-step process of primary reaction followed by final-state interaction are the following:

(a) The mechanism of the reaction is limited to short range, that is, it must occur within a definite reaction volume. This condition insures that the products of the reaction escape quickly from their birthplace and are then no longer greatly influenced by the forces that produced them. Forces between strongly interacting particles, as is well known, do have this short-range nature.

(b) The particles interacting must have low relative energy. Then they can remain close enough together after the initial reaction so that rescattering can occur.

(c) The interaction is strong and attractive. Then the particles will tend to stick together and give the maximum effect.

Watson showed by considerations of formal scattering theory that when these conditions are met the matrix element for the particles undergoing a final-state interaction is the same as that for a production reaction involving the same particles. The cross section then is $4\pi/K^2$ times the square of this matrix element, where K is the momentum

of the incoming particles (K^- and p in our example) in their center of mass.

The most common form of final-state interaction encountered in high-energy scattering experiments is a resonance having the single-level Breit-Wigner shape. For spinless particles interacting through a one-channel resonance, the cross section is

$$\frac{d\sigma}{dE} = \frac{\pi(2L+1)}{K^2} \frac{\Gamma_L \Gamma_a}{(E - E_L)^2 + \frac{1}{4}\Gamma_L^2} . \tag{3}$$

The symbol E is the energy of the interacting particles in their center of mass, E_L is the resonant energy, L is the angular momentum of the resonance, Γ_L is the width of the resonance, and Γ_a represents the rate of the primary reaction.

In the more general case that includes the interactions appearing in the present study, the initial and final particles may have spin and the resonance may proceed through more than one channel. The cross-section formula becomes

$$\left(\frac{d\sigma}{dE}\right)_b = \frac{\pi(2J+1)}{K^2 \prod_i (2S_i+1)} \frac{\Gamma_b \Gamma_a}{(E - E_J)^2 + \frac{1}{4}\Gamma_J^2} . \tag{4}$$

The notation is similar to that above, J is now the angular momentum of the resonance, S_i is the spin of an incoming particle, subscript b refers to a particular channel, and Γ_b is the partial width of the channel, following the rule $\sum_b \Gamma_b = \Gamma_J$. In general, Γ_J will be a function of E, and this behavior is discussed at more length in Sec. III. F, where Eq. (4) is put to use.

A second interaction, not often encountered in high-energy scattering, is an S-wave interaction characterized by a scattering length and an effective range:

$$q \cot \delta_0 = \frac{1}{a} + \frac{1}{2} r_0 q^2 . \tag{5}$$

Here q is the center-of-mass momentum of the particles in the interaction, a is the scattering length, r_0 is the effective range, and δ_0 is the resultant phase shift. The cross section is given by

$$\frac{d\sigma}{dq} \propto \frac{4\pi}{K^2} \frac{q^2 a^2}{1 + q^2 a^2 (1 + \frac{r_0}{a})} . \qquad (6)$$

This formula, but in relativistic form, is useful later in Sec. III. F.

Dalitz has pointed out that, in practice, there are three situations in which the forms implied by the discussion above can be distorted.[2]

(a) Dynamic interference between the particles within the interaction and one of the particles outside the interaction, such as the S-wave—scattering-length interaction mentioned above. This situation is likely if the reaction is proceeding near threshold, so that all particles have a small momentum. In the energy range considered in this paper, reaction (1) is well above threshold, so that no such dynamic effects should appear.

(b) Interference between overlapping bands. If, among the final products from a reaction, more than one pair of particles have resonant interactions, and if the kinematics allow--for certain configurations of the momenta in the final state--two or more of these pairs to be near the resonant energy simultaneously, then the amplitudes of these two interactions will superpose, with resultant interference effects. This situation occurs strongly for reaction (1) at the lower energies studied by Berge et al.[3] An analysis of the low-energy data, with S- and P-wave production assumed and the Bose statistics of the two pions taken into account was done by Dalitz and Miller.[15] The analysis yielded two ambiguous solutions, but the validity of the model is not thereby discredited. In this paper the two charge states of the $Y_1^*(1385)$ are not likely to interfere because kinematics keep them apart, but other resonances not present at lower energies may appear and give similar trouble (Fig. 9).

(c) Interference with background production. If there is an amplitude for primary production not followed by final-state interactions--that is, for production of particles according to "phase space"--this amplitude will superpose with the resonant amplitudes, again with resultant interference effects. This effect can, of course, be present at all energies. Since the phase of Breit-Wigner amplitude changes rapidly as one passes through the central energy of the resonance, and nonresonant background would have no reason for a sudden change of phase, the effects of this interference should change rapidly with the energy of the resonating pair of particles. This property is used as a check for interference in Sec. III. G.

In conclusion, the conditions for the validity of Watson's theorem are reasonably well satisfied by the reaction under consideration, providing we are alert for overlapping resonance bands and interference with background. As a first approximation, then, we can treat any observed "bumps" as resonant states that decayed as free particles.

B. Predictions Concerning $Y_1^*(1385)$

The proliferation of particles and resonances in recent years has spurred attempts by theorists to seek among these particles symmetry relations or dynamic forces that would allow one to predict the properties of some of them, given the properties of the rest. The Y_1^* (1385) has figured prominently in several such schemes. We review these schemes here.

1. Global Symmetry

In an attempt to ascribe to the strongly interacting particles a higher symmetry than the well-known isotopic spin, so that the hyperon interactions can be related somehow to the baryon interactions, Gell-Mann developed in 1957 his theory of global symmetry.[16] The basic assumptions made were (i) pions have a strong pseudoscalar coupling to hyperons comparable to their coupling to nucleons, and (ii) the coupling of K mesons to the Λ hyperon is much weaker then the coupling of pions to nucleons. He distinguished between medium-strong

interactions, in which K mesons participated, and very strong ones in which π mesons participated. Then, to first order, the pion couplings to all the baryons are the same. To place the eight baryons in a symmetric scheme, he introduced the two amplitudes

$$\begin{aligned} Y^0 &\equiv (\Lambda - \Sigma^0)/\sqrt{2} \\ Z^0 &\equiv (\Lambda + \Sigma^0)/\sqrt{2} \quad . \end{aligned} \tag{7}$$

Then the baryons are to be considered as belonging to four isotopic-spin doublets, (p, n), (Σ^+, Y^0), (Z^0, Σ^-), and (Ξ^0, Ξ^-). The pseudoscalar coupling constant for interaction of pions with each of these doublets is the same, the well-known pion-nucleon coupling constant. Of course, when the K-meson interactions are turned on, they will have a perturbing influence on the completely symmetric picture presented here.

Amati, Vitale, and Stanghellini made a model based on global symmetry in an attempt to predict the behavior of the π-Λ and π-Σ systems.[17] They introduced three parameters: Ω, a cutoff parameter; f_Λ, the π-Λ coupling constant; and f_Σ, the π-Σ coupling constant. Let

$$\delta = (f_\Lambda^2 - f_\Sigma^2) \; / \; (f_\Lambda^2 + f_\Sigma^2). \tag{8}$$

Then, if global symmetry holds approximately, δ is small; and they found that dynamic calculations predicted two $J = 3/2$ resonances, one with $I = 1$ and one with $I = 2$. The predicted resonant energies are given by

$$\begin{aligned} E_r^1 &= m_\Lambda + \Omega - \tfrac{1}{2}(m_\Sigma - m_\Lambda) - \tfrac{5}{6}\delta(m_\Sigma - m_\Lambda), \\ E_r^2 &= m_\Lambda + \Omega + \tfrac{3}{2}(m_\Sigma - m_\Lambda) + \tfrac{1}{2}\delta(m_\Sigma - m_\Lambda). \end{aligned} \tag{9}$$

The widths are then given by a phase-space factor times $\frac{1}{2}(f_\Lambda^2 + f_\Sigma^2)$, and a branching ratio for the I = 1 resonance is given by

$$\begin{aligned} R &= (Y_1^* \to \Sigma\pi)/(Y_1^* \to \Lambda\pi) \\ &= \frac{1}{2}\,(\text{relative phase space})/(1+\delta)^2. \end{aligned} \tag{10}$$

These two resonant states are related, then, through global symmetry to the well-known pion-nucleon resonance with J = 3/2, I = 3/2, mass of 1238 MeV, and width of 125 MeV. From this resonance, the value of Ω is 290 MeV. If the value of δ is taken to be zero (restricted symmetry), the predicted values are $E_r^1 = 1365$ MeV, $\Gamma_1 = 60$ MeV, and R = 0.11.[13]

For a review of early higher symmetry schemes, see Morpurgo.[18] The model of global symmetry described in Ref. 17 seems to make excellent predictions of the properties of the $Y_1^*(1385)$, but the validity of the theory is very doubtful. A systematic search for the predicted $Y_2^*(1530)$ has failed to produce any positive evidence of its existence,[19] and it is well known that many more resonances have been found whose existence is not predicted by global symmetry but which are well represented by the eightfold-way theory to be discussed later.

2. $\bar{K}$-N Bound State

Dalitz and Tuan argued that the neglect of the K interactions was not justified, especially since the absorptive cross section is so large for $\bar{K}$ - N scattering at threshold.[20] They assumed that this absorption can be attributed to S-wave interactions that are described by an effective-range formula. Since $\bar{K}$-N can be in an I = 0 or in an I = 1 state, there will be two scattering lengths, A_0 and A_1, two phase shifts, δ_0 and δ_1, and two relations between them of the form

$$k \cot \delta_1 = 1/A_1\,(k)\,. \tag{11}$$

To take account of absorption, these A's must be complex,

$$A = a + ib, \tag{12}$$

where a and b are real. From the low-energy K^--p scattering data, they obtained two solutions for the a's and b's. They made a calculation for I = 0--which is simpler than for I = 1 because only the π-Σ and not the π-Λ can be in the final state--and found that one of the solutions led to a bound state about 20 MeV below the $\bar{K}$-N threshold, whose shape depended sensitively on the π-Y phase shift at the $\bar{K}$-N threshold.

Later, Dalitz made a similar calculation for the I = 1 channel, which calculation is relevant to this paper.[21] In this case both pion-hyperon channels are present, so that the outgoing wave has a two-dimensional state function. With some simplifying assumptions, however, he again obtained a bound state with one of the low-energy solutions, and he expressed its properties in terms of the a and b of (12), as follows:

$$\begin{aligned} E_r &= M_N + m_K - (2 m_K a^2)^{-1} = 1382 \pm 20 \text{ MeV} \\ \Gamma/2 &= b/(m_K |a|^3) \approx 18 \text{ MeV}. \end{aligned} \tag{13}$$

For the branching ratio, he obtained

$$R = (Y_1^* \rightarrow \Lambda\pi) = 0.8\ R_t \tag{14}$$

for pseudoscalar K mesons, where R_t is the ratio of (I = 1)- Σ production to Λ production at $\bar{K}$-N threshold. The latter is reported to have a value of 2.46 ± 0.72,[22] so that R has a value of 1.97 ± 0.58 in this model. Of course the resonance has $J = \frac{1}{2}$, since it is S wave. Another feature of this theory is that the resonance shape as observed in the π-Y channels will, in general, have a cusp at the $\bar{K}$-N threshold, and can have a long low-energy tail. For a more detailed discussion, see reference 23.

A much more likely candidate for a $\bar{K}$-N S-wave interaction below threshold is the well-known resonance $Y_0^*(1405)$. For a discussion of this possibility, see Dalitz.[2]

Trueman[24] made calculations based on those of Amati et al.[17] but took into account also the effects of the $\bar{K}$-N system. He found that the properties of the I = 1, J = 3/2 resonance were not significantly changed by the K interactions, but that three new resonances were predicted. In particular, there should be a $J = \frac{1}{2}$ state having I = 1. Also, there are now more coupling constants to consider, so that the branching ratio R can be decreased either by decreasing the $\pi\Sigma\Sigma$ coupling constant or by increasing the $\bar{K}N\Lambda$ coupling constant.

Chand made Dalitz-Tuan—type calculations to predict the P-wave behavior of low-energy $\bar{K}$-N scattering, assuming that it is dominated by a $P_{3/2}$ Y_1^* at 1385 MeV.[25] He found that his calculations agreed with one of the solutions fit to the K^--p data for momenta up to 400 MeV/c. The conclusion is that the observed $Y_1^*(1385)$ is not inconsistent with assignment as a $P_{3/2}$ $\bar{K}$-N bound state.

3. Sakata Model

Sakata proposed that all physical particles are built up from the proton, neutron, and lambda particles and their antiparticles.[26] Ikeda, Ogawa, and Ohnuki made the theory symmetric by assuming that the properties of the three basic particles are invariant under the transformations of the group U(3).[27] This group is the unitary group of three objects. As used by these authors, it has three additive parameters, taken as baryon number, strangeness, and electric charge. All observed strongly interacting particles must then belong to some irreducible representation of this group.

Sakurai[28] has pointed out that the Sakata model is almost certainly invalid, because (i) it does not treat the Λ and the Σ in a symmetric way, contrary to all evidence, (ii) it assigns a spin of 3/2 to the Ξ, contrary to recent experiment,[29] and (iii) it forbids the reaction $p + \bar{p} \rightarrow K_1^0 + K_2^0$, again contrary to experiment.[30] An additional objection to the model, not mentioned by Sakurai, is its prediction of a K^+-p (Y = 2, B = 1) resonance, which has not yet been seen. The model is useful, however, because it gives physical insight into the eightfold-way theory.

4. Eightfold Way

But the Sakata model picks out three baryons as a basis, when there seems to be no reason why the Σ and (perhaps) the Ξ should be different. Gell-Mann[31] and, independently, Ne'eman[32] proposed that the basic set of particles was the set of eight baryons; nucleons, lambdas, sigmas, and cascades. The symmetry group chosen to describe the transformations among these particles was SU(3). In this case the baryon number has been relegated to a gauge transformation, and there remain two additive quantum numbers, which can be taken to be Y, the hypercharge, and I_z, the third component of the isotopic spin. Then SU(3) is the unitary unimodular group on three objects, but the three objects are not given physical existence in this theory. Instead, the octet, one of the irreducible representations arising from the direct product of two different three-dimensional representations, is the basic representation. Again, all observed particles must belong to some irreducible representation of the group, and matrix elements for coupling between representations are given by generalized Clebsch-Gordan coefficients for the group. For a detailed discussion of this group, see Behrends et al.[33]

The well-known $N^*(1238)$ must be in one of these representations, and the simplest assignment is a decuplet. If the $Y_1^*(1385)$ can be shown to have the same spin and parity, $J^P = 3/2^+$, then some interesting predictions can be made. These two multiplets can be assigned to the same decuplet and the existence of the two remaining multiplets, one with $Y = -1$ and $I = 1/2$ and one with $Y = -2$ and $I = 0$, is predicted. A mass formula for the eightfold way was worked out by Okubo,[34] having the form

$$m = m_0 \left\{1 + aY + b\left[I(I+1) - \frac{Y^2}{4}\right]\right\}, \qquad (15)$$

where m_0, a, and b are parameters whose values are not given by the theory, so that in general three masses must be known in a representation in order to make predictions. However, the decuplet follows

the rule $I = 1 + Y/2$, so that the mass formula degenerates to an equal spacing rule

$$m = m_0(1 + a'Y). \tag{16}$$

The masses of the decuplet under consideration would form the series 1238, 1385, 1532, and 1679, all in MeV. A resonance having $Y = -1$, $I = 1/2$, and a mass of 1532 MeV has been found (Ξ^*)[35] and has been shown to be most likely $3/2^+$.[36] More recently an example of a particle with $Y = -2$ and a mass of 1686 MeV (Ω^-) has been seen.[37] Other quantum numbers of the latter particle are not yet known. The striking success of this theory indicates that the currently assumed properties of the $Y_1^*(1385)$ are completely in accord with this theory. However, if these latter discoveries had not been made, one could still make a weak prediction on the spin and parity by associating the $Y_1^*(1385)$ with the $N^*(1238)$. Assignment of the known baryon resonances to representations has been made by Glashow and Rosenfeld.[38]

Let us assume that the $Y_1^*(1385)$ is indeed in the same representation as the $N^*(1238)$. In Rosenfeld's notation, it would then be called the Σ_δ.[39] What further predictions can be made? Behrends et al.[33] worked out the matrix elements for decay of a member of the decuplet into a member of the baryon octet and a member of the pseudoscalar octet (the latter including pions, K mesons, $\bar{K}$ mesons, and the eta meson). The widths for these decays are given by the generalized Wigner-Eckart theorem

$$\Gamma_{\mathcal{BM}} = \left(q^3 \frac{E_{\mathcal{B}}}{E_{\mathcal{B}} + E_{\mathcal{M}}}\right) |C|^2 \, |\langle \{10\}, a \,|\, \mathcal{BM}\rangle|^2 \tag{17}$$

where $\{10\}$ represents the decuplet, a is a quantum number designating a member of the decuplet, C is a normalization constant $\mathcal{B}$ refers to baryon octet, and $\mathcal{M}$ refers to pseudoscalar octet. Inserting numbers gives

$$\Gamma(Y_1^*) = 0.44\,\Gamma(N^*_{3/2}) = 64 \text{ MeV}$$
$$R = \Gamma(Y_1^* \to \Sigma\pi)/\Gamma(Y_1^* \to \Lambda\pi) = 0.16. \qquad (18)$$

The recently discovered $Y_1^*(1660)$[10] was tentatively assigned $J = 3/2-$ by Glashow and Rosenfeld,[38] but more recent researchers cast doubt on this assignment, showing a preference for $J = 3/2+$ or $5/2-$.[40,41]

The discussion in this section thus far has concerned group theory only, so that relations among masses in a representation can be predicted, but the unperturbed mass of the representation cannot be determined. Martin and Wali have made dynamic, coupled-channel calculations of the $J = 3/2+$ resonances, using the known baryon and meson masses and assuming the coupling constants are related by SU(3).[42] They were left with one adjustable parameter, which they evaluated in such a way as to give the observed physical states. Their calculations give the mass of the Y_1^* as 1610 MeV, and the branching the ratio $R = 0.06$. Unfortunately, they did not state their result for the width of the Y_1^*.

A summary of the theoretical predictions for the properties of the Y_1^* given by the theories reviewed above is presented in Table I.

C. $Y_1^*(1385)$ Angular Correlations

It is obvious that, if we are to make any progress in classifying the particles in a complete theory, we must know the spin and parity of all the particles. A large part of the analysis reported in this paper is engaged in a determination of the spin and parity of the Y_1^*; so it is important to cover carefully the theory of how these properties can be determined in final-state interactions through study of angular correlations.

Table I. Properties of Y_1^* as predicted by various theories.

Theory	Spin parity ($\hbar$)	Mass (Mev)	Width (MeV)	Branch ratio[a]	Reference number
Global symmetry	$3/2^+$	1365	60	0.11	17, 13
$\bar{K}$-N bound state	$1/2^-$	1382	36	1.97	21
Eightfold way	$3/2^+$	Input[b]	64	0.16	31
Coupled channel	$3/2^+$	1610	--	0.06	42

[a] $Y_1^* \rightarrow \Sigma\pi / Y_1^* \rightarrow \Lambda\pi^-$.

[b] Strongly corroborated by the discovery of the Ω^- at the predicted mass.[37]

1. Density Matrix

It is well known that a complete description of an experimental situation, in which pure quantum mechanical states are not to be expected in general, is properly given by density matrix.[43] For simplicity, we consider only the case for which the possible states are discrete and finite in number, though density matrix formalism can also be used when there is a continuum of states.

Let $|j\rangle$ be one of these orthonormal discrete states,

$$\langle j|j\rangle = 1, \quad \text{all } j. \tag{19}$$

We want the ensemble average of some operator Q over the states j in a given statistical ensemble, given by

$$\text{Av}(Q) = \sum_j P(j) \langle j|Q|j\rangle \tag{20}$$

where $P(j)$ is the probability of finding the ensemble in the state j. Then we have

$$\text{Av}(1) = 1 = \sum_j P(j). \tag{21}$$

Since $P(j)$ is a probability, we can require that $P(j) \geq 0$. We can rewrite the matrix element in (20):

$$\langle j|Q|j\rangle = \text{Tr}\,(Q|j\rangle\langle j|), \tag{22}$$

where Tr refers to the trace operation, that is to the sum of the diagonal elements of the operator in parentheses. Then let us define the operator

$$\rho \equiv \sum_j P(j)|j\rangle\langle j|. \tag{23}$$

Then equation (20) can be rewritten, by means of (22) and (23):

$$\text{Av}(Q) = \text{Tr}(\rho Q). \tag{24}$$

Using the above relations, we can easily establish the following properties of ρ.

$$Tr(\rho) = 1. \tag{25}$$

$$\rho^{+} = \rho. \tag{26}$$

If Q is Hermitian

$$[Av(Q)]^{*} = Av(Q). \tag{27}$$

All of the eigenvalues of ρ are positive definite. If Q is a Hermitian operator, with minimum eigenvalue q_{min} and maximum eigenvalue q_{max},

$$q_{min} \leq Tr(\rho Q) \leq q_{max}. \tag{28}$$

If ther are N complete states $|j\rangle$,

$$1/N \leq Tr(\rho^{2}) \leq 1. \tag{29}$$

The operator ρ we defined above is, of course, the density matrix. When we are studying processes involving particles with spin, operators that act on the spin wave functions can be represented by matrices of $(2J+1) \times (2J+1)$ dimensions. These matrices can be considered to belong to a linear vector space of $(2J+1)^{2}$ dimension. It is possible to select a complete set of $(2J+1)^{2}$ basis matrices that span this space. Let these matrices be denoted by S_j. Then the density matrix can be conveniently expanded in this basis:

$$\rho = (2J+1)^{-1} \sum_{j} \langle S_j \rangle S_j. \tag{30}$$

In particular, it is well known that a convenient basis for spin-$\frac{1}{2}$ particles is the three components of the Pauli matrix $\vec{\sigma}$ and the 2×2 unit matrix.

Suppose that a scattering or decay process is described by an operator M in such a manner that for a pure initial state $|i\rangle$, the final state $|f\rangle$ is given by

$$|f\rangle = M|i\rangle . \tag{31}$$

Then it is well known that the final density matrix is related to the initial one by

$$\rho_f = M\rho_i M^+. \tag{32}$$

2. Decay of Particles having Spin

Let us assume that reaction (1) proceeds through two steps,

$$K^- + p \rightarrow Y^{*\pm} + \pi^{\mp}, \; Y_1^{*\pm} \rightarrow \Lambda + \pi^{\pm} . \tag{33}$$

We assume that the K meson is pseudoscalar and that parity is conserved in both the production process and in the decay of the Y_1^*. We also assume that the Y_1^* decays as an isolated particle. It is well known that the subsequent weak decay of the Λ

$$\Lambda \rightarrow p + \pi^- \tag{34}$$

does not conserve parity and acts as an analyzer of polarization. The object of the game is to find the spin and parity of the Y_1^* from the angular decay distribution of the Y_1^* and of the Λ. This problem has been attacked by Gatto and Stapp,[44] by Capps,[45] and by Byers and Fenster.[46] The method of Byers and Fenster has been used to determine the spin of the Ξ^*,[36] and has been used on a portion of the data of this experiment on the Y_1^*. In this paper we use much of the notation of Byers and Fenster, but our approach is based more on the philosophy of Capps, so that a development of the method used is in order.

The treatment of the problem is nonrelativistic, and a justification of this approach is given where the analysis procedure is

explained in Sec. III. G. 1.

Let us be ignorant of the production process, and fix our attention on the state of the Y_1^* right after production. From the previous section, we know that this state can in general be described by a density matrix. From knowledge of the invariants of the production, we know that the elements of the density matrix must be functions only of the production angle and the energy. However, from our point of view, these elements are merely parameters which must follow (25), (26), and (29) above, but which otherwise can have any values whatever. Let us expand this density matrix in the fashion of Byers and Fenster:

$$\rho = (2J+1)^{-1} \sum_{L,M} (2L+1)\, t_L^{M*}\, T_L^M . \tag{35}$$

The matrices T_L^M are the irreducible tensors described, for example, by Rose;[47] these tensors span the vector space of matrices and under rotations have a transformation property similar to those of the $Y_L^M(\theta,\phi)$. The numbers t_L^M follow the relation

$$t_L^M = \mathrm{Tr}(\rho\, T_L^M) \tag{36}$$

so that, from (30), $t_L^M = \langle T_L^M \rangle$, that is, it is the expectation value of T_L^M. Hence $\sqrt{2L+1}\; T_L^M$ is the S_j of equation (30). From the rotation property of T_L^M, we have the relation

$$t_L^{-M} = (-)^M t_L^{M*} . \tag{37}$$

We take T_1^0 to be diagonal, so that the elements of T_L^M are given by the Clebsch-Gordan coefficients

$$(T_L^M)_{mm'} = C(JLJ;m'Mm). \tag{38}$$

In Appendix A are listed explicitly some of the T_L^M.

Let us take the normal to the production plane as the axis of quantization. Then, according to Capps, half of the elements of the density matrix vanish.[45] He shows that reflection invariance at production implies that $\rho_{ij} = 0$ for $|i-j|$ odd. From (35), those T_L^M for which some $(T_L^M)_{ij} \neq 0$ for $|i-j|$ odd must have $t_L^M = 0$. It follows then, from relation (38), that t_L^M with M odd vanish identically.

Let us turn now to the problem of determing the form of the transition operators M. The guiding principle to be followed here is proper behavior under transofrmations of the rotation group. Essentially the same problem is faced when one wishes to add two angular momentum vectors to get a third. For the guiding principle here too is the preservation of the transformation principles. The answer to the latter problem is well known; the elements of the combined representation are sums of products of elements of the two representations being combined, the weighting factors being the Clebsch-Gordan coefficients. So the elements of M must be composed of spherical harmonics multiplied by the appropriate Clebsch-Gordan coefficients, and the method of checking this construction is to check that M satisfies the defining relation (31). Some reflection shows that the proper form is

$$M_{ij}(J, \ell) = C(\ell, \tfrac{1}{2}, J; J-\tfrac{1}{2}-j+i, 3/2-i) Y_\ell^{J-\frac{1}{2}-j+i}(\hat{\Lambda}), \qquad (39)$$

where M_{ij} is the element in the ith row and jth column of a matrix representing M in a representation where the pure states of the Y_1^* are given by a column matrix with one element equal to one and the rest equal to zero. The symbol $\hat{\Lambda}$ is a unit vector pointing in the direction of the lambda momentum, which symbolizes the angles θ and ϕ that are the arguments of the spherical harmonic. The symbols J and ℓ represent the spin of the Y_1^* and the orbital angular momentum of the breakup, respectively, and because the Λ has spin $\frac{1}{2}$, they are related by

$$J = \ell \pm \tfrac{1}{2}. \qquad (40)$$

Since parity is conserved in the decay, and the Y_1^* is in a definite parity state, one or the other of the sign possibilities must hold true. Let us write explicitly the matrix for the case $J = 3/2$, $\ell = 1$ ($P_{3/2}$):

$$M = \begin{pmatrix} Y_1^1(\hat{\Lambda}) & \sqrt{2/3}\, Y_1^0(\hat{\Lambda}) & \sqrt{1/3}\, Y_1^{-1}(\hat{\Lambda}) & 0 \\ 0 & \sqrt{1/3}\, Y_1^1(\hat{\Lambda}) & \sqrt{2/3}\, Y_1^0(\hat{\Lambda}) & Y_1^{-1}(\hat{\Lambda}) \end{pmatrix}. \tag{41}$$

Then it is easily seen that each column of M is the column matrix representation for the state of the Λ resulting from the decay of a pure state of the Y_1^*, each column representing a different one of the four possible pure states. Hence M is not square in general, but is of dimension $2\times(2J + 1)$.

Let us think of ρ being expressed in matrix form in this same representation. Then relation (32) will expand in this manner:

$$\rho'_{in} = \sum_{j,k} M_{ij}(J,\ell)\rho_{jk}[M(J,\ell)]^+_{kn}$$

$$= \sum_{j,k} \rho_{jk}\, C(\ell,\tfrac{1}{2}, J; J-\tfrac{1}{2}-j+i, 3/2-i)\, C(\ell,\tfrac{1}{2}, J; J-\tfrac{1}{2}-k+n, 3/2-n) \tag{42}$$

$$\times\ Y_\ell^{J-\frac{1}{2}-j+i}(\hat{\Lambda})\, Y_\ell^{J-\frac{1}{2}-k+n*}(\hat{\Lambda}).$$

The prime here means the final density matrix, which will be 2×2. Using the equations (35) and (38), we can express the initial density matrix in terms of t_L^M, which makes the form of the final density matrix read:

$$\rho'_{in} = \sum_{j,k} (2J+1)^{-1} \sum_{L'} (2L'+1)\, t_{L'}^{k-j\,*}$$

$$\times C(J, L', J; J+1-k, k-j)\, C(\ell, \tfrac{1}{2}, J; J-\tfrac{1}{2}-j+i, 3/2-i) \qquad (43)$$

$$\times C(\ell, \tfrac{1}{2}, J; J-\tfrac{1}{2}-k+n, 3/2-n)\, Y^{J-\frac{1}{2}-j+i}(\hat{\Lambda})\, Y^{J-\frac{1}{2}-k+n\,*}(\hat{\Lambda}).$$

The above expression gives the density matrix representing the state of the Λ after the Y_1^* decay. We yet must also use the information in the Λ decay, so we need to use relation (32) once more. This time the transition operator is the familiar

$$N = \tfrac{1}{2}(S + P\vec{\sigma} \cdot \hat{p}). \qquad (44)$$

It is not hard to show that

$$\mathrm{Tr}(N\rho' N^+) = (4\pi)^{-\frac{1}{2}} \Big[(\rho'_{11} + \rho'_{22}) Y_0^0(\hat{p}) + (\rho'_{11} - \rho'_{22})\sqrt{1/3}\, a\, Y_1^0(\hat{p}) + \Big\{ -\rho'_{12}\, Y_1^{-1}(\hat{p}) + \rho'_{21}\, Y_1^1(\hat{p}) \Big\} \sqrt{2/3}\, a \Big]. \qquad (45)$$

Here a is the value of $2\mathrm{Re}S^*P$ when $|S|^2 + |P|^2 = 1$, as was assumed here, and is equal to 0.62.[48] Its value is not important in our analysis, as long as it is not zero and a consistent value is used. The direction of the proton is $\hat{p}$.

Expression (45) gives us the intensity distribution in terms of $\hat{\Lambda}$ and $\hat{p}$ when we substitute ρ' from (43). First, a simplification can be made with the relation

$$Y_\ell^m(\hat{\Lambda})\, Y_\ell^{m'}(\hat{\Lambda}) = \sum_{L,M} (4\pi)^{-\frac{1}{2}} (2\ell+1)(2L+1)^{-\frac{1}{2}}\, C(\ell, \ell, L; 0, 0)\, C(\ell, \ell, L; m, m')\, Y_L^M(\hat{\Lambda}). \qquad (46)$$

If we use the relation (37) for t_L^M and a similar one for the spherical harmonics, and let $M = -j+i+k-n$, the final expression for the intensity is given by

$$
\begin{aligned}
I(\Lambda, p) \;=\; & (4\pi)^{-1} \sum_{i,j} \sum_{n,\,L'} \sum_{L,\,M} (2L'+1)(2\ell+1) \\
& \times (2J+1)^{-1}\ (2L+1)^{-\frac{1}{2}}\ (-)^{J-\frac{1}{2}+n-j}\ C(\ell, \ell, L; 0, 0) \\
& \times C(\ell, \ell, L; J-\tfrac{1}{2}-j+i,\ -J+\tfrac{1}{2}+M+j-i)\ \ C(J, L', J; J+1-M-j+i-n, M-i+n) \\
& \times C(\ell, \tfrac{1}{2}, J; J-\tfrac{1}{2}-j+i,\ 3/2-i)\ C(\ell, \tfrac{1}{2}, J; J-\tfrac{1}{2}-M-j+i,\ 3/2-n) \\
& \times t_{L'}^{-M+i-n}\ Y_L^M(\hat{\Lambda}) \Big[Y_0^0(\hat{p})\delta_{in} + (-)^{i+1}\sqrt{1/3}\ a\ Y_1^0(\hat{p})\ \delta_{in} \\
& + \sqrt{2/3}\ a\,(-Y_1^1(\hat{p})\ \delta_{i1}\ \delta_{n2} + Y_1^{-1}(\hat{p})\ \delta_{i2}\ \delta_{n1}) \Big].
\end{aligned}
\tag{47}
$$

An abbreviated way of expressing this equation would be

$$
I(\hat{\Lambda}, \hat{p}) = \sum_{\ell' m} \sum_{L,\,M} A_{J\ell}(L, M, \ell', m)\ Y_L^M(\hat{\Lambda})\ Y_{\ell'}^m(\hat{p}), \tag{48}
$$

with $A_{J\ell}(L, M, \ell', m)$ given by the coefficients of (47). The limits on ℓ' are $\ell' \leq 1$, and the limits on L are $L \leq 2J$. The expression (47) is a cumbersome-looking one, but its derivation was straight-forward and the meaning of all its elements are well known to the experimentalist (except t_L^M, which is described above). Note that we have used the normal as the quantization axis for both the Y_1^* and the Λ, as did Capps, but not as did Gatto and Stapp nor Byers and Fenster, who used helicity states for the Λ. The latter method allows us to determine the parity separately from the spin by finding the sign of one parameter, but requires deeper knowledge of the rotation operators.[49] We use (47) and are satisfied with trying to determine spin and parity simultaneously.

Equation (47) was reduced by hand to trigonometric functions for $J = 1/2\pm$ and for $J = 3/2\pm$. The resultant equations are:

$$J = \tfrac{1}{2},\ \ell=0,\ I(\hat{\Lambda}, \hat{p})(S_{1/2}) = (4\pi)^{-2}\left[t_0^0 + \sqrt{3}\,a t_1^0 \cos\theta\right], \tag{49}$$

$$J = \tfrac{1}{2},\ \ell=1,\ I(\hat{\Lambda}, \hat{p})(P_{1/2}) = (4\pi)^{-2}\Big[t_0^0 + \sqrt{3}\,a\,t_1^0\cos\theta \times (2\cos^2\Theta - 1) + t_1^0 \sin\Theta\cos\Theta\sin\theta\cos(\Phi-\phi)\Big], \tag{50}$$

$$\begin{aligned} J = \tfrac{3}{2},\ \ell=1,\ I(\hat{\Lambda}, \hat{p})(P_{3/2}) = (4\pi)^{-2}\Big[&(t_0^0 + \sqrt{5}/2\ t_2^0) \\ &- 3\sqrt{5}/2\ t_2^0\cos^2\Theta + a(2\sqrt{3/5}\ t_1^0 + 3/2\sqrt{7/5}\ t_3^0)\cos\theta \\ &- a(\sqrt{3/5}\ t_1^0 + 9/2\sqrt{7/5}\ t_3^0)\cos^2\Theta\cos\theta \\ &- a(\sqrt{3/5}\ t_1^0 - 3\sqrt{7/5}\ t_3^0)\sin\Theta\cos\Theta\sin\theta\cos(\Phi-\phi) \\ &- \sqrt{15/2}\ |t_2^2|\sin^2\Theta\cos(2\Phi - \arg t_2^2) \\ &- \sqrt{21/2}\ a\ |t_3^2|\{\sin^2\Theta\cos\theta\cos(2\Phi - \arg t_3^2) \\ &+ 2\sin\Theta\cos\Theta\sin\theta\cos(\Phi + \phi - \arg t_3^2)\}\Big], \end{aligned} \tag{51}$$

and

$$\begin{aligned} J = \tfrac{3}{2},\ \ell=2,\ I(\hat{\Lambda}, \hat{p})(D_{3/2}) = (4\pi)^{-2}\Big[&(t_0^0 + \sqrt{5}/2\ t_2^0) \\ &- 3\sqrt{5}/2\ t_2^0\cos^2\Theta + a(2\sqrt{3/5}\ t_1^0 + 3/2\sqrt{7/5}\ t_3^0)\cos\theta \\ &+ 3a(\sqrt{3/5}\ t_1^0 + 9/2\sqrt{7/5}\ t_3^0)\cos^2\Theta\cos\theta - 15a\sqrt{7/5}\ t_3^0\cos^4\Theta\cos\theta \\ &+ 3a(\sqrt{3/5}\ t_1^0 + 2\sqrt{7/5}\ t_3^0)\sin\Theta\cos\Theta\sin\theta\cos(\Phi-\phi) \\ &- 15a\sqrt{7/5}\ t_3^0\sin\Theta\cos^3\Theta\sin\theta\cos(\Phi-\phi) \\ &- \sqrt{15/2}\ |t_2^2|\sin^2\Theta\cos(2\Phi - \arg t_2^2) \\ &- \sqrt{21/2}\ a\ |t_3^2|\sin^2\Theta(1-6\cos^2\Theta)\cos\theta\cos(2\Phi - \arg t_3^2) \\ &- \sqrt{21/2}\ a\ |t_3^2|\sin\Theta\cos\Theta(1-3\cos^2\Theta)\sin\theta\cos(\Phi + \phi - \arg t_3^2) \\ &- 3\sqrt{21/2}\ a\ |t_3^2|\sin^3\Theta\cos\Theta\sin\theta\cos(3\Phi - \phi - \arg t_3^2)\Big]. \end{aligned} \tag{52}$$

Here Θ and Φ are the polar and azimuth angles respectively of the Λ in the Y_1^* center of mass, and θ and ϕ are the equivalent angles of the proton in the Λ center of mass. The z axis is the normal to the production plane in the K^--p center of mass, and the x axis is any line in the production plane.

The above formulae are equivalent to formulae (2a) through (3d) of Capps' paper,[45] and it is possible to write relations between the parameters in his formulae and the parameters in these formulae that establish this equivalence.

The terms in these expansions can be divided into two general types: those independent of α, of θ, and of ϕ, which have an even value of L in their t_L^M's, and which are the same for the two parity cases for a given spin; and those dependent on α, θ, and ϕ, which have an odd value of L, and which in general differ for the two parity cases. The former we can call intensity terms, the latter polarization terms.

This analysis is used in Sec. III. G. 6.

3. Normal and Rotated Polarization

It was pointed out in an earlier paper that it is possible to do a spin-parity analysis when only the polar angles of the Λ and the proton are used, providing one looked at the polarization along two different directions.[9] Let us review the arguments of that paper.

First of all, we see by inspection of (49) through (52) that the intensity terms have a maximum complexity of $\cos^{2J}\Theta$, whereas the polarization terms have a maximum complexity of $\cos^{2\ell}\Theta$, in which case we are focusing our attention on the terms independent of the azimuthal angles. We can establish from (47) that this is indeed the case. But we can determine spin and parity from the polarization terms alone if we use both the normal and rotated ("magic") directions as quantization axes for determination of polarization. The latter axis is defined shortly.

Let us consider again the transition operator M, which describes the decay of the Y_1^*. From general principles we know that the unitary operator that gives a change of parity is $\vec{\sigma} \cdot \hat{\Lambda}$, since $\hat{\Lambda}$ is the reference direction in the Y_1^* frame and $\vec{\sigma}$ is the pseudovector operator that can act on the Λ spin state. Hence we have upon a change of parity of the Y_1^*

$$M \rightarrow \vec{\sigma} \cdot \hat{\Lambda} \, M \, \vec{\sigma} \cdot \hat{\Lambda}, \tag{53}$$

where we have used explicitly the fact that $\vec{\sigma} \cdot \hat{\Lambda}$ is self-adjoint. Hence, if the initial state were the same but the Y_1^* had the opposite parity, relation (32) would read

$$\rho_f = \vec{\sigma} \cdot \hat{\Lambda} \, M \, \vec{\sigma} \cdot \hat{\Lambda} \, \rho_i \, \vec{\sigma} \cdot \hat{\Lambda} \, M^+ \vec{\sigma} \cdot \hat{\Lambda}. \tag{54}$$

But by multiplying on the right and left by $\vec{\sigma} \cdot \hat{\Lambda}$, we can throw this into the form

$$\vec{\sigma} \cdot \hat{\Lambda} \, \rho_f \, \vec{\sigma} \cdot \hat{\Lambda} = M \vec{\sigma} \cdot \hat{\Lambda} \, \rho_i \, \vec{\sigma} \cdot \hat{\Lambda} M^+. \tag{55}$$

From the principle that angular momentum operators, when exponentiated, are the generators of the rotation group, we know that the expression $\exp(i\pi \frac{1}{2} \vec{\sigma} \cdot \hat{\Lambda})$ is the operator that generates a rotation by 180° about the direction $\hat{\Lambda}$, since $\frac{1}{2}\vec{\sigma}$ is the spin operator of the Λ. But if this operator is expanded in a formal power series, we see immediately that $\exp(i\pi \frac{1}{2} \vec{\sigma} \cdot \hat{\Lambda}) = \vec{\sigma} \cdot \hat{\Lambda}$, so that $\vec{\sigma} \cdot \hat{\Lambda} \, \rho \, \vec{\sigma} \cdot \hat{\Lambda}$ is exactly the description of the state in a coordinate system rotated 180° about the $\hat{\Lambda}$ direction from the original coordinate system. This transformation is illustrated in Fig. 1. The rotated z axis, which we shall call $\hat{m}$ (for "magic") is given by

$$\hat{m} = - \hat{n} + 2\hat{\Lambda} \, (\hat{\Lambda} \cdot \hat{n}). \tag{56}$$

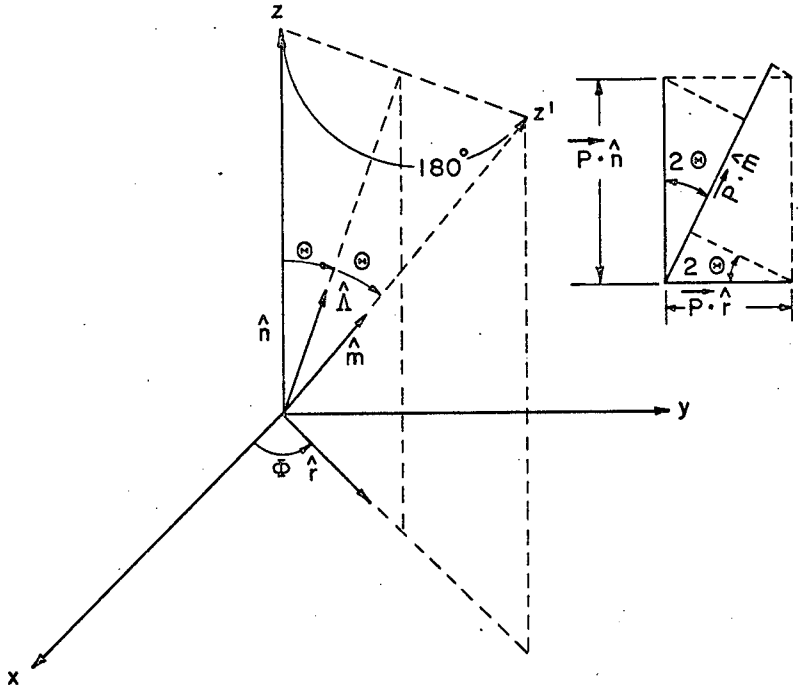

MU-34384

Fig. 1. Normal and rotated coordinate systems. The normal system has its z axis normal to the production plane. The Λ-momentum direction makes an angle Θ with this z axis. The transformation to the rbtated system is accomplished by rotating the z axis 180° about the Λ direction to the position z', which is equivalent to rotation of the same axis in the plane of the Λ and the normal by an angle 2Θ. The insert shows the relation among three projections of the polarization vector, equation (57) in the text.

The following interpretation can then be given to equation (55). The distribution observed in the rotated ("magic") coordinate system is that of parity opposite to that in the original coordinate system.

Adair was the first worker to attempt to take advantage of the rotated direction.[50] He attempted to determine whether the Y_1^* was S wave or P wave, assuming it to have spin $\frac{1}{2}$, by looking at the component of the average polarization of the Λ along the normal and along the rotated directions. If the Y_1^* is $S\frac{1}{2}$, maximum polarization of the Λ will occur along the normal direction; if it is $P\frac{1}{2}$, it will occur along the rotated direction and the ratio between the two components will be $-1/3$. The relation for any spin between these components is, with $\vec{P}$ the average polarization of the Λ,

$$\vec{P}\cdot\hat{m} = -(2\ell+1)(2\ell'+1)^{-1}\ \vec{P}\cdot\hat{n}, \qquad (57)$$

where ℓ is the orbital angular momentum of the Y_1^*, and ℓ' is the apparent orbital angular momentum when observed in the rotated system. From the discussion above, we have $\ell' = \ell \pm 1$, the sign chosen dependent on the parity of the Y_1^*, and of course, $J = \frac{1}{2}(\ell + \ell')$.

Relation (57) becomes less sensitive for higher spin, and is useless if the average polarization is nearly zero. However, the maximum complexity analysis can be used even if the latter is true, because the polarization is not likely to vanish for all values of the Y_1^* decay angle. In this case we look for a $\cos^{2\ell}\Theta$ dependence of the normal component of polarization and a $\cos^{2\ell'}\Theta$ dependence of the rotated component, with ℓ and ℓ' related as above. There is a geometrical constraint, relating the two distributions which can be used to advantage in the fitting process. Let $\hat{r}$ be a unit vector along the intersection of the plane of $\hat{n}$ and $\hat{m}$ with the production plane (see Fig. 1). Let $\vec{P}(\Theta)$ be the distribution of polarization. Then it follows from the geometry that

$$\vec{P}(\Theta)\cdot\hat{m} = \vec{P}(\Theta)\cdot\hat{n}\cos 2\Theta + \vec{P}(\Theta)\cdot\hat{r}\sin 2\Theta. \qquad (57)$$

Either $\vec{P}\cdot\hat{n}$ or $\vec{P}\cdot\hat{m}$ can have the higher complexity. Assume the parity of the Y_1^* is such that $\vec{P}\cdot\hat{m}$ has the higher complexity. Then the distributions will have the form

$$\vec{P}\cdot\hat{n} = \sum_{k=0}^{J-1/2} A_n^k \cos^{2k}\Theta, \quad \vec{P}\cdot\hat{m} = \sum_{k=0}^{J+1/2} A_m^k \cos^{2k}\Theta. \tag{58}$$

Then $\vec{P}\cdot\hat{r}$ must be of the form $\sin 2\Theta \times$ (even polynomial in $\cos\Theta$) in order that (57) shall hold for all Θ. Finally we get the relations among the coefficients,

$$A_n^0 + A_m^0 = 0 \tag{59}$$

and

$$\sum_{k=0}^{J-1/2} A_n^k - \sum_{k=0}^{J+1/2} A_m^k = 0 \tag{60}$$

by evaluating (57) with (58) inserted at $\Theta = 0$ and at $\Theta = \pi/2$, where the $\vec{P}\cdot\hat{r}$ term does not contribute. These are just the directions where the $\hat{n}$ and $\hat{m}$ are parallel and antiparallel respectively. If the parity of the Y_1^* is opposite to that assumed, simply interchange n and m and the above relations still hold.

This analysis is used in Sec. III. G. 5.

4. Adair Distribution

It was pointed out by Adair that the spin of a particle produced under circumstances similar to those we have been considering could be determined unambiguously from a specially chosen distribution.[51] Let the axis of quantization be the incident K^- direction. Since the K is spinless, the angular-momentum projection along this axis must be the $\pm\frac{1}{2}$ contribution of the proton. The π is also spinless; so the projection of the spin of the Y_1^* added to the projection of the orbital angular momentum of the final state must sum to $\pm\frac{1}{2}$. If the

production is S wave, or if the Y_1^* is traveling parallel or anti-parallel to the K direction, there will be no contribution from the orbital part, and the distribution of the Λ relative to the K will be that characteristic of the $m_J = \pm\frac{1}{2}$ states of the Y_1^*. These states have a definite form for each value of J. The forms, as given by Adair, are listed in Table II.

Table II. Adair distributions.[a]

Spin J	Distribution
1/2	1
3/2	$\frac{1}{2}(1 + \cos^2\eta)$[b]
5/2	$3/4(1 - 2\cos^2\eta + 5\cos^4\eta)$
7/2	$1/16(9 + 45\cos^2\eta - 165\cos^4\eta + 175\cos^6\eta)$

[a] Ref. 51.

[b] η is the angle between the Λ and the K.

The difficulty in using this distribution in practice, if the production is not S wave, is that the number of events satisfying the requirement that the Y_1^* travel along or opposite to the K direction is very small (theoretically equal to zero). If Y_1^* that are in a finite cone about the K direction are accepted, the effect is necessarily diluted by contributions from other m_j states. If the production state is not known, the amount of this dilution cannot be determined directly. Let us see if we can find an extrapolation technique that will get around this difficulty.

For this discussion, let η be the Adair angle ($\cos\eta = \hat{\Lambda}\cdot\hat{K}$) and let ζ be the production angle ($\cos\zeta = \hat{Y}_1^*\cdot\hat{K}$). Then the distribution in these two angles will be in general

$$I(\eta,\zeta) = \sum_m F_m(\cos\zeta)\, P_m(\cos\eta), \qquad (61)$$

where $m = |m_J| - \frac{1}{2}$ (for our purposes, we can lump together the positive and negative values of m_J), F_m is an analytic function, and P_m is an even polynomial. The observed distribution is Eq. (61) integrated over a particular range of $\cos\zeta$,

$$I'(\eta, x) = \int_x^1 \sum_m F_m(\cos\zeta)\, P_m(\cos\eta)\, d(\cos\zeta) \tag{62}$$

plus a similar integral from -1 to $-x$ which will have the same properties. The term F_m can be expanded in a Taylor's series about the point $\cos\zeta = 1$:

$$F_m(\cos\zeta) = F_m(1) + (\cos\zeta - 1)\, F_m'(1) + \cdots \tag{63}$$

If we are close enough to $\cos\zeta = 1$, we can neglect higher order terms. The polynomial $P_0(\cos\zeta)$ is the Adair function, and therefore $F_m(1)$ must vanish for $m \neq 0$. The integration is now trivial:

$$\begin{aligned} I'(\eta, x) &= (1-x)\, F_0(1)\; P_0(\cos\eta) \\ &\quad -\tfrac{1}{2}(1-x)^2 \sum_m F_m'(1)\; P_m(\cos\eta). \end{aligned} \tag{64}$$

We see here that the diluting terms enter linearly--as compared to the main effect--as the acceptance variable, $1 - x$, is increased. For analysis, we can extrapolate the observed distribution linearly, for fixed values of $\cos\eta$, to $\cos\zeta = 1$, then examine the distribution in $\cos\eta$ of the extrapolated values. We will get valid results if we remain close enough to $\cos\zeta = 1$.

This analysis is used in Sec. III. G. 4.

D. Decay Mode $\omega \to \pi^+ \pi^-$

Glashow pointed out that, when two states of matter have the same quantum numbers except for isotopic spin and have almost the same mass, electromagnetic transitions between these states may become important.[52] One case for which this behavior is possible is the pair of nonstrange vector mesons, ρ and ω. Glashow showed that the amount of mixing should be inversely proportional to the mass difference between the two states. The relevant amplitudes are

$$\begin{aligned} \tilde{\rho}^0 &= \rho^0 + \eta (\delta m)^{-1} \omega \\ \tilde{\omega} &= \omega - \eta (\delta m)^{-1} \rho^0 \end{aligned} \tag{65}$$

where $\tilde{\rho}^0$ and $\tilde{\omega}$ are the observed states that decay into two pions and three pions, respectively; ρ^0 and ω are the states of pure isotopic spin (or G parity) that are produced in the strong production process; δm is the mass difference between ρ and ω; and η is a mixing parameter. Glashow did not propose any model for the mixing, but he estimated the value of η on general grounds to be about 5 MeV, which gives a value of 5% for the branching ratio of the two-pion decay mode of the ω to the three-pion decay mode.

Gell-Mann, Sharp, and Wagner did propose a model by which they attempted to calculate the decay rates of the neutral mesons.[53] Their model proposes that the three-pion decay of the ω proceeds predominantly through the two-step process, $\omega \to \rho + \pi$ followed by $\rho \to 2\pi$. The two-pion decay mode follows the chain, $\omega \to \gamma \to \rho^0 \to 2\pi$. The direct coupling of ρ^0 and ω to γ is implied in the interpretation of these mesons as contributors to the electromagnetic form factor of the nucleons. The coupling constant for $\omega \to \rho + \pi$ can be eliminated by also assuming that the π^0 decay, whose rate is known, proceeds through the reactions $\pi^0 \to \rho^0 + \omega$, $\rho^0 \to \gamma$, $\omega \to \gamma$. In determining the branching ratio, the coupling constant for $\rho \to 2\pi$ cancels out, so that the branching-ratio figure depends on the values of the coupling

constants for $\omega \to \rho\pi$, $\rho^0 \to \gamma$, and $\omega \to \gamma$. These three constants cannot be independently determined from present experimental data; so Gell-Mann, Sharp, and Wagner made rough approximations for these numbers. Their figure for the branching ratio $\Gamma(\omega \to 2\pi)/\Gamma(\omega \to 3\pi)$ was 4.3%, but they calculated a total width of 0.5 MeV. We can adjust their theory to reproduce the observed total width of 9 ± 2 MeV[54] and the observed neutral/charged branching ratio of about 10% (Ref.12) by scaling up these coupling constants. Since there are three constants and two experimental numbers, we can apply an additional constraint of keeping the coupling constant for $\rho^0 \to \gamma$ equal to that for $\omega \to \gamma$ (predicted by unitary symmetry). When this scaling is done, the partial width for the $\omega \to 2\pi$ mode is predicted to be 350 eV, and the branching ratio $\Gamma(\omega \to 2\pi)/\Gamma(\omega \to 3\pi)$ is predicted to be 0.0001%!

For an exhaustive treatment of how interference between the ρ^0 and ω mesons can affect the shape of the $\pi^+ - \pi^-$ mass spectrum through this rare decay mode, see Bernstein and Feinberg.[55]

Many other authors have treated the problem of the electromagnetic mixing of ρ^0 and ω mesons.[56-59] Their estimates are pretty much in accord with the ones discussed above, but all of the methods would probably yield a much smaller branching ratio if the experimental total width were taken into account.

Experimental evidence from this study is discussed in Sec. III. F. 3.

E. Peripheral Production

The philosophy of this report, as stated in the Introduction, is to place much emphasis on final-state interactions and little emphasis on production processes. One production mechanism, however, can often be easily detected if it is operating in a given reaction, namely peripheral-collision mechanism in which one particle is exchanged. Two possible configurations through which reaction (1) could proceed peripherally are illustrated in Fig. 2.

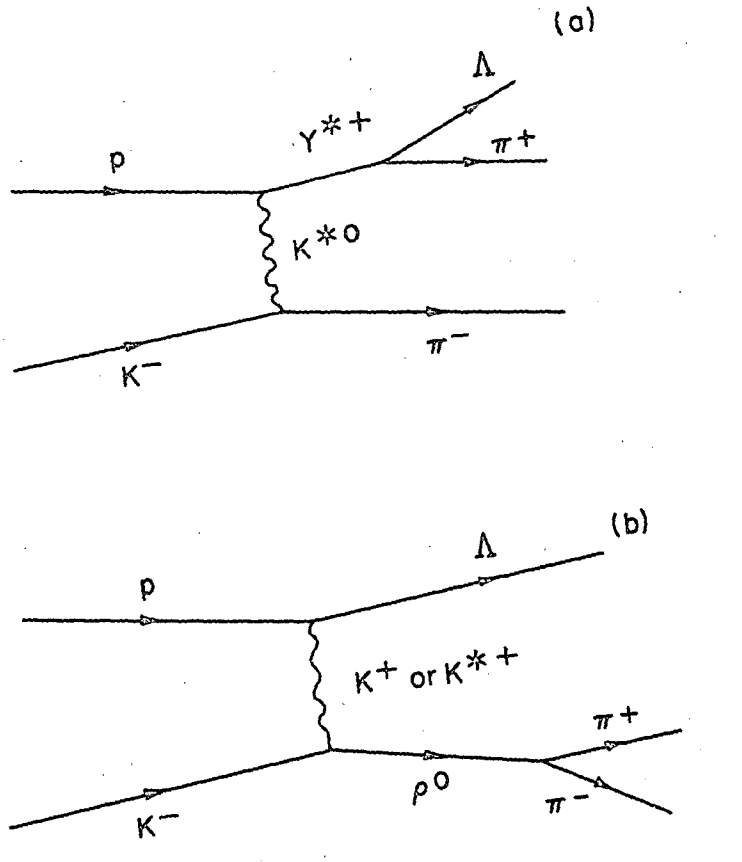

Fig. 2. Diagrams of the two exchange mechanisms that can occur in $K^- + p \rightarrow \Lambda + \pi^+ + \pi^-$. In (a), the K^- and p exchange a K^* to yield Y_{+1}^* and π^-. In (b), they exchange either a K^+ or a K^{*+} to yield Λ and ρ^0.

The exchange of K^*- mesons in the production of Y_1^*, as in Fig. 2(a), was studied theoretically by Stodolsky and Sakurai.[60] A few remarks about this mechanism are listed here.

(a) A K meson cannot be exchanged. The $K\bar{K}\pi$ vertex necessary in that case is forbidden by conservation of parity and angular momentum.

(b) Production of Y_1^{*-} is not possible from reaction (1) by this mechanism. In that event, a doubly charged meson would have to be exchanged. The K^* has $I = \frac{1}{2}$, so that there is no doubly charged member in the multiplet.

(c) From analogy with electromagnetic processes in which a gamma ray is exchanged, the process can be decomposed into contributions from various multipole moments. The calculated distributions are

$$M1 \rightarrow P_{3/2}: \quad 1 + 3(\hat{\Lambda}\cdot\hat{n})^2, \tag{66}$$

$$E2 \rightarrow P_{3/2}: \quad 1 - (\hat{\Lambda}\cdot\hat{n})^2, \tag{67}$$

$$L2 \rightarrow P_{3/2}: \quad 1 + 3(\hat{\Lambda}\cdot\hat{K})^2. \tag{68}$$

Note that the Y_1^* is explicitly assumed to be $P_{3/2}$. The symbol M1 denotes the analog of the magnetic dipole moment, E2 denotes the analog of the electric quadrupole moment, and L2 denotes the longitudinal quadrupole moment. From various theoretical considerations, Stodolsky and Sakurai argued that the predominant multipole contribution should be M1. In Sec. III.I, this mechanism is investigated.

The peripheral production of ρ mesons, as in Fig. 2(b), is not very easy to study in this reaction. The ρ is a broad resonance, there is a large background of Y_1^* production, and the K and K^* amplitudes can interfere and give complex angular correlations in the final state.[61] However, this process should be closely related to peripheral production of ω mesons from the same initial states, currently being studied by Flatté et al.[62]

III. EXPERIMENTAL ANALYSIS

A. The K^- Beam

The data upon which this study is based were taken in an extended exposure (nicknamed K-72) of the Laboratory's 72-inch bubble chamber, from September 1961 to June 1962, to a separated beam of K^- mesons. The beam was designed jointly by experimental groups at UCLA and LRL, headed by H. K. Ticho. A detailed report on the beam's design and construction is in preparation[63] but a sketch of the operation of the beam and how the analysis is thereby affected is given here.

The external-beam channel was designed to meet several requirements: (1) the momentum was variable, (2) K mesons were separated from unwanted components, and (3) a reasonable K flux was delivered to the bubble chamber.

The layout of the channel is shown in Fig. 3. Particles entering the external-beam aperture were produced in a target flipped into the primary proton beam of the Bevatron late in the acceleration cycle. Only particles emitted at 0° from the target were accepted by the optics of the channel. The target was located in a curved section of the Bevatron, so that negative particles were bent outward in the field of the Bevatron. In order to effect changes in the momentum of particles reaching the aperture, the target was made movable by remote control. Two targets at different radii were located on a support that could be moved azimuthally. In addition, a small steering magnet was placed in the hole in the magnet yoke through which the particles entered the beam aperture in order to bring the particle trajectories parallel to the beam line. Currents in the remaining magnets along the beam channel were scaled to provide the proper fields for each momenta.

Separation was necessary because the number of π's accepted by the aperture at the front end was about 10^5 per pulse. In addition, many μ particles were produced along the beam channel by decay of π's and K's. Allowing this flood of particles into the bubble chamber would

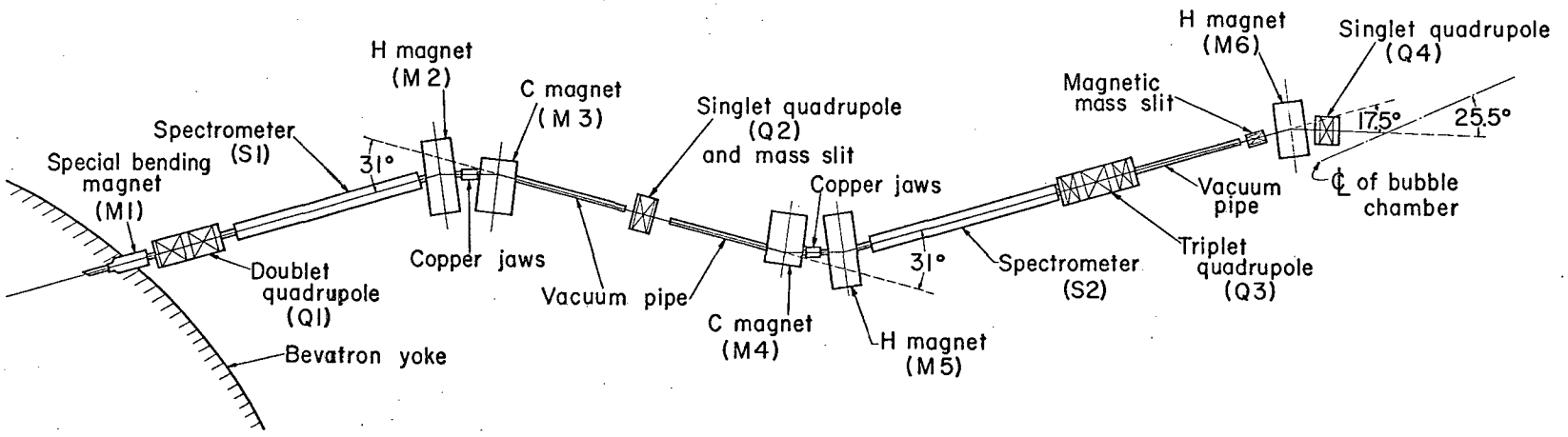

Fig. 3. Experimental setup of the K^- beam. The beam arrives from the target (not shown). M1 is a bending magnet to steer the trajectories along the beam line for each momentum setting; Q_1 is a doublet quadrupole that collimates the beam vertically; S1 is an electrostatic separator that deflects unwanted particles vertically; M2 and M3 are bending magnets that also serve to focus the beam vertically at the first slit; and Q2 is a singlet quadrupole that holds the beam together horizontally. The second stage is a reflection of the first, with M4 and M5 corresponding to M2 and M3, S2 corresponding to S1, and Q3, a triplet, corresponding to Q1. M4 gives the beam a final bend into the bubble chamber, and Q4 controls spreading of the tracks in the chamber.

make analysis of the K interactions impossible. To have a beam that is nearly all K's at the bubble chamber, a separation scheme giving a rejection ratio of 10^5 was needed. This separation was effected by crossed electric and magnetic fields. The beam entering the separator is momentum analyzed; the action of the separator is to select on the basis of velocity. The overall effect is a separation on the basis of mass. The fields were adjusted so that π's and μ's were deflected out of the horizontal plane, while K's passed through the separator undeflected.

Two stages of separation were used. By this device, the second stage can have the mass slit at the end of the first stage as its source. It was much easier to optimize separation with this cleaner source than with the target, which was the source for the first stage. Each stage contained a quadrupole, a separator, a pair of bending magnets, and a mass slit. The bending magnets acted also as focusing elements in the vertical plane, and the shape of the field of each one was adjusted with steel shims in such a manner as to correct for the chromatic aberration of the quadrupole. In each stage, the quadrupole was carefully shimmed to remove spherical aberrations. The beam was collimated at several places to remove unwanted particles such as particles that scattered from walls, particles that multiple-scattered in thin windows and gases, and particles that resulted from decay of beam particles. The beam channel was evacuated along much of its length and windows were as thin as possible.

A flux of 10 K^- per pulse into the chamber was desired. The beam length was 155 feet, 4.2 decay lengths for K particles at 1.51 BeV/c. In order to achieve the desired K^- flux when the Bevatron was operating at an average of 1.5×10^{11} protons/pulse, it was necessary to design the beam channel to accept a momentum bite of 6% full width. Elimination of chromatic aberration, mentioned above, was vital to avoid spreading of the images at the slits with consequent poor separation.

Runs were taken at momentum settings of 1.22, 1.32, 1.42, 1.51, 1.60, and 1.69 BeV/c for this Laboratory and at 1.80 and 1.95 BeV/c for UCLA. This paper uses the former set of runs as its source of data. In addition, absorber was placed into the 1.22 BeV/c beam in order to gather data down to 1.05 BeV/c for a special study at LRL of the 1815 MeV Y_0^* resonance.[64] This paper uses data from this latter source when no overlap with the special study is introduced.

B. Primary Analysis

Primary analysis of the data was done in the manner described in Sec. I of the review article by Rosenfeld and Humphrey.[65] Let us describe briefly the procedure involved.

At each pulse of the bubble chamber, three pictures were taken on one piece of film by three cameras mounted at three corners of a square on the top of the bubble chamber. About one million sets of three pictures were taken during the run. Technician personnel scanned the pictures twice to locate all interesting events. Interesting events were defined to be all cases when the beam track terminated within the chamber, with the exception of decay of beam track with one outgoing charged prong, interaction of the beam track with no outgoing charged prongs and no associated vee(s), or interaction of the beam track with two outgoing charged prongs and no associated vee(s). Events were also not recorded if they occurred too close to the walls of the chamber, if the incoming track was not a beam track, or if there were too many tracks in the picture. All three views were used to make certain that all interesting events were found and to establish the approximate geometry of the events found.

When interesting events were found, information was recorded on forms to be transferred to IBM cards. This information included, among other things, the roll, frame, and beam-track number, approximate x-y coordinates of the vertices, and the event type. Event type is a number assigned the event by the scanner to identify its topology.

Reaction (1) is found among events having event-type 32, in the language of this experiment, also known as the vee-two-prong topology. See Fig. 4 for an example of such an event. These events are identified by an interaction of the beam track resulting in two outgoing charged prongs and having associated with it a vee resulting from the decay of a neutral particle presumably produced at the primary vertex.

As desired, events were measured on Franckenstein machines--digitized measuring projectors. In each of at least two views, the position of fiducial marks etched on the top glass, the vertices, and several points along each track were located to an accuracy of about 2 microns on the film. These measurements were output on paper tape, which was converted to magnetic tape for input to the IBM 7090 computer.

A series of programs operated on these measured points to reduce them to physically interesting information. The program PANAL checks that all necessary information is present and condenses this information into a compact format. The program PACKAGE, which operates on output from PANAL, has two stages. In the PANG stage, a geometrical reconstruction of the event being processed is accomplished. In the KICK stage, a preselected series of physical hypotheses, dependent upon the event type, is assumed, and a fitting program tests whether the momenta and angles given by PANG can be adjusted to satisfy conservation of energy and momentum at each vertex for each hypothesis. A chi-squared, or figure of merit, is calculated for each hypothesis from program-estimated errors on the momenta and angles. Another mode of operation at this stage is determination of kinematic unbalance for a given assignment of masses to tracks, and expression of this unbalance as a missing mass (and its error) of a hypothetical missing neutral particle. The EXAMIN program reads the output tape from PACKAGE and lists particularly interesting information for each hypothesis that has an acceptable chi-squared on another tape. Many calculations, such as effective masses of particle

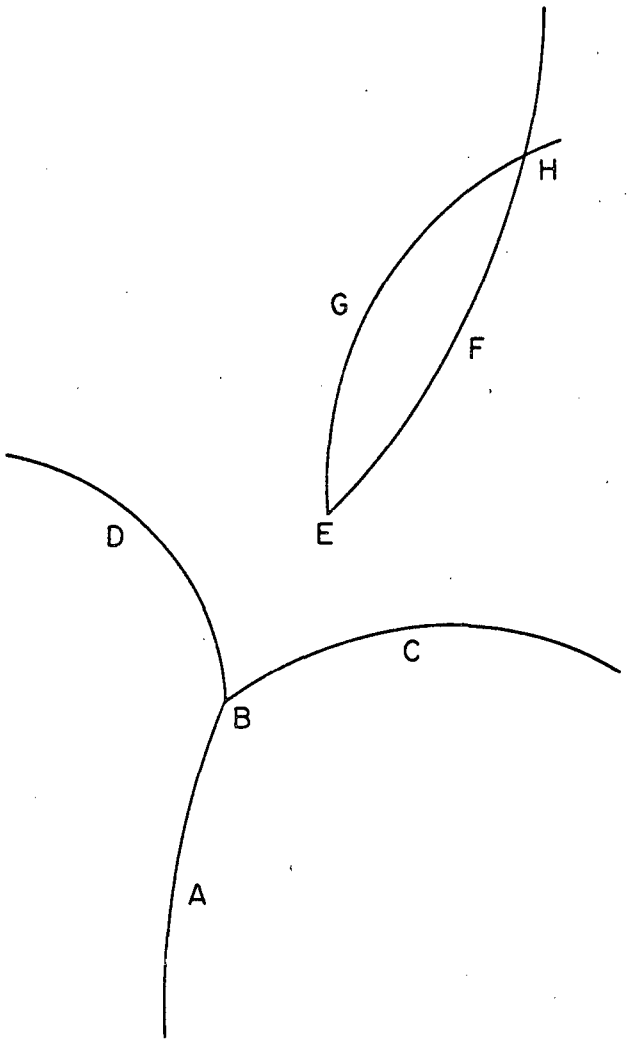

MU-34352

Fig. 4. Schematic type-32 event as seen in bubble chamber photographs. A beam particle (track A) enters the thin window of the chamber and interacts with a proton of liquid hydrogen at B, producing a negative particle (track C) a positive particle (track D), and one or more neutral particles, which leave no tracks. One of the neutral particles, a Λ or a K^0, decays at E, yielding a positive particle (track F) and a negative particle (track G). If the decay is two-body, the points B, E, and H should lie in a straight line.

pairs and angular correlations in various coordinate systems are done at this stage. READX reads the EXAMIN output, makes further calculations as needed, picks out a particular event type, and puts out separate binary tapes and printed output for each hypothesis. SUMX reads EXAMIN and READX output and constructs forms such as histograms, lists, CRT plots, and resolution functions. Finally, the LINGO program keeps a library of the experiment by collecting the scan cards into a Master List tape for each momentum setting, collecting the EXAMIN output into a Data Summary tape for each momentum setting, updating each of these tapes as necessary, and checking them against each other.

C. Measurement of Type-32 Events

All of the type-32 events were measured at the momentum settings of 1.22, 1.32, 1.42, 1.60, 1.69, and the special low-momentum settings. About 40% of type-32 events at 1.51 BeV/c were measured, but so much more data were taken at this setting that this 40% represents more events than does 100% of any other setting. Table III lists the number of events found at each setting and the number that was successfully measured, along with other related numbers.

Not all events sent to the measuring machine yield useful physical information at the end of the analysis process. A code was developed for this experiment to characterize the disposition of events in the measurement-analysis system. The measing of the more pertinent of these code numbers is:

(a) Result 0 signifies that the event was not measured. The operator of the measuring machine may have rejected it as being impossible to measure because of obscuring tracks, steeply dipping tracks, etc. Or the event may have simply been missed by the operator.

(b) Result 8 signifies that the event was rejected, before reaching the KICK stage of the analysis system, in PANAL or PANG. The operator may have left out or scrambled some of the information.

Table III. Type 32 scanning-and-measuring summary.

Item	Number of events found at momentum setting 1.22 Bev/c	1.32 Bev/c	1.42 BeV/c	1.52 BeV/c	1.60 BeV/c	1.69 BeV/c	Total
Found on scan	4087	5523	3436	23402	3025	5428	44 901
Measurement requested	4013	5411	3419	9251	2926	5211	30 231
Result 0[a] (not measured)	119	104	104	725	155	28	1 235
Result 8[a] (no reconstruction)	136	438	382	1248	393	726	3 323
Result 11[a] (hypothesis reject)	245	372	238	822	259	348	2 284
Result 20[a] (good event)	3513	4497	2695	6456	2119	4457	23 737
Remeasured result 11[a]	385	323	100	16	0	350	1 174
Became result 20[a, b]	161	139	31	0	0	172	503

[a] The results code is explained in the text.

[b] This is an extrapolated number because the $\bar{K}^0$ events were not counted directly.

Or the event may have some intrinsic difficulty that does not permit geometric reconstruction of the tracks. No physics information is available from these events.

(c) Result 11 signifies that the event was rejected by the analysis system in the KICK stage. The operator may have made a poor measurement (but not so poor that track reconstruction was impossible), the event may not really be a type 32 (such as vee not really associated with two-prong), or the event may be a physical interaction not covered in the hypotheses given (such as leptonic decay). Measured physics information is available from these events, but no hypothesis can be assigned to them, and no fitted information is available.

(c) Result 20 signifies that the event was successfully processed by the analysis system and one or more hypotheses were found to explain the event satisfactorially. Events were included here which had a good Λ fit and a missing mass significantly larger than the π^0 mass. The next section covers the further disposition of these events.

The number of events finally falling into each of these result categories is given in Table III.

In an effort to reclaim those events that did not have result 20 after the first measurement, these events were sent back, in some cases, to be measured a second time. Unfortunately, measuring-machine time was critical and a thorough remeasurement program was not possible. Events at 1.22 BeV/c were remeasured completely, about 75% of events at 1.32 BeV/c were remeasured, and only the result-11 events were remeasured at 1.69 BeV/c. The last-named measurements were made after the analysis of final-state interactions was underway, so that they were not included in the sample, but they were used as a check on possible bias at the higher momentum settings.

Events with result 0 and result 8 are not likely to be a source of bias, particularly when final-state interactions are considered, because their rejection is not closely allied to physics. Events with result 11, however, are rejected for physical reasons and may be a

source of bias. The next-to-last line of Table III gives the number of (result 11) events that were remeasured at each momentum setting, and the last line gives the number of these that did fit some hypothesis and become result-20 events. It is seen that about 40 to 50% of these events do pass a second time; these events were probably rejected because of poor measurement; but they represent only 4% of the total number measured.

Various angular and effective-mass distributions from these reclaimed result-11 events were looked at for the momentum settings 1.22 and 1.69 BeV/c. There was no qualitative difference between these distributions and the corresponding ones from original result-20 events. No significant bias was evident in these events.

A sample of 90 events that were originally result 11 and that failed again when remeasured was carefully studied on the scanning table. A variety of possible causes for failure was evident. Some causes were (i) two production vertices close together and assignment of the vee to the wrong one, (ii) production of vee from secondary interaction of an outgoing charged prong, e.g., nearby charge exchange of outgoing K^- track from elastic scatter, (iii) vee completely unassociated, (iv) Ξ^- or Ξ^0 production, (v) some track obscured, distorted, or steeply dipping. No bias is expected from this source.

D. Separation of Hypotheses

Let us turn now to the specific problem of separating reaction (1) from competing reactions that are also event-type 32. The major hypotheses tried in KICK for this experiment for type 32 are

$$K^- + p \rightarrow \Lambda + \pi^+ + \pi^-, \quad \Lambda \rightarrow p + \pi^-, \tag{1}$$

$$K^- + p \rightarrow \Sigma^0 + \pi^+ + \pi^-, \quad \Sigma^0 \rightarrow \Lambda + \gamma, \ \Lambda \rightarrow p + \pi^-, \tag{69}$$

$$K^- + p \rightarrow \Lambda + \pi^+ + \pi^- + \pi^0, \quad \Lambda \rightarrow p + \pi^-, \tag{70}$$

$$K^- + p \rightarrow \bar{K}^0 + \pi^- + p, \quad K_1^0 \rightarrow \pi^+ + \pi^-, \tag{71}$$

$$K^- + p \rightarrow \bar{K}^0 + \pi^- + \pi^+ + n, \quad K_1^0 \rightarrow \pi^+ + \pi^-, \tag{72}$$

$$K^- + p \rightarrow \bar{K}^0 + \pi^- + p + \pi^0, \quad K_1^0 \rightarrow \pi^+ + \pi^-. \tag{73}$$

Other hypotheses that cannot be fit because they are underconstrained, but whose identity can be conjectured from missing mass determinations significantly larger than a π^0 mass, are of the form

$$K^- + p \rightarrow \Sigma^0 + \pi^+ + \pi^- + \pi^0, \quad \Sigma^0 \rightarrow \Lambda + \gamma, \quad \Lambda \rightarrow p + \pi^-, \tag{74}$$

or

$$K^- + p \rightarrow \Lambda + \pi^+ + \pi^- + \pi^0 + \pi^0, \quad \Lambda \rightarrow p + \pi^-. \tag{75}$$

The fitting is done in two steps. First the neutral direction is taken to be the line connecting the primary vertex to the vertex of the vee, and the vee is fit to the two hypotheses, $\Lambda \rightarrow p + \pi^-$ and $K_1^0 \rightarrow \pi^+ + \pi^-$. This fit is a three-constraint fit. If either of these fits gives a chi-squared less than 30, the appropriate production hypotheses in the first list above are tried. If both vee fits give acceptable chi-squareds, all the production hypotheses are tried. In the latter case, if a low chi-squared (less than 10 times the number of constraints) is obtained for some production hypothesis for each interpretation of the vee, the event is classified as ambiguous between Λ production and $\overline{K}^0$ production and is eliminated from the sample to be studied for final-state interactions. For studies on $\overline{K}^0$ production, see reference 66. The percentage of events rejected for this reason compared to the number fitting some hypothesis varies from 1.2% at 1.22 BeV/c to 2.5% at 1.69 BeV/c. Little bias is expected from this rejection.

Let us now consider the unambiguous Λ events. Events that simultaneously fit (1) and (70) but do not fit (69) are about 1% or less of the total events, so that hypothesis (1) can be cleanly separated from hypothesis (70) with no difficulty. However, the number of events that simultaneously fit (1) and (69) is a significant fraction of the total number fitting either of these hypotheses. The major problem in isolating reaction (1) is distinguishing it from reaction (69).

Reaction (1) is a four-constraint fit at the production vertex since, once the vee has been fit, all the momenta and angles are known. In reaction (69), on the other hand, there are two particles whose tracks

are not seen, the Σ^0 and the γ. However, there are two vertices at which momentum and energy must be conserved, the Σ^0 decay vertex and the production vertex; these vertices can be considered to lie at the same point because of the very short lifetime of the Σ^0. The fit is made to these two vertices simultaneously, giving a two-constraint fit. It is necessary to compare the chi-squared values for these quite different fitting procedures.

Chi-squared is computed in KICK from the formula

$$\chi^2 = \sum_{i,j} (x_i - x_i^m)\,(G^{-1})_{ij}(x_j - x_j^m), \tag{76}$$

where x_i^m is the initial measured value of a track variable (angle or curvature), x_i is the final fitted value of that track variable, G is the error matrix, and the double sum is over all measured track variables. The elements of G are

$$G_{ij} = \left\langle \delta x_i \, \delta x_j \right\rangle \tag{77}$$

where δx_i is the program-estimated error to be expected in the given measurement of x_i, and $\langle\ \rangle$ indicates the taking of the average value. The errors are assumed to have a Gaussian distribution. In that case, the theoretical distribution of $M \equiv \chi^2$ is given by[67]

$$f(M) = \frac{M^{(n-2)/2}\, e^{-M/2}}{2^{n/2}[(n-2)/2]!} \tag{78}$$

where n is the constraint class, and a new figure of merit can be derived that is theoretically independent of the constraint class,

$$P(M_0) = \int_{M_0}^{\infty} f(M)\, dM, \tag{79}$$

which is just the probability that chi-squared should have a value equal to or greater than M_0.

However, the observed chi-squared distributions seem to be shifted to values higher than those of the expected distribution, Eq. (78). It is likely that the programs are underestimating the errors, or that the error distribution is not really Gaussian. In order to express this behavior in quantitative terms, it was assumed that observed chi squareds were too large by a factor A, which might vary from hypothesis to hypothesis but otherwise is constant. The corrected chi squared would be $M_c = M_0/A$. To find the best value for A, the distribution of $P(M_0/A)$ for the events of a given hypothesis [these events were required to have $P(M_0/A) > 0.01$ and $> P(M_0/A)$ for any other hypothesis] was histogrammed for a variety of values of A. If M_0/A follows the chi-squared distribution, this histogram should be flat. A chi-squared test was applied to these histograms to determine if they were flat. The values of A that gave a minimum chi-squared for each hypothesis were A = 1.44 for hypothesis (1), A = 1.52 for hypothesis (69), and A = 1.72 for hypothesis (70). Some variation with momentum setting was observed, but it was so slight that it was not compensated for. The distribution of P did not flatten out entirely, but peaked near the extreme values.

The criteria finally established, then, for acceptance of events as examples of reaction (1) were:

(a) If the vee also fit a K_1^0 decay, no $\bar{K}^0$ production hypothesis gives a satisfactory fit.

(b) $P(M_1/1.44) > 0.01$, where M_1 is the observed chi-squared for hypothesis (1).

(c) $P(M_1/1.44) > P(M_{69}/1.52)$, where M_{69} is the observed chi-squared for hypothesis (69).

(d) $P(M_1/1.44) > P(M_{70}/1.72)$, where M_{70} is the observed chi-squared for hypothesis (70).

To test whether criterion (c), which is the one expected to give the most difficulty, is really yielding a clean sample, we must find some alternate way of estimating the probability that an event is really

a Λ event or a Σ^0 event. We selected a sample of events that fit either (1) or (69) but not (70) (by using criteria similar to those above). The information from the vee was ignored, and the missing mass was determined from the beam track and the two charged prongs alone. The missing mass is given simply by

$$MM = \left[\left(\sum_i E_i - \sum_o E_o \right)^2 - \left(\sum_i \vec{P}_i - \sum_o \vec{P}_o \right)^2 \right]^{1/2}, \qquad (80)$$

where the index i runs over the incoming particles and the index o runs over the outgoing particles. In the present case, if there were no measurement error, the missing mass would have one of two values, 1115 MeV for a missing Λ, or 1190 MeV for a missing Σ^0. Measurement error is expected to broaden these spikes into bell-shaped curves with a finite width (called resolution function and discussed below). A histogram of this quantity is shown in Fig. 5.

The curve drawn through the data on Fig. 5 is the sum of two resolution function curves centered at 1115 and 1190 MeV respectively. The resolution function for a variable x having a value x_i with a program-estimated error of δx_i for the ith event in a collection of events is given by

$$RF(x) = (2\pi)^{-\frac{1}{2}} \sum_i \exp\left[-\tfrac{1}{2} (x - \bar{x})^2 / (\delta x_i)^2 \right]. \qquad (81)$$

In other words, it is a sum of Gaussian forms, each representing the expected distribution of one event, but all centered at the same arbitrary value of x. It can be easily determined with program SUMX. In this case, the data used in the sum were the points within 25 MeV of 1115 MeV for one curve and within 30 MeV of 1190 MeV for the other. As one would expect, both curves have the same width. Normalization of these curves consists basically of normalizing to the observed number of events in the strips from which the data were taken, but it was necessary to use an iteration procedure because each curve has a tail extending under the peak of the other. The 8516 Λ events

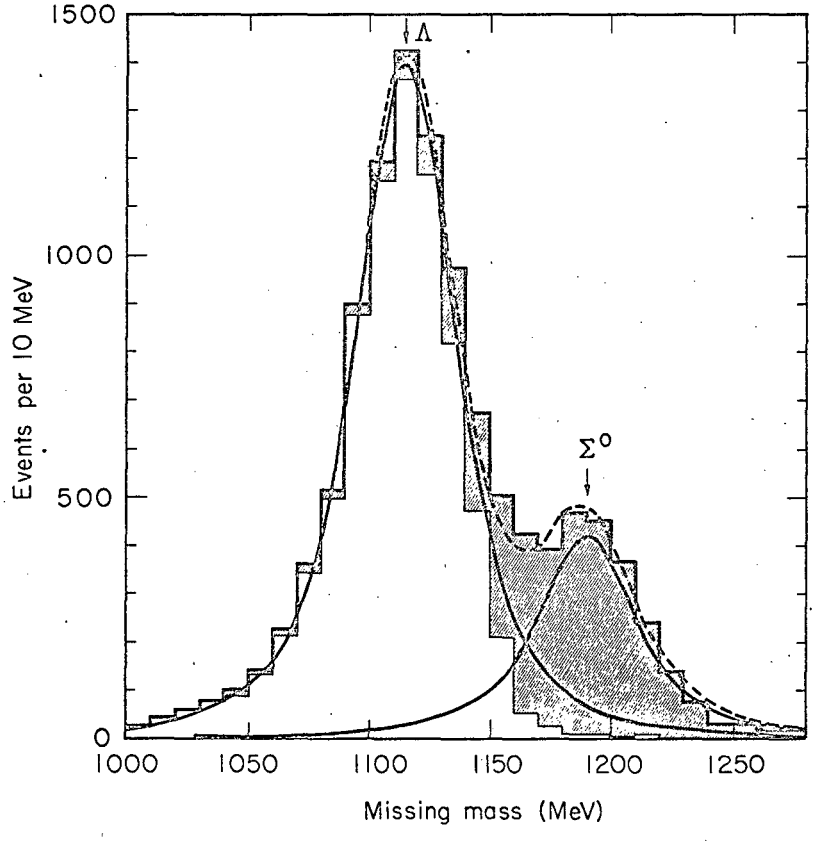

MU-34353

Fig. 5. Missing-mass spectrum of all neutrals in a sample of 11 285 events selected to fit either $K^-+p \rightarrow \Lambda+\pi^++\pi^-$, or $K^-+p \rightarrow \Sigma^0+\pi^++\pi^-$. All momentum settings, including those from a special low-energy study, are included. The two solid curves are normalized resolution-function curves for the events in the vicinity of the Λ peak and the Σ^0 peak, respectively. The dashed curve is the sum of the two solid curves. Shaded events are those eliminated by criterion (c) of Sec. III.D of the text.

and 2579 Σ^0 events under the respective curves represent all momentum settings.

From our earlier discussion on the distribution of chi squared, we suspect that the program-estimated error is too small. A scale factor was determined in this case by plotting the chi-squared distribution for a sample of events of reaction (1) on a special graph paper that has a nonlinear scale such that the theoretical distribution, formula (78), is a straight line with a 45° slope.[68] The observed distribution also approximated a straight line, but with a slope that was 1/1.62 that of the theoretical line. The scale factor used, then, was $(1.62)^{\frac{1}{2}}$. This factor is nearly the same as the ones $[(1.44)^{\frac{1}{2}}$ and $(1.52)^{\frac{1}{2}}]$ mentioned earlier and determined by more complicated procedures. This method of finding the scale factor is further justified by the fit of the curves to the histogram in Fig. 5.

The histogram was then separated into two parts by means of series of values of the quantity $L = \log_{10}[P(M_{\Lambda 2\pi})/P(M_{\Sigma^0 2\pi})]$. That is, a series of numbers X_i was selected and separate histograms were plotted for data with $L < X_i$ and $L > X_i$. In each case, these histograms were compared with the respective resolution-function curves on Fig. 5. From these comparisons, an estimate was made (a) for each X_i of the degree of separation of Λ's from Σ^0s, and (b) vice versa, and (c) of the number of good events lost from each hypothesis. Results of this study are graphed in Fig. 6. Recall that criterion (c) for separating reaction (1) from reaction (69) is equivalent to setting $X_i = 0$. The separation of events by this criterion is indicated by shading in Fig. 5. On Fig. 6(a), we see that this criterion eliminates essentially all of the Σ^0 events from the Λ events, but that about 13% of the Λ events are lost in the process.

A further check was made on this separation by generation of 1500 events of reaction (1) and 400 events of reaction (69) with the Monte Carlo event-generating program FAKE.[69] The events were generated at 1.61 BeV/c, and the conditions of the actual experiment were copied as well as possible. The same scale factor, $(1.62)^{\frac{1}{2}}$, used in the resolution function calculations was used to scale up all

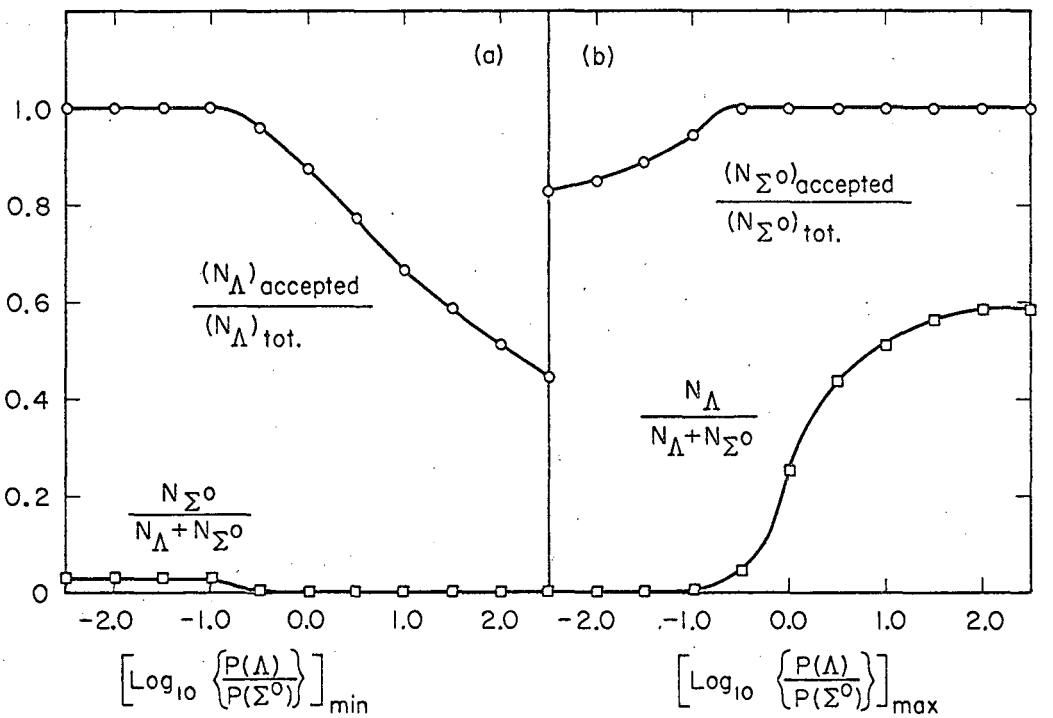

MU-34354

Fig. 6. Separation of events of the two reactions, $K^-+p \rightarrow \Lambda+\pi^++\pi^-$(i) and $K^-+p \rightarrow \Sigma^0+\pi^++\pi^-$ (ii), as a function of the limits placed on the ratio of confidence levels of the two fits. (a) Separation of Σ^0's from Λ's. The lower curve represents the fractional contamination [of reaction (ii)] contained in the sample which one obtains when one seeks reaction (i) by placing a lower limit on the logarithm of this ratio. The upper curve gives the fraction of events of the desired reaction (i) which survive this selection procedure. (b) Separation of Λ's from Σ^0's. The two curves give the corresponding fractions when the roles of the two reactions are reversed and an upper limit is placed on the logarithm. The optimum point of division is about -0.75 in this variable; a value of 0.0 was used in the actual separation.

errors, since FAKE uses the same error-estimating formulas as PANG does. Chi-squared distributions from the simulated events agreed very well with those from physical events. Reaction (1) was made to go entirely through $Y_1^{*+}\pi^-$ with the observed production-angle distribution; reaction (69) was generated isotropically.

Of the 1500 events of reaction (1) generated, 1429 made it successfully through the analysis system; 58 of the rejected events failed all hypotheses, and 13 of them encountered program difficulties, such as tape-reading errors. When the criteria for accepting events as reaction (1) were applied, 213 were eliminated as being more likely reaction (69), 8 were eliminated as being more likely reaction (70), and 36 (compared with expected 15) had a probability lower than 1 percent for all hypotheses. Remaining were 1192 events, or 83.5%, that passed the criteria.

Of the 400 events generated as reaction (69), 373 survived the analysis system, and only two of these events fulfilled the criteria to be accepted as reaction (1).

The conclusion is that we have succeeded in obtaining a clean sample of events of reaction (1), but have lost events in the process. A look at angular- and effective-mass distributions of the FAKE events that were rejected compared to the distributions of those that were accepted shows no sign of obvious bias introduced by this procedure.

E. Beam Momentum and Chi-Squared Distributions

Our sample of reaction (1) events is certainly quite pure and we feel that it is not badly biased. Let us proceed to examine these events and learn what we can.

The fitted beam-momentum distribution for all events in the sample, including those from the special low-momentum run, is histogrammed in Fig. 7. Beam averaging was used. The resolution function was plotted for this quantity at several places, with the same procedure described in the last section. The full width of this curve is about 30 MeV at all momenta, which is considerably narrower than

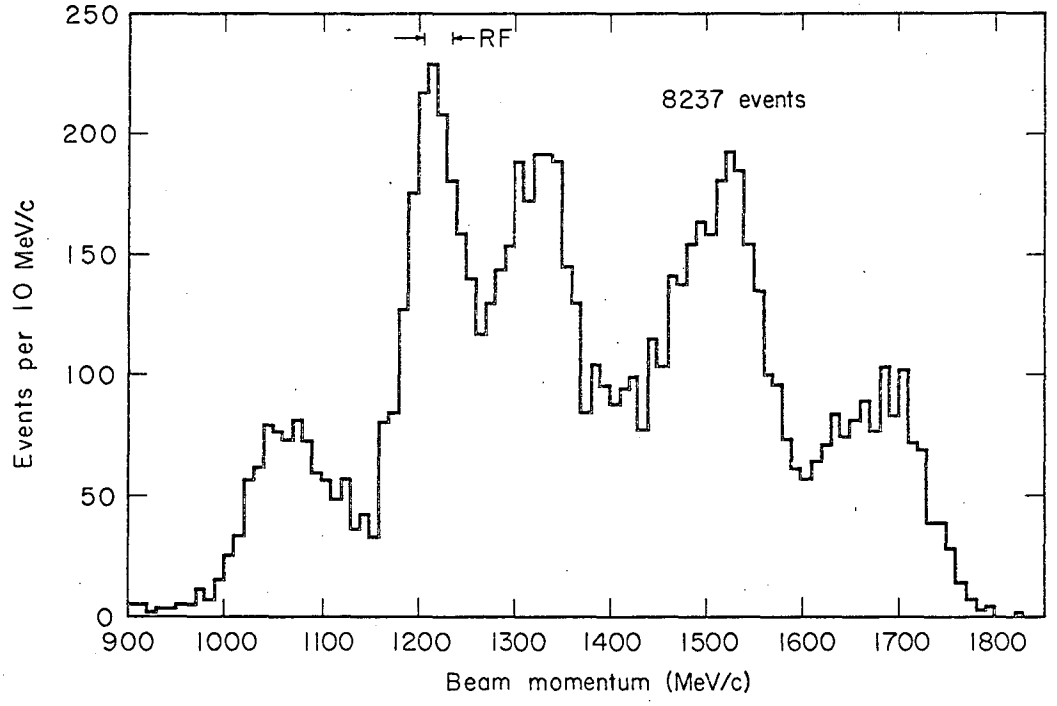

MU-34355

Fig. 7. Distribution of laboratory momentum of the K^--beam particles for the sample of events that fulfilled the criteria for the reaction $K^-+p \rightarrow \Lambda+\pi^++\pi^-$. All momentum settings, including those for the low-energy study, are included. The settings at 1.42 and 1.60 BeV/c had so few events that no resolved peaks show. The vertical marks labeled "RF" show the full width of the resolution function, which has about the same value throughout the sample.

that for the momentum-distribution curves for the separate momentum settings. Accordingly, it is possible to divide the sample into intervals by selecting on beam momentum without sacrificing information. The remainder of the analysis will divide the sample into 150 MeV/c intervals in beam momentum, 1.00-1.15 BeV/c, 1.15-1.30 BeV/c, 1.30-1.45 BeV/c, 1.45-1.60 BeV/c, and 1.60-1.75 BeV/c. Except for the first interval, which embraces the special low-momentum study and which is used here only in special circumstances, each interval contains 1000-2000 events, sufficient for reasonable statistical accuracy.

Before studying the effective-mass distributions, let us look at the chi-squared distributions. Figure 8(a) shows the lambda-decay distribution, a three-constraint fit, and Fig. 8(b) shows the production distribution, a four-constraint fit. The horizontal scale has been stretched by the scale factor of 1.62 determined above, and the data are then seen to fit the shape given by equation (78) quite well. The latter distribution is cut off at about 20 by criterion (b).

F. Effective-Mass Distributions

1. Dalitz Plots

Resonant states are usually detected by examination of the effective-mass distribution of groups of particles. For a three-body final state, as in this study, one would look at pairs of particles. The effective mass of a pair of particles, a Lorentz-invariant quantity, is

$$M_{12} = \left[(E_1 + E_2)^2 - (\vec{P}_1 + \vec{P}_2)^2 \right]^{\frac{1}{2}}, \qquad (82)$$

where E_i and $\vec{P}_i$ are the energy and momentum, respectively, of the ith particle. This quantity M_{12} is just the energy in their c.m. of the particle pair; if the particle resonate in the final state, as in relation (4), a peak in this quantity should occur at the resonant energy.

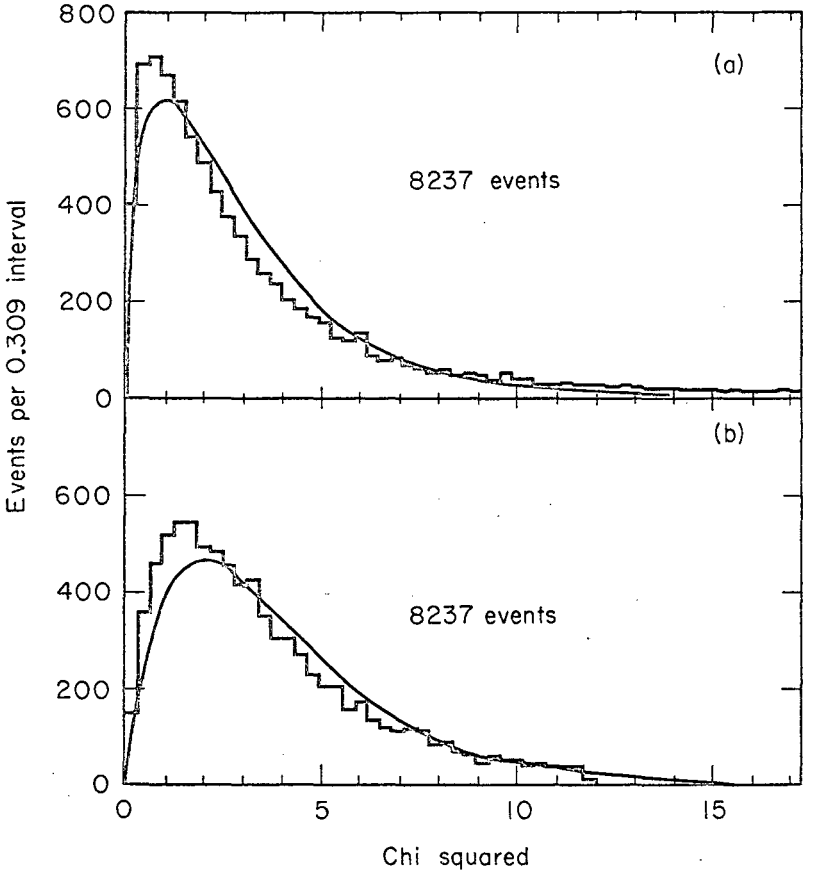

Fig. 8. Distribution of chi squared for the sample of events fitting $K^- + p \rightarrow \Lambda + \pi^+ + \pi^-$. In (a) is shown the distribution for the Λ decay, $\Lambda \rightarrow p + \pi^-$, a three-constraint fit; in (b) is shown the distribution for the production fit, a four-constraint fit. The solid curves show the distributions expected for the given number of events and constraints.

The classical method of analyzing three-body final states is to make a Dalitz plot. Gell-Mann and Rosenfeld[70] (Appendix C of their review article) showed that the element of Lorentz-invariant phase space is proportional to $dT_i\ dT_j$ for a three-body final state, where T_i and T_j are the kinetic energies of any two of the particles. It is easy to prove the relation

$$(M_{ij})^2 = (W - m_k)^2 - 2WT_k \tag{83}$$

where i, j, and k = 1, 2, and 3, respectively in any permutation; W is the total c.m. energy of the three-body system (constant for a given Dalitz plot); and m_k is the mass of the kth particle. Hence $d(M_{ij}^2)\ d(M_{ik}^2)$ is also proportional to an element of phase space, and has the further advantage that it is in units directly related to the energy of resonant states. The form of the Dalitz plot that we will use, then, is a two-dimensional scatter plot with the effective mass squared of the Λ-π^- along one axis and the effective mass squared of the Λ-π^+ along the other axis. Each event is represented by a point on this plot.

The kinematic limits for such a plot are given by those points in the given variables where the momenta of the three particles are collinear. Figure 9 shows the kinematic envelopes for a number of energies pertinent to this experiment. Because the two pions have the same mass, the envelopes are symmetric about a line at 45° to the coordinate axes. From the relation

$$\sum (M_{ij})^2 = W^2 + \sum m_k^2,$$

we see that this 45° line is also perpendicular to lines of constant effective mass squared of the π^+-π^- pair. Unfortunately, the zero of this latter quantity shifts with different values of W, so that pion-pion resonances will be spread out by the spread in c.m. energy. The bands where $Y_1^*(1385)$ is expected to give concentrations of points are also shown in this figure.

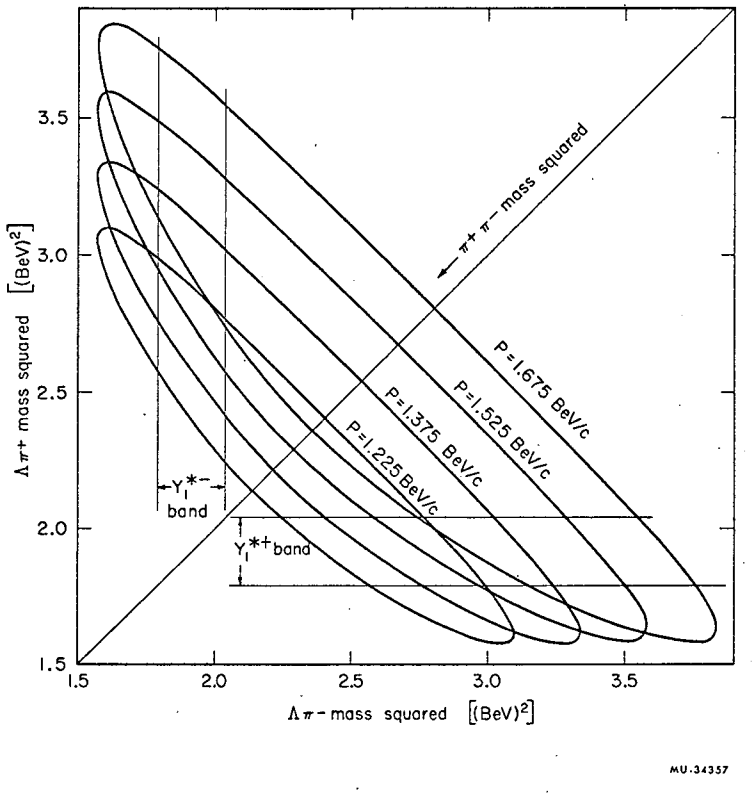

Fig. 9. Kinematic envelopes showing the limits on the effective mass squared of the Λ-π^+ pair and the Λ-π^- pair for the reaction $K^-+p \rightarrow \Lambda+\pi^++\pi^-$ at various laboratory momenta representative of this experiment. Each envelope is labeled with the corresponding momentum. The bands where concentration of events from the $Y_1^*(1385)$ resonance can be expected to be heavy are indicated; these bands correspond to Λ-π mass limits of 1340 and 1430 MeV.

Figure 10 shows Dalitz plots for four momentum intervals of 150 MeV/c each. These plots were made directly by the computer, using program SUMX, on its cathode-ray tube. The scale was changed on each one in order to make maximum use of the tube face. Envelopes for the maximum and minimum momentum are shown. The $Y_1^*(1385)$ resonance is a prominent feature of each of these plots, and no other features stand out clearly.

2. Lambda-Pion System

Figures 11 and 12 show the Λ-π^+ and Λ-π^- effective-mass distributions, respectively, for the four momentum intervals. Figures 13 and 14 show the same distributions with all momenta summed together. Again, the $Y_1^*(1385)$ is the only prominent feature on these projections of the Dalitz plot. The resolution function was plotted for events in the Y_1^* bands for each momentum interval, and was found to have a full width of about 7 MeV at all momenta.

The events in the momentum interval 1.15-1.30 BeV/c and the invariant-mass intervals 1340 MeV $< M_{\Lambda\pi} <$ 1430 MeV were selected for a study of the mass and width of the Y_1^*. It was felt that interference with background and with the opposite charge state of the Y_1^* should be a minimum at this energy (at lower energies the Y_1^* bands overlap, at higher energies other resonances appear). The program ATHOS was used to calculate the shape of an S-wave Breit-Wigner resonance (not a bad approximation since q = 208 MeV/c) distribution multiplied by three-body phase space for various values of the energy and width of the resonance. A small amount of nonresonant background was added incoherently, but the results were not sensitive to this addition. A chi-squared test was performed with each combination of mass and width values against the observed distributions. The confidence level for each test was plotted at the appropriate point on a mass-vs-width plot. Contour lines of constant confidence level were drawn through these points and the location of the point of maximum

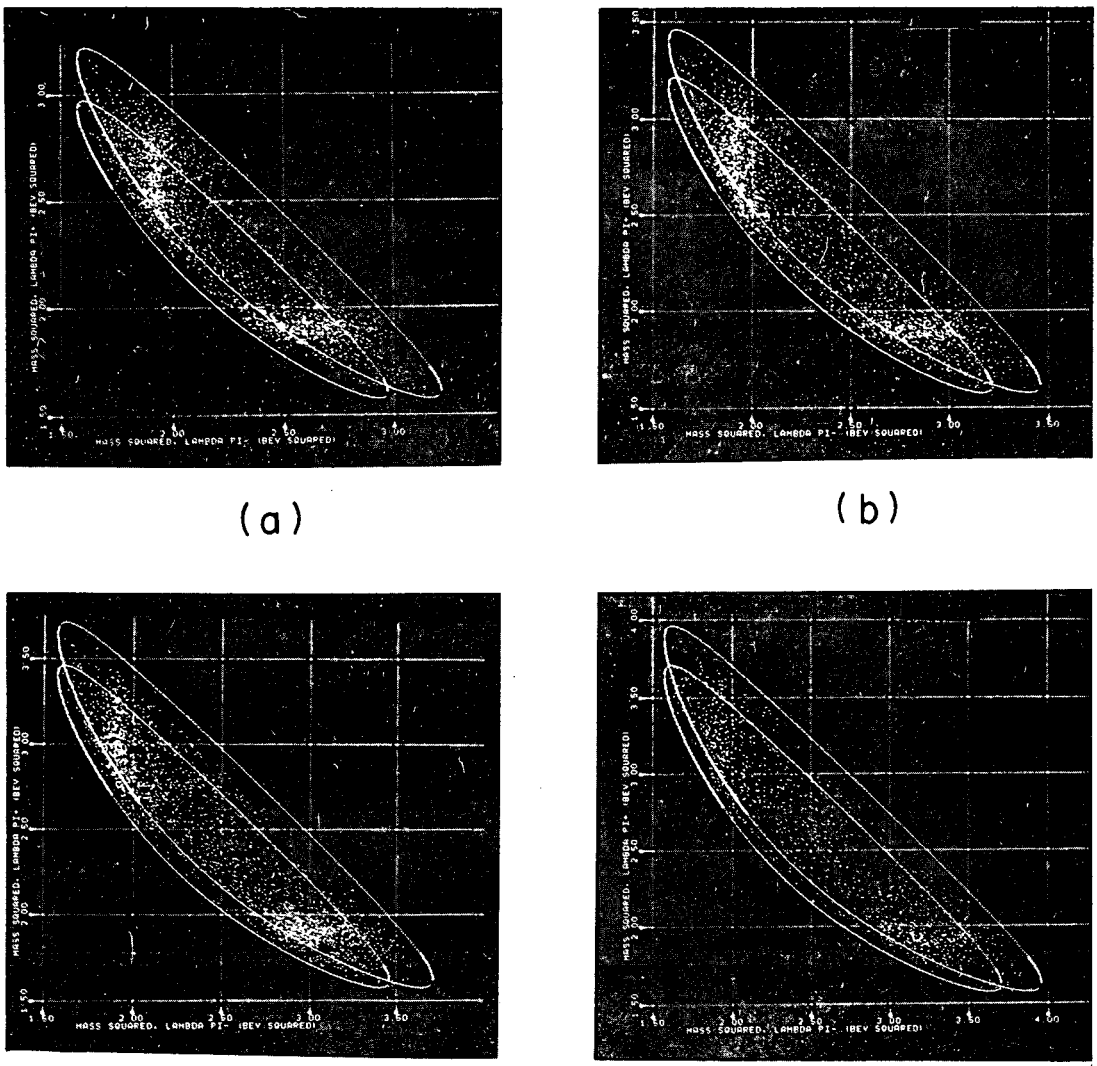

ZN-4357

Fig. 10. Dalitz plots for events from the reaction $K^- + p \rightarrow \Lambda + \pi^+ + \pi^-$ for the K^- laboratory-momentum intervals of (a) 1.15-1.30 BeV/c, (2130 events) (b) 1.30-1.45 BeV/c, (2054 events) (c) 1.45-1.60 BeV/c, (2046 events) and (d) 1.60-1.75 BeV/c (1070 events). Each dot represents one event. The kinematic envelopes for each plot are plotted for the minimum and maximum laboratory momentum in that sample. Scales on the four plots are different in order to make most efficient use of the face of the tube.

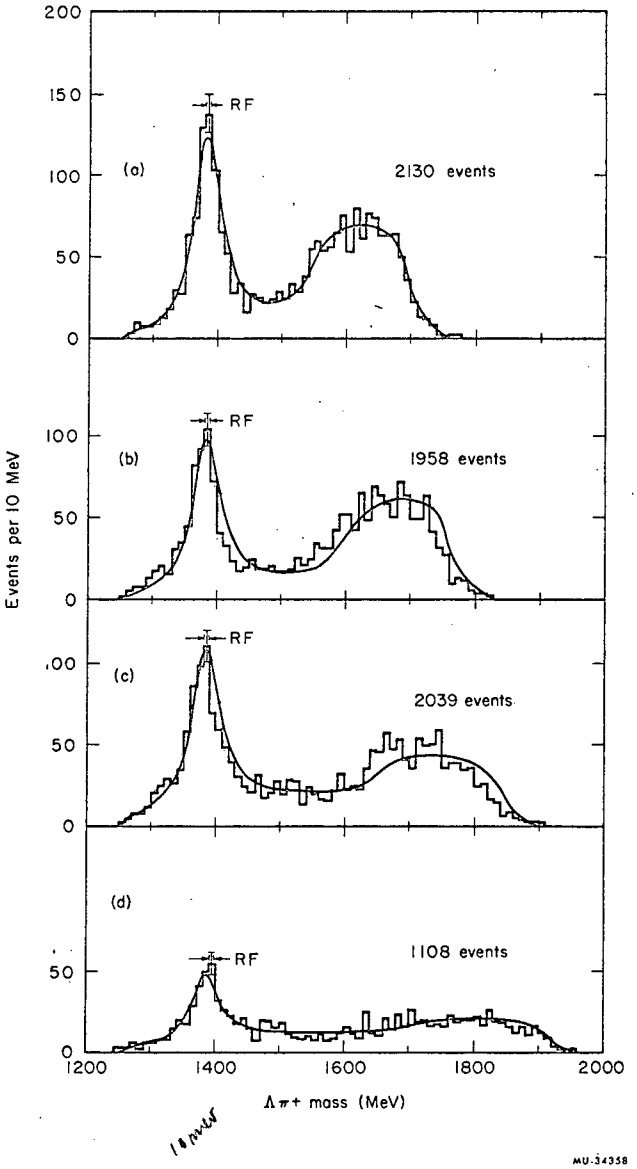

Fig. 11. Effective mass distribution of the Λ-π^+ pair from the reaction $K^-+p \rightarrow \Lambda+\pi^++\pi^-$ at (a) 1.15-1.30 BeV/c, (b) 1.30-1.45 BeV/c, (c) 1.45-1.60 BeV/c, and (d) 1.60-1.75 BeV/c. The sample of events was selected by the criteria described in the text. The spacing marks labeled "RF" give the FWHM of the resolution function for the events in the Y_1^* peak. The solid curve on each graph is the expected shape, projected on this axis, of phase space and Y_1^{*+}, Y_1^{*-}, and ρ^0 resonances weighted according to the populations given in Table IV.

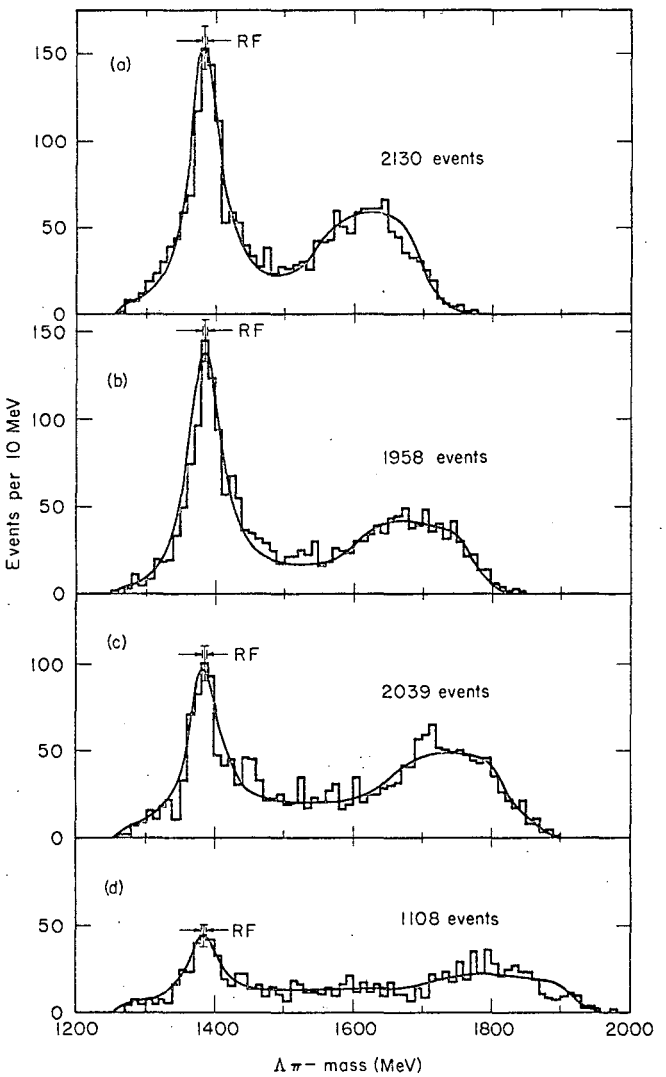

Fig. 12. Effect mass distribution of the Λ-π^- pair. Caption same as that for Fig. 11.

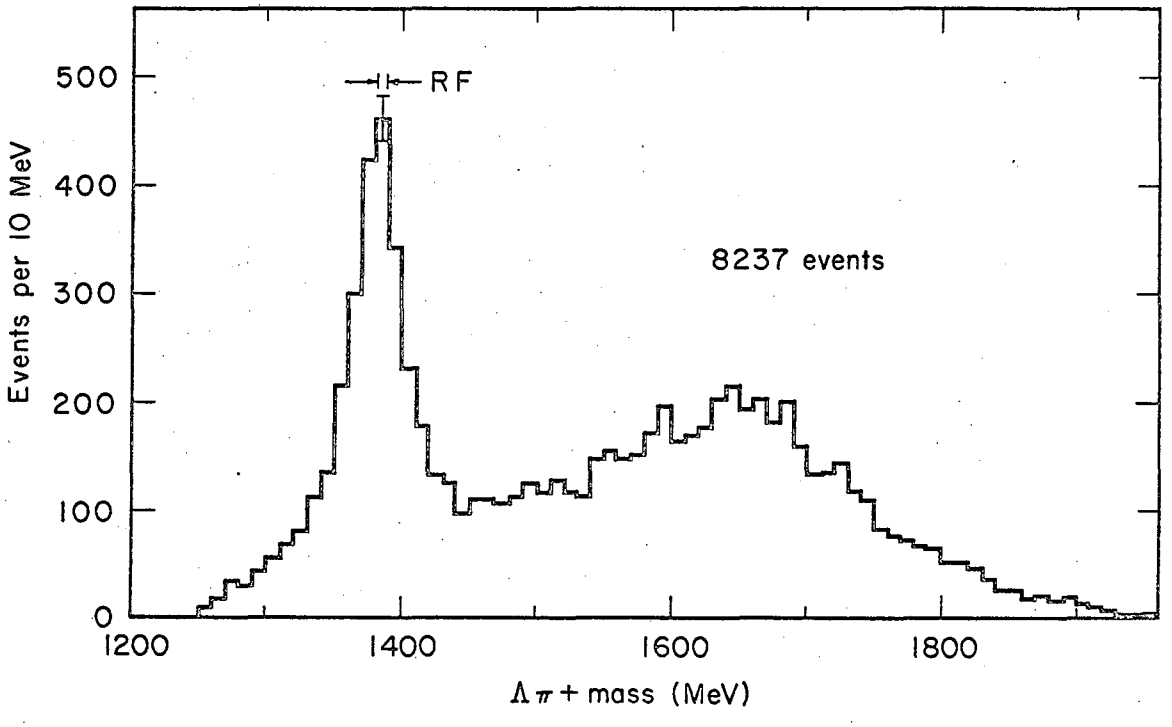

MU-34360

Fig. 13. Effective-mass distribution of the Λ-π^+ pair from the reaction $K^-+p \rightarrow \Lambda+\pi^++\pi^-$ for all momenta, including those from the special low-energy study, from 1.00-1.75 BeV/c. The sample of events was selected by the criteria described in the text. The spacing marks labeled "RF" give the FWHM of the resolution function for the events in the Y_1^* peak.

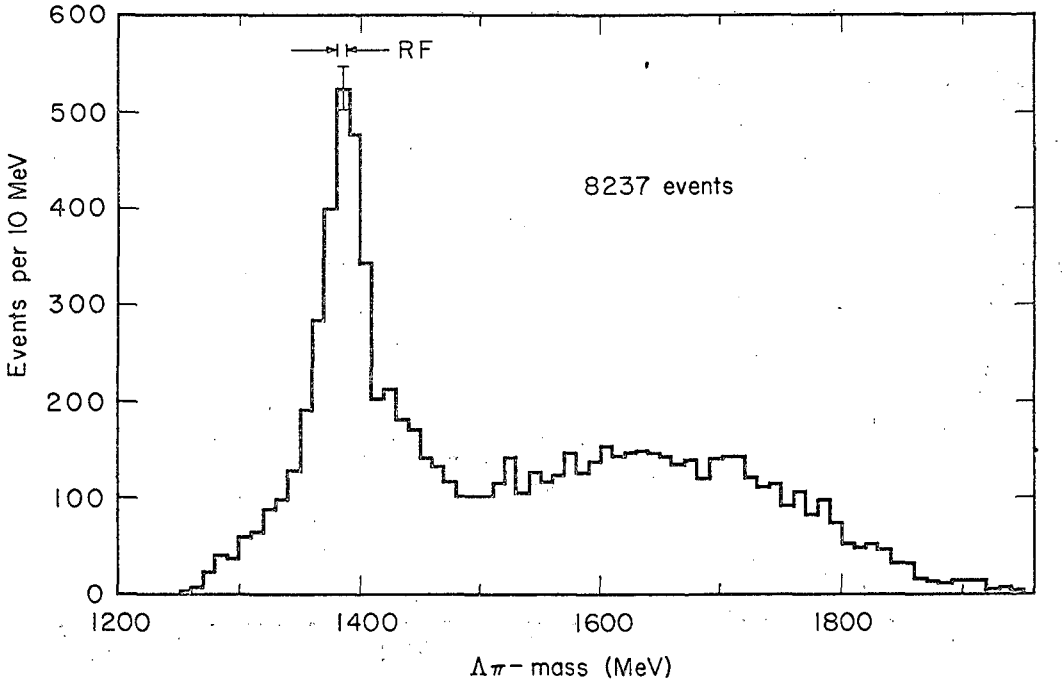

Fig. 14. Effective-mass distribution of the Λ-π^- pair. Caption same as that for Fig. 13.

confidence level was determined. This analysis gave

$$\begin{aligned} M(Y_1^{*+}) &= 1381.0 \pm 1.6 \text{ MeV}, \\ \Gamma(Y_1^{*+}) &= 46.5 \pm 3.0 \text{ MeV}, \end{aligned} \tag{84a}$$

and

$$\begin{aligned} M(Y_1^{*-}) &= 1385.3 \pm 1.5 \text{ MeV}, \\ \Gamma(Y_1^{*-}) &= 62.0 \pm 7.0 \text{ MeV}. \end{aligned} \tag{84b}$$

The $Y_1^{*-} - Y_1^{*+}$ mass difference is then 4.3 ± 2.2 MeV, compared with 17 ± 7 MeV reported elsewhere[71] and with 8.0 ± 0.4 for the $\Sigma^- - \Sigma^+$ mass difference. If the two samples of data are combined and the same analysis is performed, the values are

$$\begin{aligned} M(Y_1^{*}) &= 1383.5 \pm 1.6 \text{ MeV} \\ \Gamma(Y_1^{*}) &= 51.4 \pm 4.2 \text{ MeV}. \end{aligned} \tag{85}$$

The confidence-level map for this combined analysis is shown in Fig. 15. When treated separately, maps for the charge states have about the same shape, except that the center of the pattern is at a different point on the graph. The results of equation (85) should represent the average mass of the multiplet, and are in good agreement with the generally accepted values of $M = 1385$ MeV and $\Gamma = 50$ MeV.

The confidence level at the maximum point in the above maps is at about the 1% level, indicating some departure from the S-wave Breit-Wigner shape. One source of distortion is interference with background amplitudes. Another source arises from ignoring the energy dependence of the width. We show that this resonance is P wave or higher, so that the S-wave shape is only approximate, and deviations may occur even for a narrow resonance with $q = 205$ MeV/c. A formula is given by Gell-Mann and Watson for the shape of the $P_{3/3}$ N^*(or $\Delta\delta$) resonance.[72] More discussion of this energy behavior

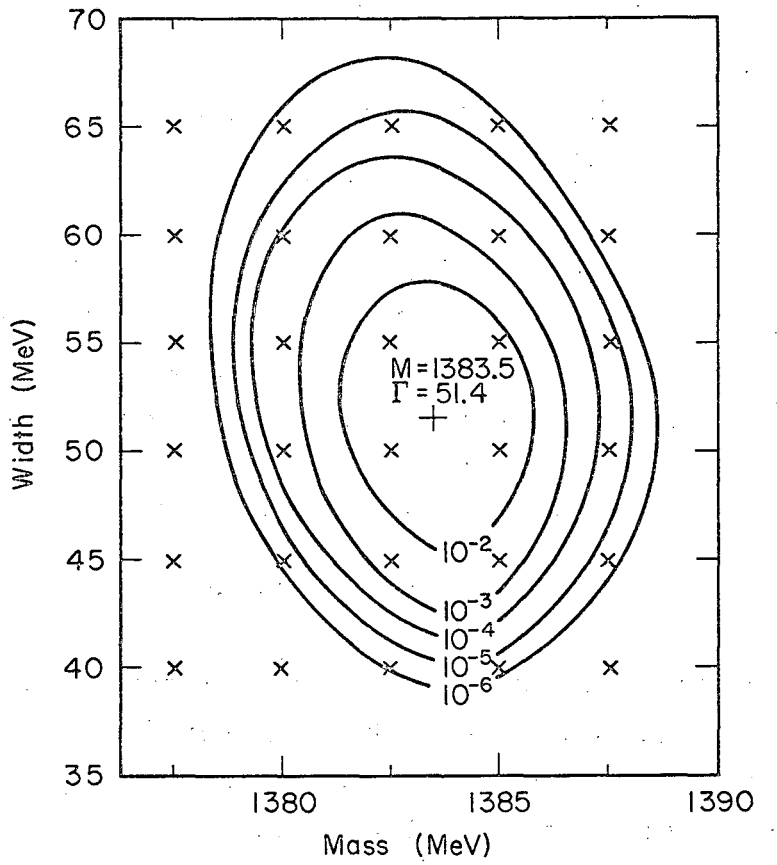

MU-34362

Fig. 15. Contour map of the confidence level of a fit of the combined Y_1^{*+} and Y_1^{*-} events to a simple Breit-Wigner resonance shape as a function of the mass and width parameters. The events are selected according to criteria described in the text. A small amount of background was assumed, but the map is insensitive to the amount of background. Chi-squared and confidence-level calculations were made at the points marked by crosses.

is given in Appendix D. If there is any appreciable coupling with $\bar{K}$-N, the shape can be affected near the $\bar{K}$-N threshold at 1430 MeV, as we pointed out in the section on the $\bar{K}$-N bound-state theory for the Y_1^*. From the discussion there, we probably can expect a cusp at this threshold and above that energy a general depletion of the high-energy tail as $\bar{K}$-N competes with Λ-π.

If we look at Figs. 11 through 14, we see that the Y_1^{*+} peak is slightly depleted on the high-energy side, whereas the Y_1^{*-} peak is considerably enhanced on the high-energy side, when compared to the simple Breit-Wigner shape. In the latter case, there may well be a break in the slope at the $\bar{K}N$ threshold. But unfortunately these effects could be solely the result of interference. The mechanisms operating in this experiment are not well enough understood to permit a more quantitative treatment.

Still, the S-wave Breit-Wigner shape does seem to be a reasonable zeroth-order approximation to the observed distribution, with the values from Eq. (85) for mass and width of the resonance used. A study was made to ascertain the approximate composition of the final state. The predominant resonances were assumed to be Y_1^{*+}, Y_1^{*-}, and ρ meson (these are justified in the next section). The effect of each of these resonances in each of the three channels was determined with the program ATHOS. A linear combination of these three shapes plus nonresonant phase space was assumed, and a minimum-chi-squared fit was made to the data in the vicinity of the resonance in each of the three channels. The restriction to the vicinity of the resonances was made because the "sideways" shape (reflection of resonance peak onto the axis of the nonresonating pair of particles on the Dalitz plot) of the resonance bumps is not predicted reliably (it is sensitive to the distribution of total energy and to anisotropy of decay angle), and because resonances of lesser significance are not taken into account. In the $\pi^+\pi^-$ channel, it was found necessary to exclude the Y_1^* bands in order to make the fit sensitive to the ρ^0 meson (this cutoff is covered in the next section). The coefficients

of the fit were then interpreted as giving the number of each final state produced. Table IV lists the results of this analysis, and the curves on Figs. 11 and 12 are based on these figures.

Another resonance, the $Y_1^*(1660)$, has previously been reported in part of this data.[10] It can be seen in Fig. 10(c) on the Dalitz plot for the interval 1.45-1.60 BeV/c, but its presence is not apparent at any other energy on the Dalitz plot. This resonance appears only in the positive-charge state in this experiment. In the projection, Fig. 11(c), it is ragged and difficult to identify because of the large, ragged background provided by the "sideways" projection of the $Y_1^{*-}(1385)$. If we make an "eyeball" estimate of the background in Fig. 13, we see an excess of 167±35 events in the region of this resonance for the complete momentum interval covered in this study. The error given is purely statistical. By contrast, the above analysis yields 2790±90 $Y_1^{*+}(1385)$ in the same sample (which includes the special low-momentum data).

Table IV. Composition of final state.

Momentum interval (BeV/c)	Number nonresonant	Number Y_1^{*+}	Number Y_1^{*-}	Number ρ^0
1.15-1.30	185±118	859±47	1086±49	0±51
1.30-1.45	42±129	665±41	1030±47	221±68
1.45-1.60	312±131	708±40	610±38	409±76
1.60-1.75	482± 86	280±38	268±26	78±49

3. Pion-Pion System

Figure 16 shows the π^+-π^- effective-mass spectrum for each of the four momentum intervals, and Fig. 17 shows the same spectrum for all data lumped together. The curves drawn through the data in Fig. 16 are those given by the analysis described in the previous section.

But a large background of Y_1^* events occurs in these distributions. The features of pion-pion interactions stand out much more clearly if the Y_1^* bands are eliminated from the sample. Accordingly, we selected a sample that included only those events that had $M_{\Lambda\pi^+} > 1430$ MeV and $M_{\Lambda\pi^-} > 1430$ MeV. The resultant portion of the kinematically allowed region on the Dalitz plot is an approximate trapezoid (see Fig. 9). In the analysis described in the previous section, this sample was used for the pion-pion channel, suitably normalized to allow for the reduced value of total phase space. In that analysis the ρ meson was assumed to have $M = 750$ MeV and $\Gamma = 100$ MeV, commonly accepted values.[73]

Figure 18 shows the π^+-π^- spectrum for this restricted sample, again with all energies lumped together. This time a mass-squared scale was used to take advantage of the rougly triangular shape expected for phase space in this mass-squared coordinate system. The dashed curve on this graph shows the phase space, plus the small amount of Y_1^* remaining outside the bands, which is given by the analysis of the previous section normalized to the reduced amount of total phase space. There are two regions where there is a significant excess of events above this curve, one near threshold and one in the vicinity of the ρ mass.

a. Low-mass enhancement

The excess near threshold might be the anomaly discovered by Abashian, Booth, and Crowe.[74,75] In a later paper, they established a good fit to the hypothesis that this anomaly is an $I = 0$, S-wave pion-pion interaction characterized by a scattering length.[76] Let us attempt to fit their solution to our data.

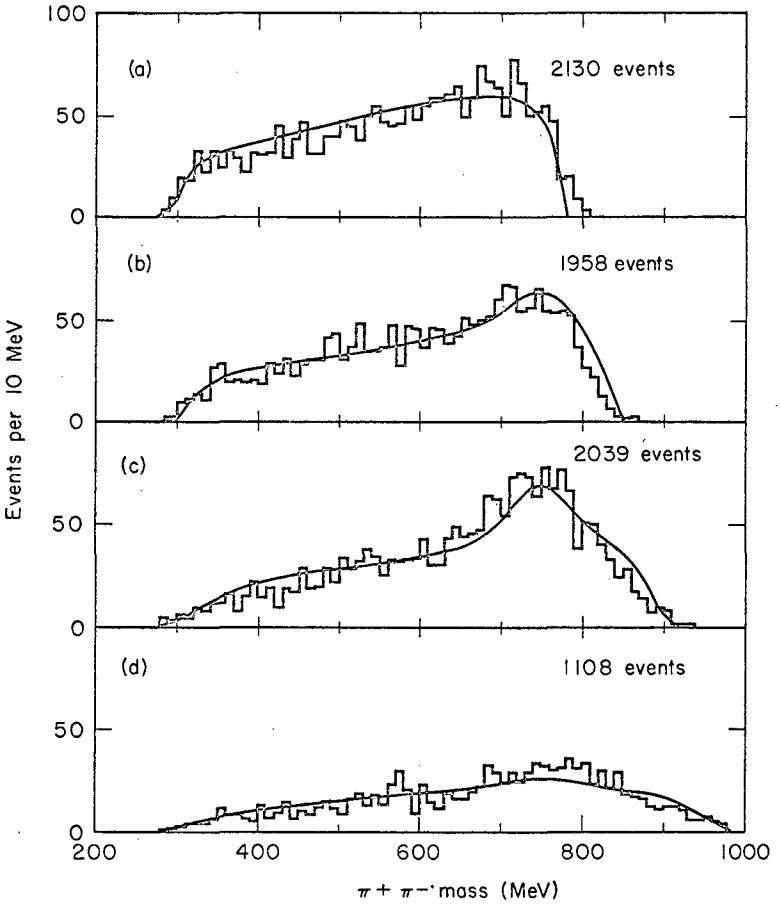

MU-34363

Fig. 16. Effective-mass distribution of the π^+-π^- pair from the reaction $K^-+p \rightarrow \Lambda+\pi^++\pi^-$ at (a) 1.15-1.30 BeV/c, (b) 1.30-1.45 BeV/c, (c) 1.45-1.60 BeV/c, and (d) 1.60-1.75 BeV/c. The sample of events was selected by the criteria described in the text. The solid curve on each graph is the sum of phase space and Breit-Wigner resonance shapes for Y_1^{*+}, Y_1^{*-}, and ρ^0, as projected on this axis, weighted according to the populations given in Table IV.

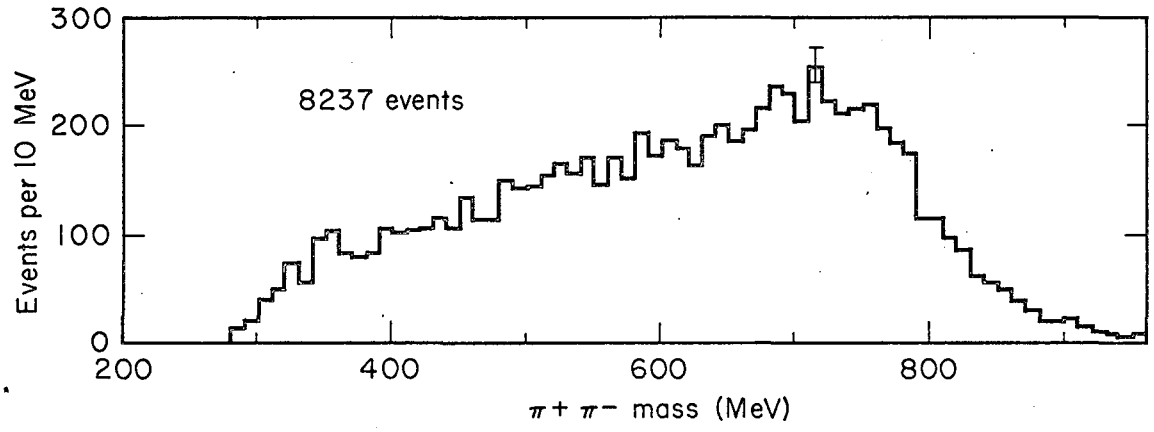

MU-34364

Fig. 17. Effective-mass distribution of the π^+-π^- pair from the reaction $K^-+p \rightarrow \Lambda+\pi^++\pi^-$ for all momenta, including those from the special low-energy study, from 1.00-1.75 BeV/c. The sample of events was selected by the criteria described in the text.

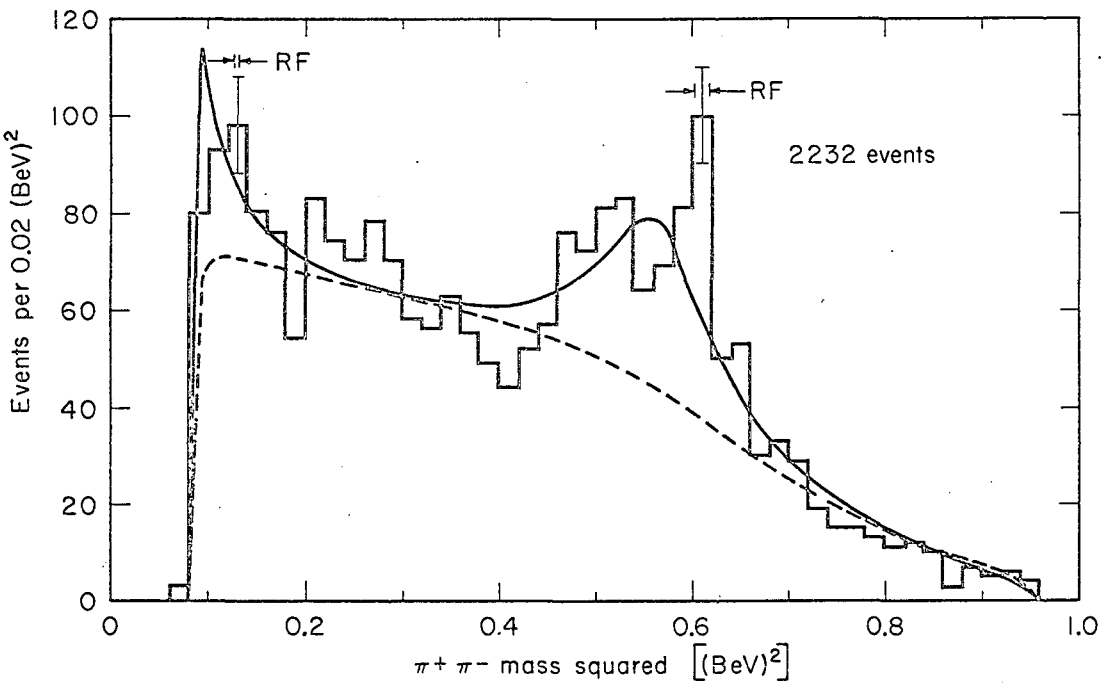

MU.34365

Fig. 18. Effective-mass-squared distribution of the π^+-π^- pair from the reaction $K^-+p \rightarrow \Lambda+\pi^++\pi^-$ at all momenta, including those of the special low-energy study, from 1.00-1.75 BeV/c. In addition to the general criteria described in the text, a restriction on the Λ-π masses was imposed. Events were chosen only if the effective mass of the Λ-π pair was greater than 1430 MeV for both charge states. The spacing marks labeled "RF" give the FWHM of the resolution function for the events in the vicinity of the marks. The dashed curve represents nonresonant phase space, plus some contribution from the Y_1^* states, weighted according to Table IV (with low-energy events added) with allowance for restriction of phase space by the limits imposed on the Λ-π masses. The solid curve is the sum of 74% of the dashed curve, 26% of S wave, I = 0 enhancement folded into phase space, and of a Breit-Wigner resonance shape, with M = 750 MeV and Γ = 100 MeV, for the total number of ρ° mesons given in Table IV.

They used a relativistic form of the zero-effective-range formula

$$\cot\delta = a^{-1}\left[(\nu+1)/\nu\right]^{\frac{1}{2}} + (2/\pi) \times \ln\left[(\nu)^{\frac{1}{2}} + (\nu+1)^{\frac{1}{2}}\right] \tag{86}$$

where $\nu = q^2/m^2$, q is the center-of-mass momentum, m is the pion mass, a is the scattering length, and δ is the phase shift. The enhancement is given by

$$F(\nu) = \left[(\nu+1)/\nu\right]\sin^2\delta \ . \tag{87}$$

There is an additional enhancement for a pair of I = 0, S-wave pions due to Bose statistics. The enhancement from this source is given by

$$B(\nu) = 1 + \exp\left[-(R/2.15)^2(4\nu)\right] \tag{88}$$

where R is the radius of the sphere of interaction. The best fit to their data was reported by the above authors to be a = 1.3 and R = 2.1, expressed in natural units based on the pion mass.

We do not know the proportion of I = 0 in our data. The enhancements (87) and (88) were first multiplied together and the product then multiplied by the phase space. A linear combination of this shape and phase space was constructed so that the area under the resultant curve matched the number of observed data to the left of $0.18\,(\text{BeV})^2$ on Fig. 18. A combination of 74% phase space and 26% I = 0, S-wave enhancement was found to yield this result. The solid curve on Fig. 18 shows the result of adding this enhancement and of including the amount of ρ^0 meson concluded in the previous section. This model certainly does fit the data better than phase space alone, but it does not agree in detail with the data. In particular, the enhancement peaks at a lower mass value than the observed events do. A narrow resonances at about 350 MeV would probably agree with the data better. The above authors included a form factor for the nucleus in the final state, but no form factor was used for the Λ in the present treatment. We cannot confirm or deny the presence of the enhancement.

b. Decay moade $\omega \to \pi^+\pi^-$

Turnitn to the ρ^0 peak, we find that it has somewhat the same "double-peaked" shape observed by Button et al. in proton-antiproton annihilations.[77] In that experiment, the two apparent peaks had about the same width and most likely arose from a statistical fluctuation in the shape of a single peak. In this experiment, on the other hand, the higher mass peak has a width comparable to the resolution at that energy and falls at 780 MeV, the mass of the ω meson as observed in the three-pion spectrum of reaction (70) in this experiment. According to our discussion in Sec. II. D, we can interpret this peak as the decay mode $\omega \to \pi^+\pi^-$, facilitated by electromagnetic mixing of the ρ^0 and ω mesons. An earlier report on this phenomenon was made on part of these same data.[12] (The experiment of Button et al. did not show this decay mode. In the reactions they studied--

$$\begin{aligned} &\bar{p} + p \to \pi^+ + \pi^- + \pi^+ + \pi^- \\ &\bar{p} + p \to \pi^+ + \pi^- + \pi^+ + \pi^- + \pi^0 \end{aligned} \tag{89}$$

only 100 ω mesons were observed in the latter reaction, so that the $\pi^+\pi^-$ decay mode would be seen in the former reaction above a large background only if the branching ratio were very large.)

Many other workers have reported evidence for this rare decay mode in other reactions. Some early papers were based on insufficient data and cannot be said to support the existence of the mode.[78, 79] Fickinger et al.[80] studied

$$\begin{aligned} &\pi^- + p \to n + \pi^+ + \pi^- \\ &\pi^- + p \to n + \pi^+ + \pi^- + \pi^0 . \end{aligned} \tag{90}$$

The second reaction could not be fit because there are two missing particles in the final state. A cutoff was imposed on the momentum transfer in the first reaction in order to eliminate much of the ρ^0 background. The ρ^0 is produced copiously by one-pion exchange in this reaction, but the ω meson cannot be so produced because of the

conservation of G parity. They assume that the second reaction accounts for all of the large-missing-mass events, and that it is all ω production; and they report 5 to 7% for the branching ratio $R_\omega = \Gamma(\omega \to \pi^+\pi^-)/\Gamma(\omega \to \pi^+\pi^-\pi^0)$.

Walker et al.[81] also looked at reaction (90) and deduced that $R \leq 15\%$. None of the experiments using reaction (90), however, are reliable because of the inability to fit $\omega \to 3\pi$ events.

Armenteros et al.[54] looked at

$$\begin{aligned} &\bar{p} + p \to K + K^- + \pi^+ + \pi^- \\ &\bar{p} + p \to K + K^- + \pi^+ + \pi^- + \pi^0 . \end{aligned} \tag{91}$$

They observed no peak where $\omega \to \pi^+\pi^-$ should show up and put an upper limit of 5% on R_ω.

In a later paper, Walker et al.[82] reported on many more events of reaction (90) plus some four prongs,

$$\begin{aligned} &\pi^- + p \to \pi^- + p + \pi^+ + \pi^- \\ &\pi^- + p \to \pi^- + p + \pi^+ + \pi^- + \pi^0 . \end{aligned} \tag{92}$$

They concluded that some of the contradictory results in earlier work, including our paper,[12] might be brought into agreement by considering the interference of ρ^0 and ω, discussed in Sec. II. D, since the ω has been shown to have a larger width than had been expected.[54] Their analysis takes into account only the number of events observed in the peak and not the detailed shape of the peak. This treatment represents about the best one can do when the resolution is about as wide as the peak is. Let us review the analysis of these authors and attempt to modify it to fit the conditions of this experiment. We write the total amplitude of $\pi^+\pi^-$ as

$$
\begin{aligned}
A_t &= A_\omega + A_\rho , \\
|A_\rho|^2 &= (dN_\rho/dm^*), \\
|A_\omega|^2 &= (dN_\rho/dm^*)_{max}\, \Gamma_\omega^{\,2}/4 \left[(m_\omega - m^*)^2 + \Gamma_\omega^{\,2}/4 \right]^{-1} , \\
|A_t|^2 &= |A_\omega|^2 + |A_\rho|^2 + 2|A_\omega||A_\rho|\cos(\theta_\omega - \theta_\rho), \\
\tan\theta_\omega &= \Gamma_\omega/2\ (m_\omega - m^*)^{-1} .
\end{aligned}
\tag{93}
$$

We now integrate over the range of m^*, assuming that quantities specific to the ρ^0 will remain constant over the small interval (< 20 MeV) in which quantities specific to the ω have any appreciable magnitude, getting an observed excess

$$
\begin{aligned}
\delta &= \int |A_t|^2 dm^* - \int |A_\rho|^2 dm^* \\
&= N_\omega + \left[2\pi \Gamma_\omega N_\omega (dN_\rho/dm^*) \right]^{\frac{1}{2}} \sin\theta_\rho
\end{aligned}
\tag{94}
$$

for the observed excess of events at the ω mass in the π^+-π^- spectrum. The term N_ω represents the number of pion pairs that would be seen if the ω were produced all by itself. The solution for N_ω is

$$
\begin{aligned}
N_\omega &= \delta + \pi \Gamma_\omega (dN_\rho/dm^*) \sin^2\theta_\rho \\
&\quad \mp \left[2\delta\pi \Gamma_\omega (dN_\rho/dm^*) \sin^2\theta_\rho \right. \\
&\quad \left. + \pi^2 \Gamma_\omega^{\,2} (dN_\rho/dm^*)^2 \sin^4\theta_\rho \right]^{\frac{1}{2}} .
\end{aligned}
\tag{95}
$$

In this formula, only the value of θ_ρ is not experimentally known, and the sign of the square root depends on the sign of θ_ρ so that there is no real ambiguity. Walker et al. chose to assume that $\sin\theta_\rho = 1$, i.e., complete interference between the ω and the ρ^0 at the peak of the ω resonance. They then varied Γ_ω and found that the value that gave agreement among the considered experiments agreed with the

directly measured value. This procedure seems unjustifiable, and we choose instead to use the measured value of Γ_ω and let θ_ρ vary over its possible range.

This experiment has a considerable nonresonant background, compared to the π^--p experiments, but it seems reasonable to assume that the phase of this background will be random compared to that of the ω and the ρ^0 over the large range of energy interval of this experiment. On the other hand, if the production mechanisms of the ρ^0 and of the ω are similar (K and K^* exchange, say), we might expect a net interference between the two mesons over the experiment.

From Fig. 18, assuming the ρ^0 intensity is given by the solid curve, we have $\delta = 42 \pm 10$ events, and $\pi(dN_\rho/dm^*) = 6.06$ events/MeV. The number N_ω, which is calculated from (95), must still be corrected, because (a) the limits imposed on the Λ-π^+ mass and the Λ-π^- mass restrict the available phase space for the observation of $\omega \to \pi^+ \pi^-$, and (b) alignment of the ω may make the density in the observed portion of phase space different from the average density over all phase space. The first effect is purely kinematical and can be computed exactly for each c.m. energy. The second effect can be inferred from the observed alignment of the three-pion decay mode observed in suitably chosen events of reaction (70) of the same sample of type-32 events. If the ω had zero width, the alignment would be the same for all decay modes; we assume that any distortion caused by interference with the ρ^0 is small, at least compared with the uncertainty in θ_ρ. The overall correction factor, weighted over various momentum intervals by the number of $\omega \to 3\pi$ in these intervals, is 1.74. Finally, for the denominator, 2831 events of the form

$$K^- + p \to \Lambda + \omega, \qquad \omega \to \pi^+ + \pi^- + \pi^0 \tag{96}$$

were found in the same sample of type-32 events.

Table V shows a series of values for the branching ratio for various values of θ_ρ, calculated according to the above discussion and with the experimental value of Γ_ω.[54] The range in θ_ρ represented there gives the total range of R_ω allowed, so that we can place limits on the branching ratio:

$$(0.6 \pm 0.2)\% \leq \frac{\Gamma(\omega \to \pi^+ \pi^-)}{\Gamma(\omega \to \pi^+ \pi^- \pi^0)} \leq (11.3 \pm 1.0)\% . \qquad (97)$$

The upper limit is of little value, but the lower limit establishes that this decay mode does have a nonvanishing branching ratio. The work of Armenteros et al.[54] sets a valid upper limit, since the ρ^0 does not seem to be produced in reaction (91) and interference is thus no problem. One can say that this number lies between 0.6 and 5% without reference to the π^--p experiments with their problem of intense ρ^0 background and unfittable hypotheses. The fact that the previously reported "zero-interference" branching ratio from the 1.51 BeV/c data alone[12] is larger than the corresponding value found here with all the data indicates more constructive interference at 1.51 BeV/c than the net value for all momenta. Our lower limit also agrees with an upper limit from a compilation over all available data.[83]

There is no evidence in this experiment for the I = 1 resonance reported to be at 575 MeV.[84,85]

Table V. The branching ratio, $\frac{\Gamma(\omega \to \pi^+ \pi^-)}{\Gamma(\omega \to \pi^+ \pi^- \pi^0)}$.

θ_ρ (deg)	Branching ratio
90°	0.0058 ± 0.0023
60°	0.0070 ± 0.0026
30°	0.0117 ± 0.0038
0°	0.0258 ± 0.0062
-30°	0.0568 ± 0.0085
-60°	0.0950 ± 0.0097
-90°	0.1130 ± 0.0100

G. Y_1^* Angular Distributions and Correlations

We established above that a large fraction of reaction (1) proceeds through the two-step process, $K^- + p \rightarrow Y_1^{*\pm} + \pi^{\mp}$, $Y_1^{*\pm} \rightarrow \Lambda + \pi^{\pm}$. Angular distributions and correlations of the Y_1^* and its decay products can reveal details of the structure of this resonance and the mechanism of its production. We regard as Y_1^* those events having 1340 MeV $< M_{\Lambda\pi} <$ 1430 MeV.

1. Lorentz Transformations

Many of the particles involved in each event have relativistic velocities. Proper treatment of the angular distributions then requires that the full Lorentz group be considered, velocity transformations[86] as well as rotations. Fortunately, Stapp has shown that proper choice of velocity transformations performed on the experimental data and proper selection of the coordinate system in which each momentum direction is measured enables one to use the more familiar nonrelativistic representations of the quantum mechanical operators.[87] Figure 19 illustrates how this process is carried out in this experiment.

The initial measurements are made in a coordinate system having a fixed relation to the fiducial marks on the top glass of the bubble chamber. This coordinate system is given a rotation that brings its x axis into the direction of the K^- at the point of interaction; it is given a velocity transformation, along this new x axis, that takes it into the K^--p center of mass; then the inverse rotation is applied. Measurements on the K^- direction, the Y_1^* direction, and the normal to the plane of these two vectors,

$$\hat{n} = (\vec{K}^- \times \vec{Y}_1^*)/|\vec{K}^- \times \vec{Y}_1^*|, \qquad (98)$$

are referred to this system. That is, the three coordinates of each of these vectors as seen in this coordinate system are recorded.

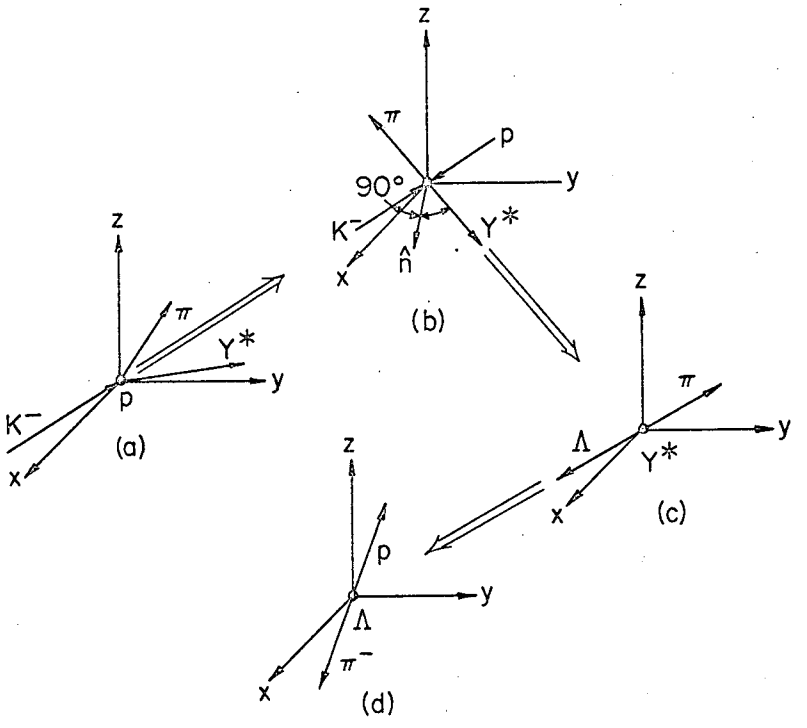

MU-34385

Fig. 19. Diagram of the successive Lorentz transformations performed in order to study the chain of interactions, $K^- + p \rightarrow Y_1^* + \pi$, $Y_1^* \rightarrow \Lambda + \pi$, $\Lambda \rightarrow p + \pi^-$. (a) Laboratory coordinate system. (b) Is obtained from (a) by transformation along the K^- direction into the K^--p center of mass; (c) is obtained from (b) by transformation along the Y_1^* direction into the Y_1^* rest system; and (d) is obtained from (c) by transformation along the Λ direction into the Λ rest frame. In each case the transformation is the "direct Lorentz transformation" described in the text.

The coordinate system is then rotated so that the x axis lies along the Y_1^* direction, a velocity transformation that takes it into the Y_1^* center of mass is applied, and the inverse rotation is performed. The three coordinates of the Λ direction in this coordinate system are recorded. In the same manner, by rotation of the x axis to the Λ direction, velocity transformation to the Λ center of mass, and inverse rotation, the coordinate system is found in which to record the three components of the proton direction from the Λ decay. Note that in each case the direction of the relative velocity between the two frames has the same direction cosines with respect to the coordinate axes in the new frame as it had with respect to those in the old frame. Stapp calls this transformation a "direct Lorentz transformation."

When this chain of transformations is completed, each vector of interest has three coordinates assigned to it in a particular coordinates assigned to it in a particular coordinate system. Now if these three numbers are assumed to be the components of this vector in some unphysical coordinate system, all vectors being assigned to this same unphysical frame, the physics of these vectors in this frame is given, according to Stapp, by nonrelativistic formulae. This prescription is intuitively plausible. Each vector is obtained in a rest frame where its description can be given nonrelativistically, and the transformations are done in a way that avoids introducing rotations through the velocity transformations.

In the remainder of this report, when dot products of vectors and similar operations are mentioned, it is always done in the manner described above.

2. Y_1^* Decay Angle

The natural variable in the decay of the Y_1^* is the angle between the Λ and the Y_1^* directions. Figure 20 shows the histogram of the cosine of this angle for each charge state and for each momentum interval. Events are used that have 1340 MeV $< M_{\Lambda\pi} <$ 1430 MeV for the given charge state. It is well known that if parity is conserved in the decay process and if there are no interferences between particles in the final state, this distribution must be symmetric about 90°.

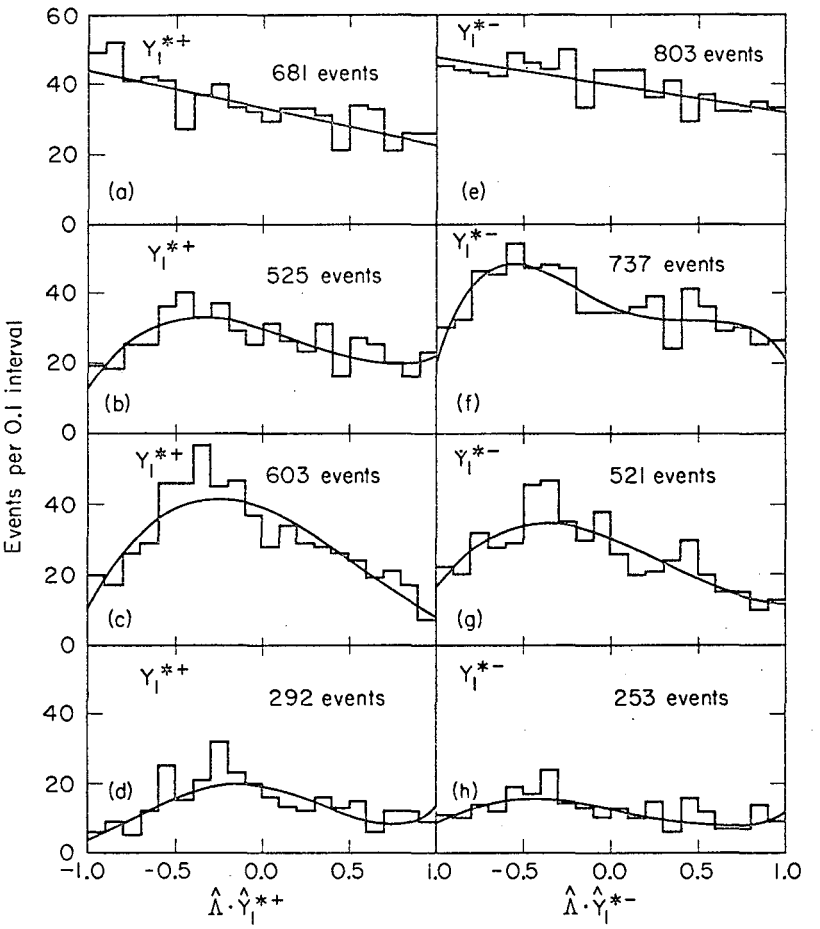

Fig. 20. Distribution of the cosine of the decay angle of the Y_1^* relative to its line of flight at (a) 1.15-1.30 BeV/c, (b) 1.30-1.45 BeV/c, (c) 1.45-1.60 BeV/c, and (d) 1.60-1.75 BeV/c for the Y_1^{*+}; and at (e) 1.15-1.30 BeV/c, (f) 1.30-1.45 BeV/c, (g) 1.45-1.60 BeV/c, and (h) 1.60-1.75 BeV/c for the Y_1^{*-}. Criteria for selection of events are explained in the text. The solid curves are best fits to the series, $1 + A_1(\hat{\Lambda}\cdot\hat{Y}_1^*) + A_2(\hat{\Lambda}\cdot\hat{Y}_1^*)^2 + A_3(\hat{\Lambda}\cdot\hat{Y}_1^*)^3 + A_4(\hat{\Lambda}\cdot\hat{Y}_1^*)^4$, the coefficients of which are listed in Table VI.

It is evident by inspection that the distribution is not symmetric in the cases considered here. The coefficients of a fit to a power series are listed in Table VI, along with some corresponding information from other experiments at lower energies. Since we have already seen other evidence of interference in the final state, such interference seems the likely explanation of the observed asymmetry. Note that the asymmetry has decreased from its value at lower momenta, but that higher terms in the power series become important at higher energies. The latter effect is likely due to more resonances, namely the ρ^0 and the $Y_1^*(1660)$, in the final state.

3. Y_1^* Production-Angle Distribution

When we discussed the spin-space density matrix in Sec. II.C, we found that there are in general $(2J+1)^2$ parameters that give the configuration of the final state if the resonance has spin J and can be considered to decay as an isolated particle. Simplication is gained by using the normal to the production plane as the axis of quantization, the number of parameters then being $\frac{1}{2}(2J+1)^2$. At a certain c.m. energy, these parameters are functions of the production angle alone. In principle, from knowledge of the distribution of each of these parameters with production angle, the partial waves participating in the production could be ascertained, and the relative amplitude of each of them could be determined. For spin $J > \frac{1}{2}$ such a procedure is quite complicated. Since the philosophy of this paper is to concentrate on the final state, no serious attempt at a partial-wave analysis was made.

Figure 21 shows the histograms of the production-angle distribution, which is just the distribution of the parameter t_0^0 in the language of Sec. II. C. Events used have 1340 MeV $< M_{\Lambda\pi} <$ 1430 MeV for the given charge state. Distribution of some of the other parameters was also looked at, but none showed startling behavior. In particular, the value of t_1^0, or the polarization, is consistent with zero at all production angles and all energies. These distributions were fit to power series in the cosine of the production angle. Details of acceptable fits are given in Table VII, and the corresponding curves are drawn on Fig. 21.

Table VI. Y_1^* decay coefficients fit to a power series.[a]

Lab momentum (BeV/c)	A_1	A_2	A_3	A_4
		Y_1^{*+}		
0.76[b]	-0.24± 0.20			
0.85[b]	-0.92± 0.26			
1.15[b]	-0.70± 0.26			
1.15-1.30	-0.32± 0.07			
1.30-1.45	-0.52± 0.17	-0.41± 0.12	0.67± 0.25	
1.45-1.60	-0.50± 0.13	-0.76± 0.09	0.47± 0.18	
1.60-1.75	-0.42± 0.18	-0.47± 0.47	0.66± 0.26	0.90± 0.50
		Y_1^{*-}		
0.76[b]	-0.16± 0.20			
0.85[b]	-0.24± 0.24			
1.15[b]	-0.02± 0.20			
1.15-1.30	-0.20± 0.06			
1.30-1.45	-0.60± 0.17	0.69± 0.45	0.60± 0.24	-1.12± 0.49
1.45-1.60	-0.65± 0.16	-0.55± 0.11	0.59± 0.23	
1.60-1.75	-0.75± 0.27	-0.23± 0.19	0.87± 0.40	

[a] From fit to $\sum_k A_k (\hat{\Lambda} \cdot \hat{Y}_1^*)^k$, normalized so that $A_0 = 1$.

[b] From reference 3.

Table VII. Y_1^* production-angle distributions.[a]

Lab momentum (BeV/c)	Fit to production-angle distribution
	Y_1^{*+}
1.15-1.30	$(148\pm 18) - (330\pm 56)x + (1164\pm 147)x^2 + (386\pm 86)x^3 - (1009\pm 173)x^4$
1.30-1.45	$(130\pm 17) - (208\pm 48)x + (668\pm 129)x^2 + (159\pm 76)x^3 - (489\pm 153)x^4$
1.45-1.60	No satisfactory fit at or below 10th order.
1.60-1.75	$(192\pm 20) - (409\pm 60)x - (734\pm 217)x^2 + (1137\pm 245)x^3 + (1748\pm 610)x^4 - (839\pm 222)x^5 - (1104\pm 454)x^6$
	Y_1^{*-}
1.15-1.30	$(275\pm 23) - (317\pm 61)x + (707\pm 163)x^2 + (152\pm 93)x^3 - (588\pm 186)x^4$
1.30-1.45	$(242\pm 25) - (130\pm 95)x - (46\pm 353)x^2 - (261\pm 419)x^3 + (2107\pm 1053)x^4 + (280\pm 385)x^5 - (1999\pm 798)x^6$
1.45-1.60	$(152\pm 20) - (120\pm 77)x - (196\pm 287)x^2 - (24\pm 351)x^3 + (2405\pm 877)x^4 - (38\pm 328)x^5 - (2176\pm 673)x^6$
1.60-1.75	No satisfactory fit at or below 10th order.

[a] For convenience, $x \equiv (\hat{Y}_1^* \cdot \hat{K}^-)$. Normalized so that $\int_{-1}^{1} f(x)dx = N$.

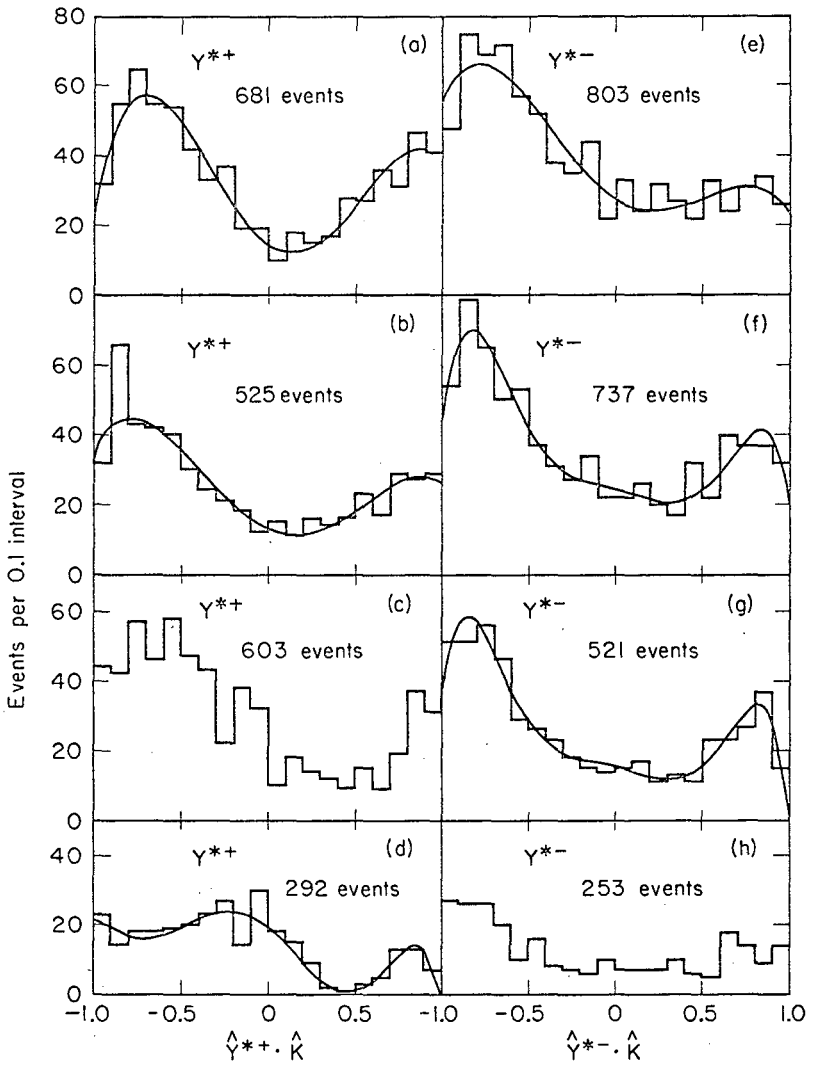

Fig. 21. Distribution of the cosine of the production angle of the Y_1^* relative to the incoming K^- momentum direction at (a) 1.15-1.30 BeV/c, (b) 1.30-1.45 BeV/c, (c) 1.45-1.60 BeV/c, and (d) 1.60-1.75 BeV/c for the Y_1^{*+}; and at (e) 1.15-1.30 BeV/c, (f) 1.30-1.45 BeV/c, (g) 1.45-1.60 BeV/c, and (h) 1.60-1.75 BeV/c for the Y_1^{*-}. Criteria for selection are explained in the text. The solid curves are best fits to the power series $\Sigma_i A_i(\hat{Y}_1^* \cdot \hat{K}^-)^i$, the coefficients of which are given in Table VIII.

The form of the curves fitting the data seems to change little at lab momenta up to 1.45 BeV/c(c. m. energy = 2 BeV) compared to that found by Ely et al. at 1.11 BeV/c.[5] Qualitatively, there is a large backward peak, a small forward peak, and a dip in the extreme backward direction. Distribution of some of the other moments confirms this picture; nothing is changing very fast in the production mechanism over this energy range. Above 1.45 BeV/c, the curves do change character, but increased background at the higher energies may be partly responsible for this effect.

No correction has been made to these data for events where the Λ escapes from the chamber or for events where the Λ is too short to be recognized as a vee. Some investigation of the order of magnitude of these biases showed that the corrections would be too small to substantially change the qualitative conclusions discussed above.

4. Adair Distribution

This distribution is discussed theoretically in Sec. II. C. 4. Attempts to use it on Y_1^* have not been successful, generally because the small number of events that fit the criteria for use in this distribution renders the results statistically insignificant. In the analysis by Dalitz and Miller, in which interference between the charge states and Bose statistics were taken into account, the result was still ambiguous.[15] Block et al.[88] studied the reaction

$$K^- + {}^4\mathrm{He} \rightarrow \Lambda + \pi^- + {}^3\mathrm{He} \qquad (99)$$

when the K^- stopped in the liquid helium chamber. Using the conclusions of Day and Snow,[89] they argued that K^- is captured in ^{4}He in an S wave. Since ^{4}He has spin 0 and ^{3}He has spin $\frac{1}{2}$, the Adair argument can be applied to all production angles. From 30 events, they concluded that $J = \frac{1}{2}$ for the Y_1^*. However, a later report on the same reaction, but with 146 events, described results ambiguous between $J = \frac{1}{2}$ and $J = 3/2$ but favoring the latter.[90] Coffin et al.[91] studied

$$\pi^- + p \rightarrow \Lambda + K^0 + \pi^0 \qquad (100)$$

in a spark chamber at 1.5 BeV/c. Preliminary results obtained with the Adair distribution (accepting $0.4 < |Y_1^* \cdot \pi^-| < 1.0$) gave strong evidence for $J = \frac{1}{2}$, but a later analysis assuming S and P waves in the production favors $J = 3/2$.[92]

In this experiment, it is evident from the production-angle distributions that higher partial waves are present, very likely D or F waves. An extreme cutoff in production angle is apt to be necessary in order to insure validity of the distribution. However, it is legitimate to lump together data from a wide range of energy since the prediction of the Adair distribution is unique and additive, whereas contributions from interference with the background will tend to cancel because of random phases. Accordingly, data from 1.00-1.45 BeV/c (including data from special low-energy study) were used; the background problem is considered too severe for momenta above 1.45 BeV/c. Both charge states of the Y_1^* were lumped together. In this manner, we found 171 events that fit the criterion $|Y_1^* \cdot K^-| > 0.95$ as well as $1340 \text{ MeV} < M_{\Lambda\pi} < 1430 \text{ MeV}$ for either charge state. This distribution is shown in Fig. 22. The curves represent the predictions of the Adair distribution, listed in Table II. The symmetry of the distribution suggests that interference terms have indeed tended to cancel each other. But it is evident that the data do not favor uniquely any one of the theoretical curves.

From the theoretical discussion, we reasoned that the coefficients of a power-series fit would approach the values predicted by the Adair distribution linearly as the cutoff approaches 1.0. To study this effect, the data for various values of the cutoff were fitted to a curve of the form $N(1 + a \cos^2\eta)$, where η is the Adair angle. The values of a from these fits are depicted graphically in Fig. 23. It is evident that the coefficient a does increase in a linear fashion for cutoff values larger than 0.9. But is is difficult to extrapolate the error because the errors are highly correlated, the data for each point also being contained in that for every point to the left of it.

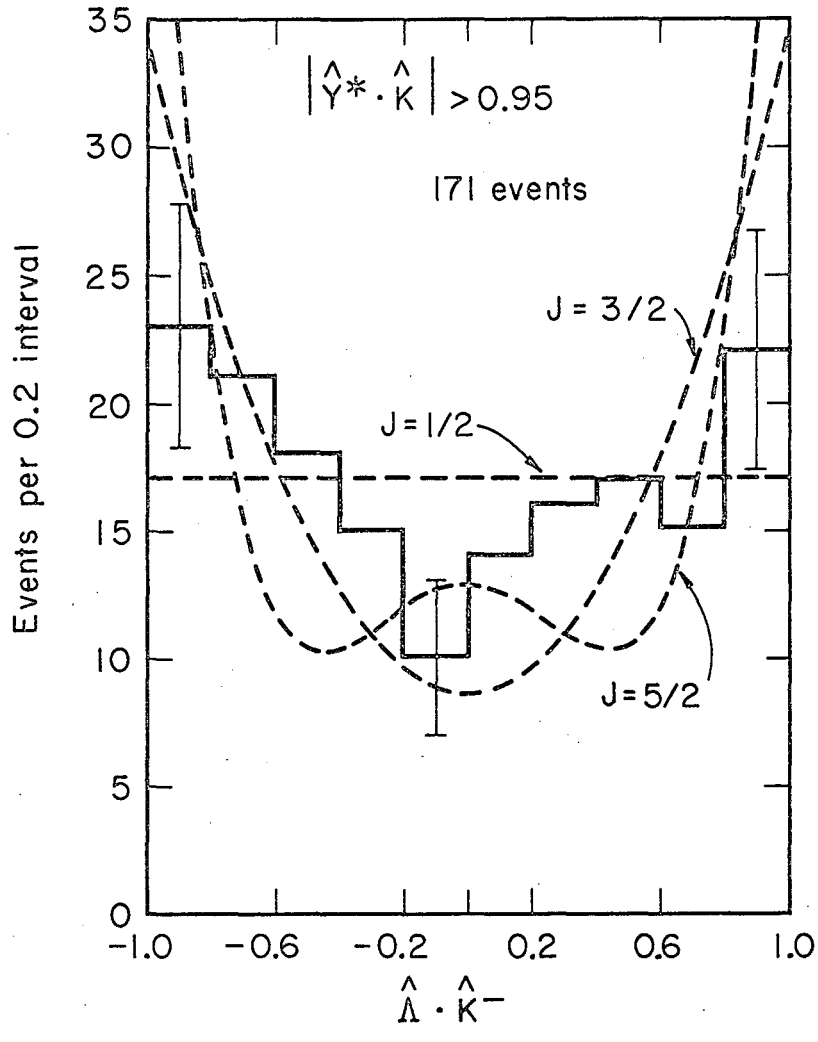

MU-34368

Fig. 22. Adair distribution, or distribution of the cosine of the angle between the Λ direction and the K^- direction, for the reaction $K^-+p \rightarrow \Lambda+\pi^++\pi^-$, in the momentum interval 1.00-1.45 BeV/c (including special low-energy study). Criteria for selection of events are explained in the text. The dashed curves are the theoretical distributions, each labeled with the spin of the Y_1^* which its shape implies (see Table II).

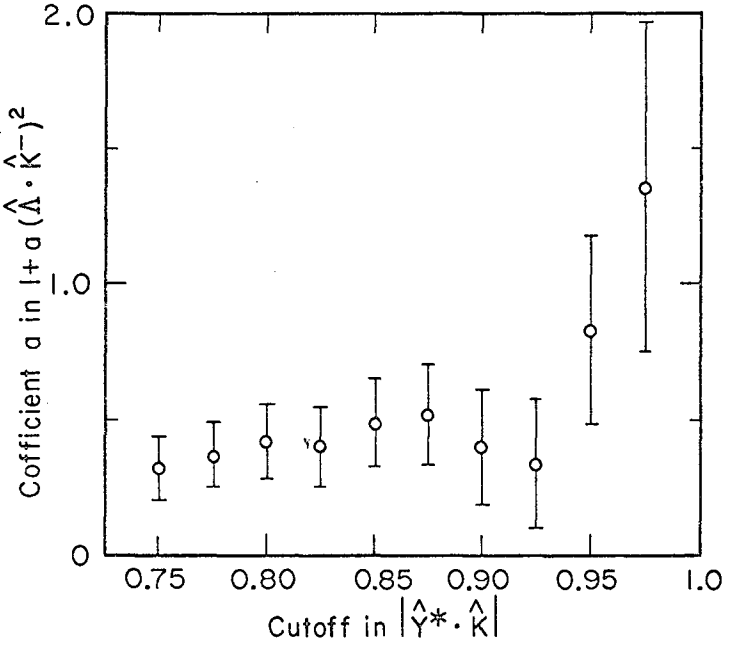

MU-34369

Fig. 23. Dependence of the coefficient a on lower limit allowed on $|\hat{Y}_1^* \cdot \hat{K}^-|$, when the Adair distribution is fit to $1 + a\,(\hat{\Lambda} \cdot \hat{K}^-)^2$. Events are from the reaction $K^- + p \rightarrow \Lambda + \pi^+ + \pi^-$ in the momentum interval 1.00-1.45 BeV/c (including special low-energy study). In addition to the general criteria for this reaction described in the text, it was required that 1340 MeV < $M_{\Lambda\pi}$ < 1430 MeV.

In order to obtain the correct treatment of errors, the data in each bin of cosη for $|\hat{Y}_1^* \cdot \hat{K}^-| > 0.9$ were extrapolated linearly to $|\hat{Y}_1^* \cdot \hat{K}^-| = 1.0$. The linear fits all had acceptable chi squareds. The extrapolated values and their errors are plotted in Fig. 24. Events having 1340 MeV < $M_{\Lambda\pi}$ < 1430 MeV for either charge state are used. Again the theoretical curves from Table II are drawn on the figure. The results of a chi-squared test, that the data are represented by each of these curves, are listed in Table VIII. It is seen that J = 3/2 is preferred, but J = 1/2 and J = 5/2 cannot be ruled out, the betting odds against each being about 5 to 1. The Adair distribution fails to give a certain spin determination.

Table VIII. Confidence level of Adair distribution.

J	Chi squared	Confidence level
1/2	7.27	0.12
3/2	2.57	0.63
5/2	6.83	0.15

5. Distributions Relative to the Production Normal

More success has been achieved by studying angular distributions relative to the normal to the production plane. In Sec. II. C. 2 we discussed the complete angular distribution relative to this direction. In practice, most experiments have used just a portion of this distribution.

Ely et al.[5] examined the normal decay angle of the Λ decay of the Y_1^*. This distribution, when fit to $N(1+ a \cos^2\Theta)$, gave $a = 1.5 \pm 0.4$. Equations (49) and (50) show that a must be 0 for a spin-$\frac{1}{2}$ Y_1^*. The conclusion was reached that $J > \frac{1}{2}$ with a confidence $> 3\sigma$. In order to obtain this result, they found that they had to restrict the production angle, $-0.5 < Y_1^* \cdot K^- < 0.5$, indicating a correlation between these angles.

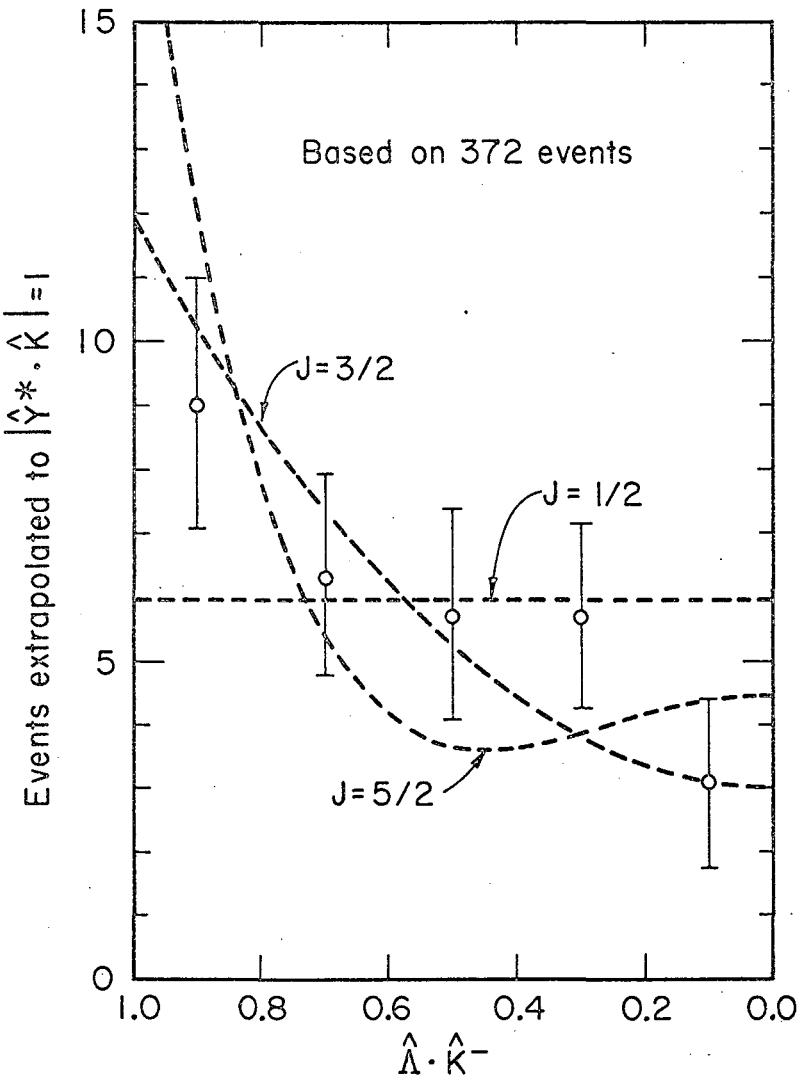

MU-34370

Fig. 24. Adair distribution, or distribution of the cosine of the angle between the Λ direction and the K^- direction, for the reaction $K^-+p \rightarrow \Lambda+\pi^++\pi^-$ in the momentum interval 1.00-1.45 BeV/c (including special low-energy study). The data were folded about $\hat{\Lambda} \cdot \hat{K}^- = 0$, and the events in each bin of this variable were extrapolated to $|\hat{Y}_1^* \cdot \hat{K}^-| = 1$, as explained in the text. The dashed curves represent the theoretical expectation for the value of J indicated for each curve (see Table II).

Colley et al. studied

$$\pi^- + p \rightarrow \Lambda + \pi^- + K^+ \qquad (101)$$

at 2.0 BeV/c in a propane chamber.[93] They found $Y_1^*(1385)$ as well as $K^*(880)$. The same analysis as that of Ely et al. (except that no limits on production angle are mentioned) gave $a = 1.29 \pm 0.78$. This quantity is proportional to t_2^0 in the irreducible representation of the density matrix. From the condition on the density matrix that $Tr(\rho^2) \leq 1$, an inequality can be derived for t_1^0, which is proportional to the polarization $\overline{P}$ of the Λ. For the observed value of a, Colley et al. deduced that $|\overline{P}|_{max} = 0.47 \pm 0.09$ for a $P_{3/2}$ Y_1^* and $|\overline{P}|_{max} = 0.28 \pm 0.05$ for a $D_{3/2}$ Y_1^*. They observed $|\overline{P}| = 0.82 \pm 0.27$, which is closer to the $P_{3/2}$ limit than to the $D_{3/2}$ limit. They concluded that if Y_1^* has $J = 3/2$, then it has positive parity. Erwin et al. looked at reaction (101) and the corresponding reaction with $K^0\pi^0$ in the final state at 1.89 BeV/c in a hydrogen bubble chamber.[94] They reported isotropy in the normal distribution of the Λ (and also in the Adair distribution), but they also found a very large polarization of the Λ, $\alpha\overline{P} = 0.61 \pm 0.28$, favoring the parity states $S_{1/2}$, $P_{3/2}$, etc.

Bertanza et al.[7] looked at reaction (1) at 2.24 BeV/c in a hydrogen bubble chamber and reported a large alignment. They found a value of the parameter a of 4.2 ± 1.0. They concluded that the spin of the Y_1^* had to be greater than $\frac{1}{2}$.

Previous work on part of the data used in this report used the distribution of polarization, referred to both the normal direction $(\vec{P} \cdot \hat{n})$ and to the rotated direction $(\vec{P} \cdot \hat{m})$, as a function of the normal distribution of the Λ $(\hat{\Lambda} \cdot \hat{n})$ in order to investigate the spin and parity of the Y_1^*.[9] The theory of this analysis is covered in that paper and in Sec. II.C.3 of this paper. The unit vector $\hat{m}$ is defined in formula (56). The normal distribution itself can also be used, of course, in the manner of Ely et al.[5] These two analyses taken together constitute a study of the diagonal elements of the density matrix. The analysis was extended to

cover the range of energy used in the previous section for the Adair analysis, K^- lab momentum of 1.00-1.45 BeV/c. The normal distribution for each of the three intervals--1.00-1.15, 1.15-1.30, and 130-1.45 BeV/c--is shown in Fig. 25. The polarization distributions for each energy interval are shown in Fig. 26. The distributions have much the same shape at each of these energies. Confirming earlier remarks that the production mechanism seems to be changing slowly over this energy interval. Consequently, it seems valid to lump data together in this analysis also, and Figs. 27 and 28 show the above distributions for the entire interval, 1.00-1.45 BeV/c. In all cases the production-angle interval, $-0.8 < Y_1^* \cdot K^- < 0.8$, and the invariant-mass interval $1340 \text{ MeV} < M_{\Lambda\pi} < 1430 \text{ MeV}$, are used, the two charge states of the Y_1^* are lumped together, and the data are folded. If the data are not folded, the asymmetry terms are small. This observation is not inconsistent with the observation of large asymmetry terms in the decay relative to the Y_1^* direction, since we are now looking at an orthogonal direction. Some cancellation of asymmetry also results from the lumping together of charge states. The polarization is determined for each bin of the observation by projection,

$$N\alpha\vec{P}\cdot\hat{n} = 3\sum_{i}^{N}(\hat{p}\cdot\hat{n})_i , \qquad (102)$$

and similarly for $N\alpha\vec{P}\cdot\hat{m}$, where i runs over the events in the bin and $\hat{p}$ is the direction of the proton from the Λ decay. Note that the unnormalized value of the polarization is used, (this is the natural quantity to use if the density matrix is normalized to the total number of events) and that the error in this quantity is given simply by $(3N)^{\frac{1}{2}}$.

The normal distributions were each fit to even-power series in $\cos\Theta$. The maximum complexity possible for spin J is $\cos^{2J-1}\Theta$. Each fit yields a chi squared and a confidence level depending on chi squared and the number of degrees of freedom. Table IX lists the goodness-of-fit parameters for each distribution. In the same manner, the polarization distributions are expected to display maximum complexity as a function of the orbital angular momentum as explained in

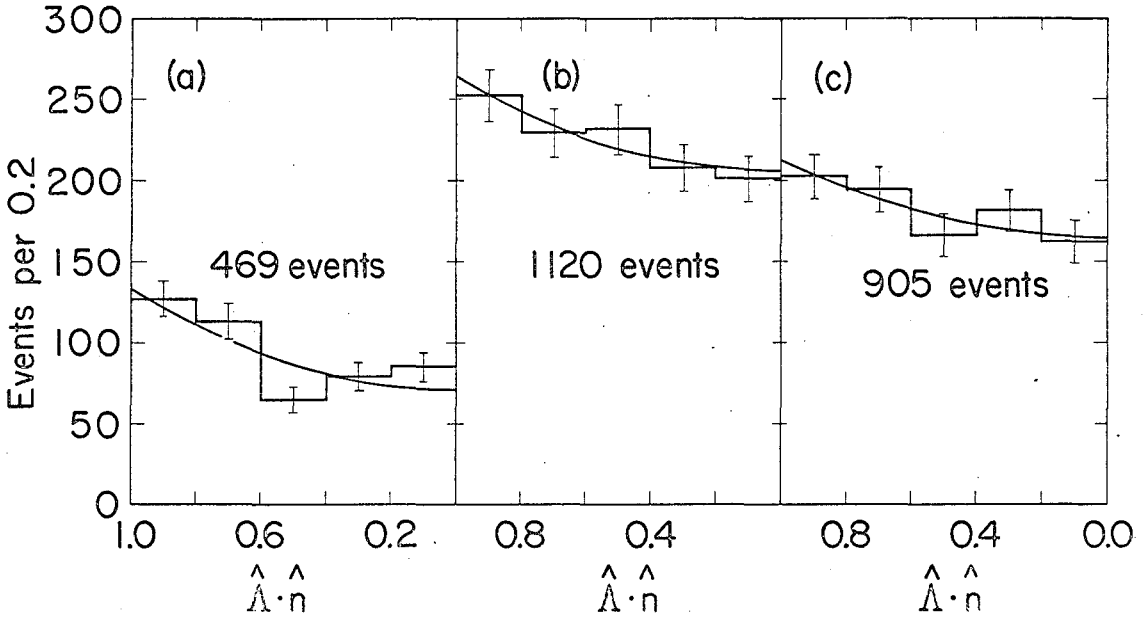

Fig. 25. Normal decay distribution of the Y_1^* for (a) P = 1.00-1.15 BeV/c (from special low-energy study), the solid curve is $(71\pm6) + (64\pm16)\,(\hat{\Lambda}\cdot\hat{n})^2$; (b) P = 1.15-130 BeV/c, the solid curve is $(204\pm10) + (60\pm23)\,(\hat{\Lambda}\cdot\hat{n})^2$; and (c) P = 1.30-1.45 BeV/c, the solid curve is $(165\pm9) + (47\pm21)\,(\hat{\Lambda}\cdot\hat{n})^2$. The data are from the reaction $K^- + p \rightarrow \Lambda + \pi^+ + \pi^-$. Criteria for selection of events are explained in the text. The solid curves are least-square fits to $a + b\,(\hat{\Lambda}\cdot\hat{n})^2$. $\hat{n} = (\hat{K}^- \times \hat{Y}_1^*)/|\hat{K}^- \times \hat{Y}_1^*|$.

Fig. 26. Distribution of the polarization of the Λ from decay of the Y_1^* (a) relative to the normal to the production plane, $\hat{n} = (\hat{K}^- \times \hat{Y}_1^*)/|\hat{K}^- \times \hat{Y}_1^*|$, for P = 1.00-1.15 BeV/c (special low-energy study), the solid curve is $-(9\pm8) + (89\pm22)\,(\hat{\Lambda}\cdot\hat{n})^2$; (b) relative to the rotated direction, $\hat{m} = -\hat{n} + 2\hat{\Lambda}(\hat{\Lambda}\cdot\hat{n})$, for P = 1.00-1.15 BeV/c (special low-energy study), the solid curve is $(9\pm8) - (197\pm68)\,(\hat{\Lambda}\cdot\hat{n})^2 + (268\pm74)\,(\hat{\Lambda}\cdot\hat{n})^4$; (c) relative to the normal for P = 1.15-1.30 BeV/c, the solid curve is $-(42\pm13) + (164\pm34)\,(\hat{\Lambda}\cdot\hat{n})^2$; (d) relative to the rotated direction for P = 1.15-1.30 BeV/c, the solid curve is $(42\pm13) - (526\pm105)\,(\hat{\Lambda}\cdot\hat{n})^2 + (607\pm113)\,(\hat{\Lambda}\cdot\hat{n})^4$; (e) relative to the normal for P = 1.30-1.45 BeV/c, the solid curve is $-(18\pm12) + (73\pm30)\,(\hat{\Lambda}\cdot\hat{n})^2$; and (f) relative to the rotated direction for P = 1.30-1.45 BeV/c, the solid curve is $(18\pm12) - (223\pm94)\,(\hat{\Lambda}\cdot\hat{n})^2 + (259\pm101)\,(\hat{\Lambda}\cdot\hat{n})^4$. The data are from the reaction $K^- + p \rightarrow \Lambda + \pi^+ + \pi^-$. Criteria for selection of events are explained in the text. The solid curves are simultaneous least-square fits of the normal projection to $A_0 + A_2(\hat{\Lambda}\cdot\hat{n})^2$ and of the rotated projection to $B_0 + B_2(\hat{\Lambda}\cdot\hat{n})^2 + B_4(\hat{\Lambda}\cdot\hat{n})^4$ subject to the constraints $A_0 + B_0 = 0$ and $A_0 + A_2 - B_0 - B_2 - B_4 = 0$. This behavior is that appropriate to a $P_{3/2}$ state.

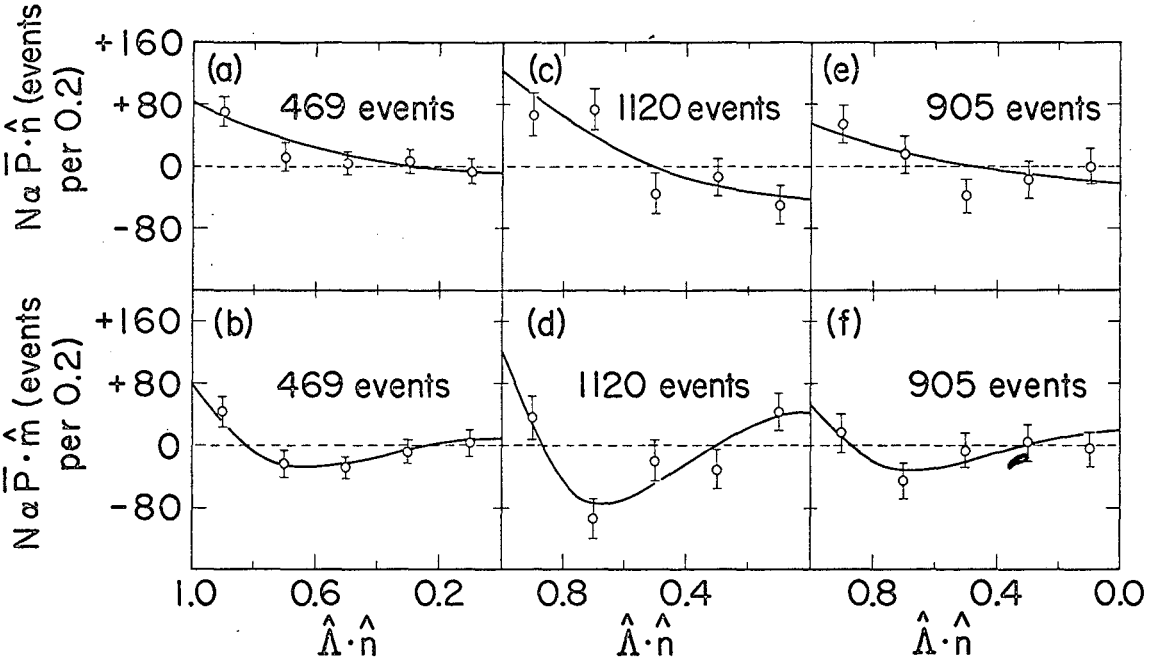
(a)
469 events
(c)
1120 events
(e)
905 events
(b)
469 events
(d)
1120 events
(f)
905 events
+160
+80
0
-80
N α P̄ · n̂ (events per 0.2)
N α P̄ · m̂ (events per 0.2)
1.0
0.6
0.2
0.8
0.4
0.0
Λ̂ · n̂
MU-34372

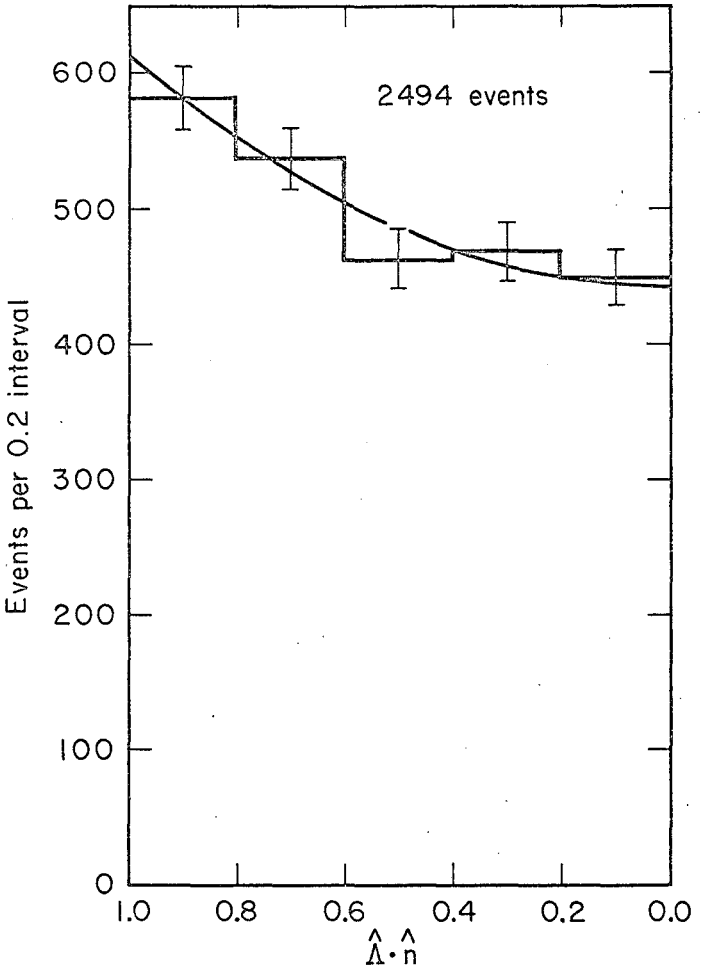

Fig. 27. Normal decay distribution of the Y_1^* for P = 1.00-1.45 BeV/c (includes special low-energy study). The solid curve is a fit to $a+b(\hat{\Lambda}\cdot\hat{n})^2$, with a = 442±15 and b=170±37. The data are from the reaction $K^-+p \rightarrow \Lambda+\pi^++\pi^-$. Criteria for selection of events are explained in the text. $\hat{n} = (\hat{K}^-\times\hat{Y}_1^*)/|\hat{K}^-\times\hat{Y}_1^*|$.

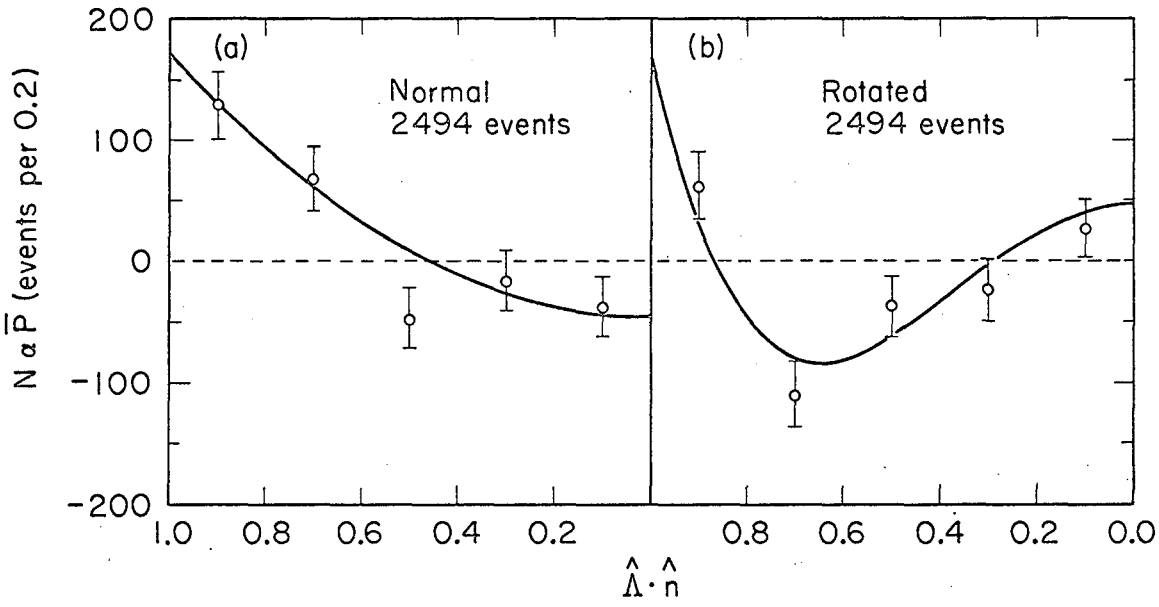

MU-34374

Fig. 28. Distribution of the polarization of the Λ from decay of the Y_1^* for P=1.00-1.45 BeV/c (includes special low-energy study) (a) relative to the normal to the production plane, $\hat{n}=(\hat{K}^-\times\hat{Y}_1^*)/|\hat{K}^-\times\hat{Y}_1^*|$, the solid curve is $-(70\pm20)+(326\pm51)(\hat{\Lambda}\cdot\hat{n})^2$; and (b) relative to the rotated direction, $\hat{m}=-\hat{n}+2\hat{\Lambda}(\hat{\Lambda}\cdot\hat{n})$, the solid curve is $(70\pm20)-(936\pm157)(\hat{\Lambda}\cdot\hat{n})^2+(1121\pm169)(\hat{\Lambda}\cdot\hat{n})^4$. Criteria for selection of events are explained in the text. The solid curves are a simultaneous fit of the normal projection to $A_0+A_2(\hat{\Lambda}\cdot\hat{n})^2$ and of the rotated projection to $B_0+B_2(\hat{\Lambda}\cdot\hat{n})^2+B_4(\hat{\Lambda}\cdot\hat{n})^4$ subject to the constraints $A_0+B_0=0$ and $A_0+A_2-B_0-B_2-B_4=0$. This behavior is that appropriate to a $P_{3/2}$ state.

Table IX. Confidence level of normal decay distributions.

Spin	Degrees of freedom	Chi squared	Confidence level
		P = 1.00-1.15 BeV/c	
1/2	4	26.8	2.2×10^{-5}
3/2	3	10.7	0.013[a]
5/2	2	7.3	0.026[a]
		P = 1.15-1.30 BeV/c	
1/2	4	7.4	0.12
3/2	3	0.8	0.85
5/2	2	0.7	0.71
		P = 1.30-1.45 BeV/c	
1/2	4	6.6	0.16
3/2	3	1.7	0.63
5/2	2	1.7	0.42
		P = 1.00-1.45 BeV/c	
1/2	4	24.8	5.5×10^{-5}
3/2	3	1.6	0.67
5/2	2	1.4	0.50

[a]These confidence levels are low because of the large deviation of the bin at 0.5 from its neighbors [Fig. 25(a)].

Sec. II. C.3, the coefficients of the fit to normal and rotated projections being related by equations (59) and (60). Table X lists the confidence level parameters for each spin-parity hypothesis for each pair of distributions. Finally, these two independent investigations can also be regarded as one analysis by summing the chi-squared values and the degrees of freedom for each hypothesis. Results of this combination are shown in Table XI.

The conclusions of the previous paper are strengthened; $S_{1/2}$, $P_{1/2}$, and $D_{3/2}$ are ruled out quite strongly as spin-parity states of the Y_1^* whereas $P_{3/2}$, $D_{5/2}$, and $F_{5/2}$ are allowed. If normal decay and polarization chi-squared values are combined, this conclusion can be reached independently with the 1.00-1.15 BeV/c and with the 1.15-1.30 BeV/c data; the 1.30-1.45 data favor this conclusion but are inconclusive. Lumping together all energies raises the relative confidence level by about three orders of magnitude, showing again that things are varying slowly.

Adair has raised the objection that the many experiments in which anisotropies rule out $J = \frac{1}{2}$ may all be manifestations of interference between a $J = \frac{1}{2}$ Y_1^* and a combination of background states.[95] Such an explanation could be true, but the number of experiments that have reported anisotropies makes it unlikely. One test for interference, as explained in Sec. II.A, is to examine the above distributions for different mass intervals. Since the phase of the Y_1^* is changing rapidly as a function of this mass, interference effects are expected to behave differently in the different mass intervals. Accordingly, the data used above were divided into three mass intervals, 1335-1375 MeV, 1375-1395 MeV, and 1395-1435 MeV, each including about the same number of events, and the above analysis through D-3/2 was done for each of these portions. The selection criterion $|\hat{Y}^* \cdot \hat{K}| < 0.8$ was retained. The normal decay distributions are shown in Fig. 29, and the polarization distributions in Fig. 30. Combined confidence-level figures are tabulated in Table XII. The apparent alignment and polarization do obviously change with mass, low mass having strong alignment and weak

Table X. Confidence level of polarization distributions.

Spin-parity	Degrees of freedom	Chi squared	Confidence level
	P = 1.00-1.15 BeV/c		
$S_{1/2}$	9	19.3	0.022
$P_{1/2}$	9	25.2	0.0027
$P_{3/2}$	7	3.3	0.85
$D_{3/2}$	7	16.5	0.021
$D_{5/2}$	5	0.7	0.98
$F_{5/2}$	5	0.5	0.99
	P = 1.15-1.30 BeV/c		
$S_{1/2}$	9	39.4	9.6×10^{-6}
$P_{1/2}$	9	39.2	1.1×10^{-5}
$P_{3/2}$	7	9.2	0.24
$D_{3/2}$	7	33.9	1.8×10^{-5}
$D_{5/2}$	5	8.9	0.11
$F_{5/2}$	5	9.2	0.10
	P = 1.30-1.45 BeV/c		
$S_{1/2}$	9	13.0	0.16
$P_{1/2}$	9	12.9	0.17
$P_{3/2}$	7	6.0	0.54
$D_{3/2}$	7	12.4	0.087
$D_{5/2}$	5	2.0	0.85
$F_{5/2}$	5	2.3	0.81
	P = 1.00-1.45 BeV/c		
$S_{1/2}$	9	57.7	1.9×10^{-8}
$P_{1/2}$	9	59.3	1.7×10^{-8}
$P_{3/2}$	7	9.7	0.21
$D_{3/2}$	7	52.6	1.9×10^{-8}
$D_{5/2}$	5	6.7	0.24
$F_{5/2}$	5	6.8	0.24

Table XI. Confidence level of combined normal decay and polarization distributions.

Spin-parity	Degrees of freedom	Chi squared	Confidence level
	P = 1.00-1.15 BeV/c		
$S_{1/2}$	13	46.1	1.4×10^{-5}
$P_{1/2}$	13	52.0	1.4×10^{-6}
$P_{3/2}$	10	14.0	0.17
$D_{3/2}$	10	27.3	0.0024
$D_{5/2}$	7	8.1	0.33
$F_{5/2}$	7	7.9	0.35
	P = 1.15-1.30 BeV/c		
$S_{1/2}$	13	46.8	1.0×10^{-5}
$P_{1/2}$	13	46.6	1.1×10^{-5}
$P_{3/2}$	10	10.0	0.44
$D_{3/2}$	10	34.7	1.4×10^{-4}
$D_{5/2}$	7	9.6	0.21
$F_{5/2}$	7	9.8	0.20
	P = 1.30-1.45 BeV/c		
$S_{1/2}$	13	19.6	0.11
$P_{1/2}$	13	19.5	0.11
$P_{3/2}$	10	7.7	0.66
$D_{3/2}$	10	14.1	0.17
$D_{5/2}$	7	3.7	0.82
$F_{5/2}$	7	4.0	0.78
	P = 1.00-1.45 BeV/c		
$S_{1/2}$	13	82.5	3.7×10^{-12}
$P_{1/2}$	13	84.1	1.9×10^{-12}
$P_{3/2}$	10	11.2	0.34
$D_{3/2}$	10	54.2	4.5×10^{-8}
$D_{5/2}$	7	8.1	0.32
$F_{5/2}$	7	8.1	0.32

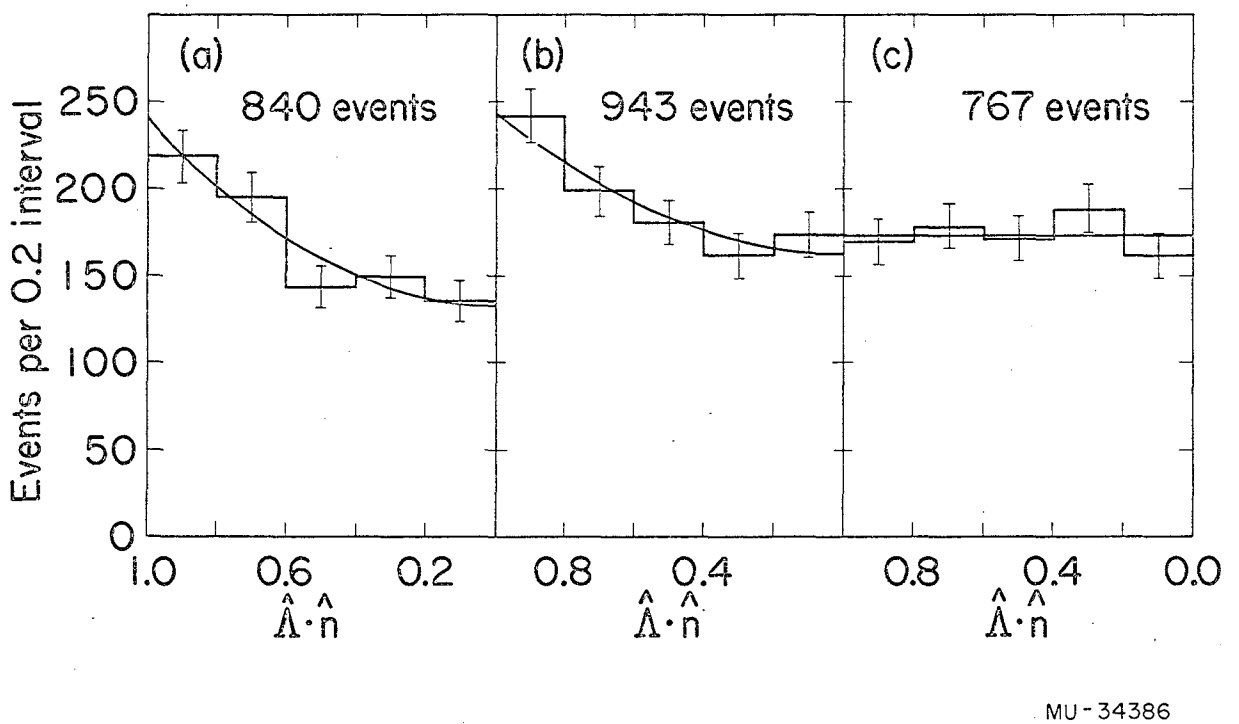

Fig. 29. Normal decay distribution of the Y_1^* for P=1.00-1.45 BeV/c (includes special low-energy study) and for (a) 1335 MeV < $M_{\Lambda\pi}$ < 1375 MeV, the solid curve is (132±8) + (107±21) $(\hat{\Lambda}\cdot\hat{n})^2$; (b) 1375 MeV < $M_{\Lambda\pi}$ < 1395 MeV, the solid curve is (162±9) + (80±22) $(\hat{\Lambda}\cdot\hat{n})^2$; and (c) 1395 MeV < $M_{\Lambda\pi}$ < 1435 MeV, the solid curve is (173±9) - (0±20) $(\hat{\Lambda}\cdot\hat{n})^2$. Criteria for selection of events are explained in the text. The solid curves are least-square fit to a $a+b(\hat{\Lambda}\cdot\hat{n})^2$. $\hat{n}=(\hat{K}^-\times\hat{Y}_1^*)/|\hat{K}^-\times\hat{Y}_1^*|$.

Fig. 30. Distribution of the polarization of the Λ from decay of the Y_1^*, for P=1.00-1.45 BeV/c (includes special low-energy study) (a) relative to the normal to the production plane, $\hat{n}=(\hat{K}^- \times \hat{Y}_1^*)/|\hat{K}^- \times \hat{Y}_1^*|$, for 1335 MeV $< M_{\Lambda\pi} <$ 1375 MeV, the solid curve is $(24\pm11) + (28\pm30)(\hat{\Lambda}\cdot\hat{n})^2$; (b) relative to the rotated direction, $\hat{m}=-\hat{n}+2\hat{\Lambda}(\hat{\Lambda}\cdot\hat{n})$, for 1335 MeV $< M_{\Lambda\pi} <$ 1375 MeV, the solid curve is $-(24\pm11) - (26\pm91)(\hat{\Lambda}\cdot\hat{n})^2 + (103\pm99)(\hat{\Lambda}\cdot\hat{n})^4$; relative to the normal for 1375 MeV $< M_{\Lambda\pi} <$ 1395 MeV, the solid curve is $-(58\pm12) + (179\pm32)(\hat{\Lambda}\cdot\hat{n})^2$; (d) relative to the rotated direction for 1375 MeV $< M_{\Lambda\pi} <$ 1395 MeV, the solid curve is $(58\pm12) - (505\pm96)(\hat{\Lambda}\cdot\hat{n})^2 + (569\pm104)(\hat{\Lambda}\cdot\hat{n})^4$; (e) relative to the normal for 1395 MeV $< M_{\Lambda\pi} <$ 1435 MeV, the solid curve is $-(39\pm12) + (129\pm29)(\hat{\Lambda}\cdot\hat{n})^2$; and (f) relative to the rotated direction for 1395 MeV $< M_{\Lambda\pi}$ Λ 1435 MeV, the solid curve is $(39\pm12) - (360\pm92)(\hat{\Lambda}\cdot\hat{n})^2 + (410\pm98)(\hat{\Lambda}\cdot\hat{n})^4$. The data are from the reaction $K^-+p\rightarrow\Lambda+\pi^++\pi^-$. Criteria for selection of events are explained in the text. The solid curves are simultaneous least-square fits of the normal projection to $A_0+A_2(\hat{\Lambda}\cdot\hat{n})^2$ and of the rotated projection to $B_0+B_2(\hat{\Lambda}\cdot\hat{n})^2+B_4(\hat{\Lambda}\cdot\hat{n})^4$ subject to the constraints $A_0+B_0 = 0$ and $A_0+A_2 - B_0 - B_2 - B_4 = 0$. This behavior is that appropriate to a $P_{3/2}$ state.

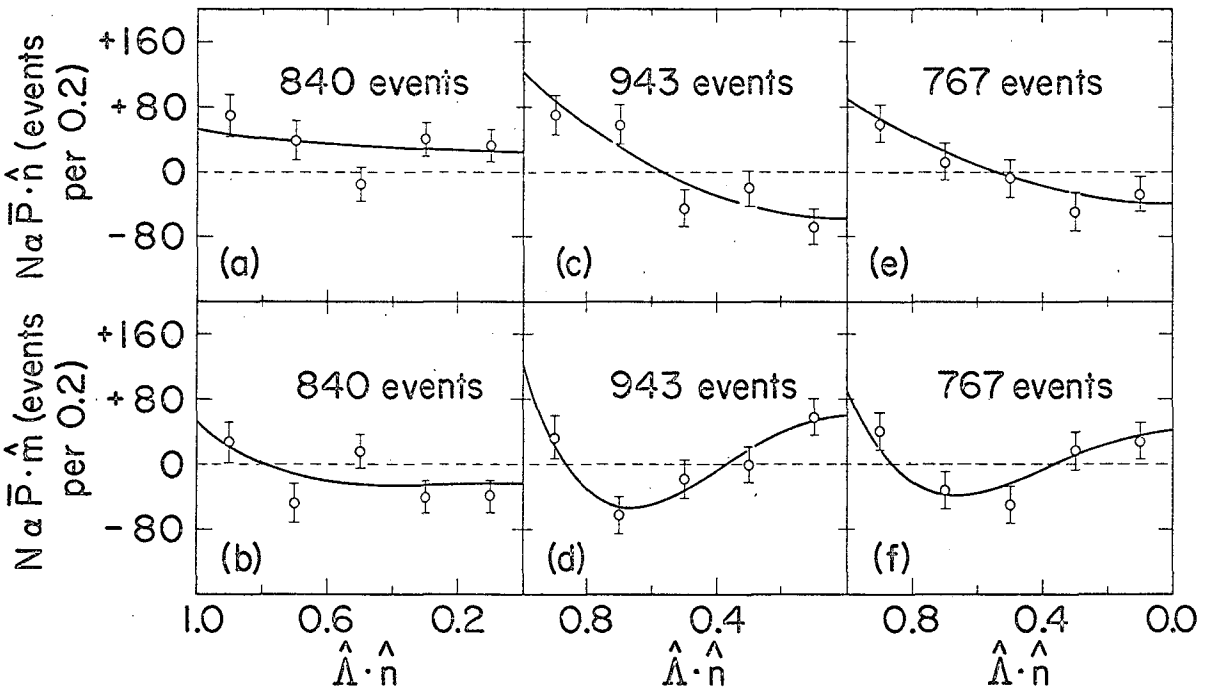
840 events
943 events
767 events
(a)
(c)
(e)
(b)
(d)
(f)
+160
+80
0
-80
N α P̄·n̂ (events per 0.2)
N α P̄·m̂ (events per 0.2)
1.0
0.6
0.2
0.8
0.4
0.0
Λ̂·n̂
MU-34375

Table XII. Confidence level versus Y_1^* mass.

Spin-parity	Degrees of freedom	Chi squared	Confidence level
	{1335 MeV< Λ-π mass < 1375 MeV}		
$S_{1/2}$	13	43.9	3.2×10^{-5}
$P_{1/2}$	13	54.8	4.5×10^{-7}
$P_{3/2}$	10	16.4	0.088
$D_{3/2}$	10	16.8	0.079
	{1375 MeV < Λ-π mass < 1395 MeV}		
$S_{1/2}$	13	55.6	3.3×10^{-7}
$P_{1/2}$	13	50.6	2.3×10^{-6}
$P_{3/2}$	10	7.4	0.68
$D_{3/2}$	10	33.1	2.6×10^{-4}
	{1395 MeV < Λ-π < 1435 MeV}		
$S_{1/2}$	13	27.7	0.0098
$P_{1/2}$	13	24.7	0.025
$P_{3/2}$	10	6.4	0.78
$D_{3/2}$	10	23.8	0.0083

polarization, high mass having weak alignment and strong polarization. But the combined goodness of fit excludes $S_{1/2}$, $P_{1/2}$ and $D_{3/2}$ (except in the low-mass bin) in each mass interval independently. Interference is unquestionably distorting the distributions, but it seems very unlikely that it solely is responsible for the departures from isotropy.

6. Complete Analysis of Angular Correlations

The above analysis determines the diagonal elements of the density matrix. A complete analysis should find all the elements. Equation (47) shows that we need to examine the distribution, not only of the polar angles of the Λ and the proton from the Λ decay, but also of the azimuthal angles of these two directions--four variables in all. Unfortunately it is impossible to depict on a figure the correlated behavior of four variables, so that a complete analysis must be altogether numerical, and it is not possible to keep a physical feeling for intermediate stages of the analysis.

A previous complete analysis was done on part of these data by means of a method of projection.[11] The t_L^M of equation (47) were obtained by certain projection formulae derived by Byers and Fenster.[46] Spin was essentially determined by that value of L above which the t_L^M with L even vanish within statistical errors. Parity was determined by comparison of two independent determinations of each t_L^M with L odd, one from the projection of transverse polarization, the other from that of longitudinal polarization. Coefficients are the same except for a change in sign for the two parity cases. See the original paper for more details.

A different method of approach to the complete analysis problem was developed independently and is described here. The basic technique for this method is to fit the data to a set of t_L^M's for each spin-parity hypothesis and compare the predicted moments (to be defined) with the same moments determined by projection. A single chi squared value for each hypothesis gives the overall goodness of fit.

A likelihood function L is defined by

$$L(\vec{t}) = \prod_i I(\hat{\Lambda}_i, \hat{p}_i; \vec{t}) , \qquad (103)$$

where I is the function defined in equation (47), $\vec{t}$ stands for the set of $t_L^{M_1}$s and the product is over all the events in the sample. The $\vec{t}$ that maximizes the value of L is the best estimate of the true value of $\vec{t}$, when the hypothesis being tried is assumed to be the correct one. In practice, the logarithm is taken of both sides of (103) so that the product becomes a sum. The logarithm is a monotonic function for real positive argument, so that a maximum value of log (L) corresponds to a maximum value of L. No weighting for experimental error or bias was done. Error on the angle determination should be small compared to the structure of the distribution for small values of J, but may well be significant at higher values of J. No significant biases are felt to be present.

The fitting program developed to find the maximum value of L did not use equation (47) directly. Instead, the steps of the derivation of this equation were repeated by the computer for each event, and the transformation to irreducible representation was not done until the end of the run. In this manner most of the Clebsch-Gordon coefficients, which are time consuming to compute in the general case, were eliminated in the event-by-event calculations. The distribution $I(\vec{t})$ is a linear function of the $t_L^{M_1}$s, so that the analytic first and second derivatives of log (L) could be easily calculated, and Newton's method was used in an iterative fashion to search for the maximum. The search was started in every case from the most chaotic, and hence a priori the most probable, form of the density matrix; in the irreducible representation, this form is characterized by all $t_L^{M_1}$s = 0 except for t_0^0. No search for additional maxima was made. All solutions found were physical in the sense that $Tr(\rho^2) \leq 1$. The highest value of J investigated was 7/2; the search in the 32-parameter space took about 10 iterations. All maxima found were quite sharp. The numerical values of the solutions are not important to our argument, but some of them are listed for reference in Appendix B.

The solutions from the fitting program described above give a representation of the data that is dependent on the hypothesis assumed.

On the other hand, because of the completeness of the spherical harmonics, we can assume that a quite general expansion of the form of equation (48) would be valid independent of physical assumptions. In other words, let

$$I(\hat{\Lambda}, \hat{p}) = \sum_{\ell, m} \sum_{L, M} A(L, M, \ell, m)\, Y_L^M(\hat{\Lambda})\, Y_\ell^m(\hat{p}). \tag{104}$$

Then, from the orthogonal property of the spherical harmonics, we can project out each A,

$$A(L, M, \ell, m) = \oint d\Omega_\Lambda d\Omega_p\, I(\hat{\Lambda}, \hat{p})\, Y_L^{M\,*}(\hat{\Lambda})\, Y_\ell^{m\,*}(\hat{p}). \tag{105}$$

For the experimental situation, we perform the sum

$$(4\pi)^3 A(L, M, \ell, m) = (1/N) \sum_i Y_L^{M\,*}(\hat{\Lambda}_i)\, Y_\ell^{m\,*}(\hat{p}_i), \tag{106}$$

where N is the total number of events and i runs over all events in the sample. The error matrix is given by

$$\begin{aligned}(4\pi)^6 & G(L, M, \ell, m; L', M', \ell', m') \\ &= (1/N^2) \sum_i Y_L^{M\,*}(\hat{\Lambda}_i)\, Y_\ell^{m\,*}(\hat{p}_i)\, Y_{L'}^{M'\,*}(\hat{\Lambda}_i)\, Y_{\ell'}^{m'\,*}(\hat{p}_i) \\ &\quad - (1/N^3) \left[\sum_i Y_L^{M\,*}(\hat{\Lambda}_i)\, Y_\ell^{m\,*}(\hat{p}_i)\right] \left[\sum_j Y_{L'}^{M'\,*}(\hat{\Lambda}_j)\, Y_{\ell'}^{m'\,*}(\hat{p}_j)\right].\end{aligned} \tag{107}$$

It was found by counting that there are 73 of these moments, as we shall call the A's, which are pertinent through $J = 7/2$. They are listed for reference in Appendix C.

The final step is to take the coefficients of equation (47), plug in the values of the t_L^M's from the fitting program, and get a set of predicted moments. Those moments not appearing as coefficients are predicted to be zero. A chi-squared test can now be applied to the difference between the projected and predicted values of the moments.

Equation (76) is used, where now x_i^m is the projected value of one of the moments, x_i is the corresponding predicted value, and G is given by (107). The number of degrees of freedom is just the difference between the number of moments taken into account in the chi-squared determination and the number of parameters in the fitting procedure--that is, the number of A's minus the number of $t_L^{M_L}$'s. A confidence level can then be associated with each hypothesis for each momentum interval studied. The same intervals were used as were used in the previous section (including the same cutoff on production angle, same Y_1^* mass band, etc.), the projected moments were computed though J = 7/2, and confidence levels were obtained for all hypotheses through J = 7/2. These confidence levels are listed in Table XIII and plotted in Fig. 31.

Study of these values shows that $P_{3/2}$ is the most likely assignment, $D_{5/2}$ is not ruled out, and $F_{7/2}$ is remotely possible. All other assignments are uniformly excluded by large margins at all momenta. The complete analysis is not significantly better than the analysis of the previous section for $J \leq 3/2$, but it does allow additional conclusions for possibilities of higher spin.

A solution given by the fitting program can be expressed in terms of trigonometric functions by use of equations of the type (49) through (52). The analysis of the last section is naturally expressed in trigonometric functions. The diagonal terms of the $P_{3/2}$ solutions from the fitting program of the complete analysis were compared with the $P_{3/2}$ solutions of the previous section by evaluating the coefficients of the corresponding trigonometric functions. When the errors from the previous section were used and correlations among the errors were ignored a chi-squared test that these coefficients are the same gave a chi-squared value of 4.78 for twelve pairs of coefficients (four from each momentum interval). This excellent agreement between the programs shows that there are no significant mistakes in the two programs. In addition, the parameters from the P-3/2 solution on 1.15-1.30 BeV/c data of the complete analysis developed here agree very well with those of the independently developed complete treatment by moment projection[11] on approximately the same data.

Table XIII. Confidence levels from complete analysis.

Spin parity	P = 1.00-1.15 BeV/c	1.15-1.30 BeV/c	1.30-1.45 BeV/c
$S_{1/2}$	1.2×10^{-7}	3.1×10^{-8}	3.7×10^{-8}
$P_{1/2}$	1.1×10^{-7}	1.3×10^{-8}	2.1×10^{-8}
$P_{3/2}$	0.24	0.023	0.052
$D_{3/2}$	6.7×10^{-4}	2.8×10^{-8}	6.9×10^{-5}
$D_{5/2}$	0.14	6.0×10^{-3}	0.017
$F_{5/2}$	1.1×10^{-5}	1.2×10^{-9}	6.0×10^{-6}
$F_{7/2}$	3.7×10^{-6}	0.14	1.4×10^{-3}
$G_{7/2}$	4.0×10^{-9}	1.4×10^{-9}	4.3×10^{-15}

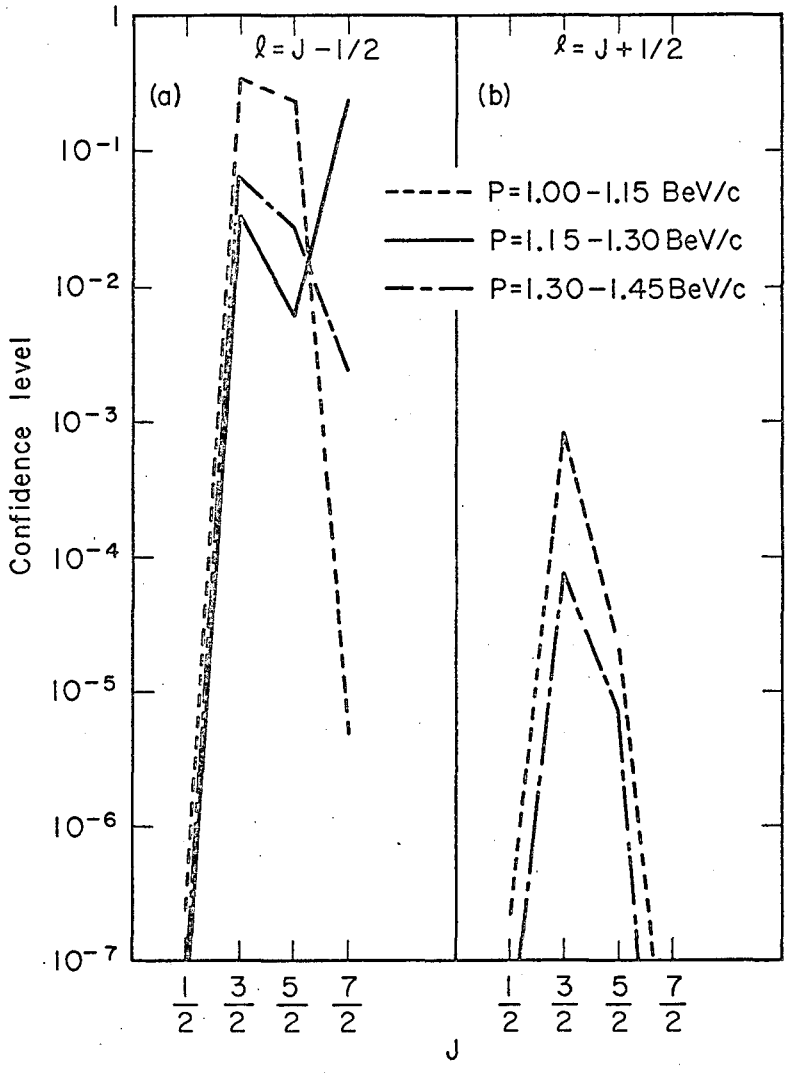

Fig. 31. Plot on a logarithmic scale of confidence-level determinations from the complete analysis of the spin and parity of the $Y_1^*(1385)$. Part (a) shows the confidence levels for hypothesized Y_1^* states having $\ell = J - \frac{1}{2}$, part (b) shows those having $\ell = J + \frac{1}{2}$. Each momentum interval studied can be identified by means of the box. Note that one line never appears above the lower limit of the graph in part (b); all confidence levels for P=1.15-1.30 BeV/c for this parity were less than 10^{-7}.
– – – P=1.00-1.15 BeV/c; ——— P=1.15-1.30 BeV/c; —·— P=1.30-1.45 BeV/c.

As an additional check on the effects of interference, the 1.15-1.30 BeV/c data were divided into two portions, one with Λ-π mass < 1385 MeV, the other with Λ-π mass > 1385 MeV. The $P_{3/2}$ analysis was performed on these portions separately. When correlations among the errors were ignored, chi-squared tests gave values of chi squared of 5.20 and 6.44 respectively, that the solution for each subset of data was the same as the solution for the undivided set of data. Within errors, this analysis finds no significant interference.

H. Y_1^* Branching Ratio

One of the sensitive predictions made by various theories covered in Sec. II. B has been the branching ratio of the Y_1^*. Earlier determinations of this ratio gave values of the order of 1 to 5% but were hampered by poor statistics.[13]

Events of the reaction

$$K^- + p \rightarrow \Sigma^0 + \pi^+ + \pi^- \qquad (69)$$

were taken from the same sample of type-32 events for the entire momentum range of 1.00-1.75 BeV/c. These events had been selected by a somewhat different set of criteria than the one described above; chi squared for reaction (69) (a two-constraint fit) was required to be less than 20, and also less than one-half the chi squared for reaction (1) (four-constraint) and less than twice that for reaction (70) (one-constraint). Accordingly, the reaction (1) denominator, used in the analysis below, was normalized to correspond to these same criteria.

The $\Sigma^0\pi^+$ and $\Sigma^0\pi^-$ effective-mass distributions are shown in Fig. 32. The curves drawn through the data represent the analysis described below. The π^+-π^- effective-mass distribution shows no significant deviation from phase space.

We expect to find nonresonant events, $Y_1^*(1385)$ events, $Y_1^*(1660)$ events, and events that are really reaction (1) but are accepted by the criteria given above. In order to find the expected

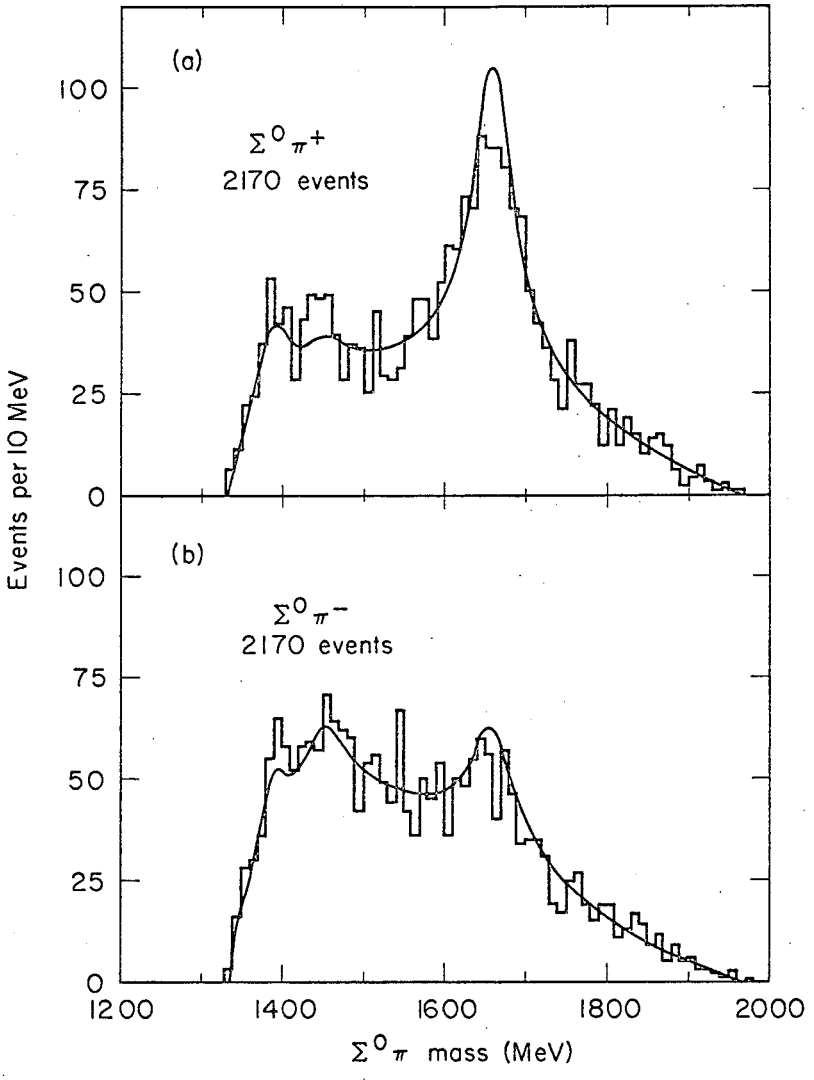

Fig. 32. Effective-mass distributions (a) of the Σ^0-π^+ pair and (b) of the Σ^0-π^- pair from the reaction $K^-+p \rightarrow \Sigma^0+\pi^++\pi^-$ at P=1.00-1.75 BeV/c (includes special low-energy study). Criteria for selection of events are explained in the text. The solid curve is the sum of nonresonant-phase-space and Breit-Wigner shapes for the $Y_1^*(1385)$, $Y_1^*(1660)$, and the $Y_1^*(1385)$ which is produced as a Λ-π state but fit as a Σ^0-π state, in the proportions given by Table XIV.

contribution of the last-named source of events, we looked at the events simulated by the FAKE program mentioned in Sec. III. D above. Mass distributions of events generated as reaction (1) but fulfilling the criteria of reaction (69) are shown in Fig. 33. These events had been generated as proceeding through the $Y_1^{*+}(1385)$ resonance. When fit as reaction (69), these events still show a peak, but it is broadened and shifted to higher mass. The curve shown in Fig. 33 is that expected from a Breit-Wigner resonance of mass 1450 MeV and width 60 MeV, which fits the simulated-data curve very well. In addition, the fitted beam momentum in these events peaks about 35 MeV/c higher than the momentum at which they were generated as reaction (1).

A model was chosen in which the data in the two channels of Fig. 32 are represented by the incoherent sum of nonresonant production plus production of Breit-Wigner resonances of $M = 1385$ MeV, $\Gamma = 50$ MeV, of $M = 1450$ MeV, $\Gamma = 60$ MeV, and of $M = 1660$ MeV, $\Gamma = 60$ MeV. The shape of each of these contributions was calculated by the program ATHOS, which integrated over the momentum intervals by weighting with the total number of reaction (69) in each interval and adding. A linear sum of these shapes was assumed, and the coefficients that gave a minimum chi squared over all the data plotted in Fig. 32 were determined. These coefficients give an estimate of the number of events in each final state. Table XIV lists these estimates, and the curves in Fig. 32 show the shape of the solution.

Table XIV. Composition of $\Sigma^0\pi^+\pi^-$ final state.

Final state	Number of events
Nonresonant	812 ± 106
$Y_1^{*+}(1660)\,\pi^-$	609 ± 47
$Y_1^{*-}(1660)\,\pi^+$	211 ± 41
Misfit Λ-$Y_1^{*+}(1385)\,\pi^-$	63 ± 36
Misfit Λ-$Y_1^{*-}(1385)\,\pi^+$	167 ± 41
$Y_1^{*}(1385)\,\pi^-$	156 ± 22
$Y_1^{*-}(1385)\,\pi^+$	153 ± 24

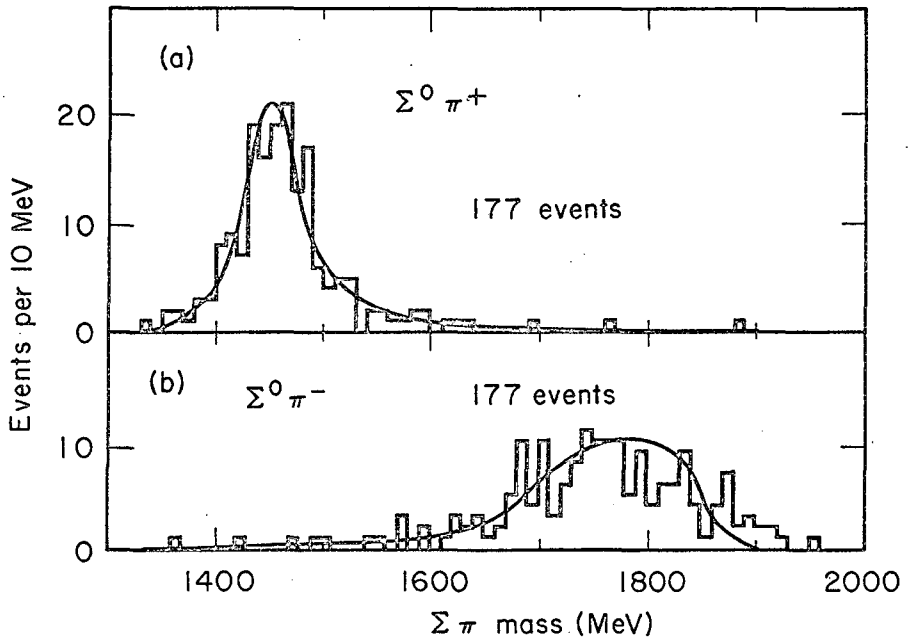

MU-34378

Fig. 33. Distribution of effective mass (a) of the Σ^0-π^+ pair and (b) of the Σ^0-π^- pair of events which were generated by the FAKE program as $K^-+p \rightarrow Y_1^{*+}(1385)+\pi^-$, $Y_1^{*+}(1385) \rightarrow \Lambda+\pi^+$, but which fit, according to the general criteria described in the text, the reaction $K^-+p \rightarrow \Sigma^0+\pi^+ +\pi^-$. The events were generated with the properties of the 1.51 BeV/c data of the physical experiment. The curves are the projections on the two axes of the Breit-Wigner shape between the Σ^0 and the π^+ with M=1450 MeV, Γ=60 MeV, for P=1.545 BeV/c.

The corresponding numbers from reaction (1), normalized to the different criteria and with the misfit events added on, come to 3035 $Y_1^{*+}(1385)$ and 3841 $Y_1^{*-}(1385)$. The branching ratios then are

$$N(Y_1^{*+} \to \Sigma^0 \pi^+)/N(Y_1^{*+} \to \Lambda \pi^+) = 0.051 \pm 0.007 \tag{108}$$

$$N(Y_1^{*-} \to \Sigma^0 \pi^-)/N(Y_1^{*-} \to \Lambda \pi^-) = 0.040 \pm 0.006. \tag{109}$$

Combination of these data gives

$$N(Y_1^{*\pm} \to \Sigma^0 \pi^\pm)/N(Y_1^{*\pm} \to \Lambda \pi^\pm) = 0.045 \pm 0.005. \tag{110}$$

Charge symmetry requires a similar number of events in which a charged Y_1^* decays into a charged Σ. The branching ratio is, therefore

$$R = N(Y_1^* \to \Sigma\pi)/N(Y_1^* \to \Lambda\pi) = 0.09 \pm 0.04. \tag{111}$$

The statistical error has been quadrupled to allow for large uncertainties in the model used.

In an earlier paper, the similar branching ratio for the $Y_1^*(1660)$ was estimated to be 6/7.[10] We mentioned in Sec. III.E.3 that this resonance was not resolved in the mass distributions of reaction (1), but an estimate of 167 ± 35 $Y_1^{*+}(1660)$ events was made by counting the number of excess events in the resonance region. Taking this number, normalizing to different criteria, and comparing with Table XIV, we obtain

$$N[Y_1^*(1660) \to \Sigma\pi]/N[Y_1^*(1660) \to \Lambda\pi] = 6.8 \pm 3.0. \tag{112}$$

Here the statistical error has been doubled to give a realistic error. In any event, when one looks at more data it is clear that the earlier estimate of this branching ratio is not substantiated.

I. Peripheral Production of Y_1^*

The experiment of Bertanza et al.[7] on reaction (1) at 2.24 BeV/c showed significant production of $Y_1^{*+}(1385)$ at this energy, but no $Y_1^{*-}(1385)$. In addition, the Y_1^*'s were strongly aligned, consistent with equation (66) for M1 K^* exchange. From the theory of Stodolsky and Sakurai[60] (discussed in Sec. II.E), it is apparent that the Y_1^{*+} is being produced by the peripheral exchange of a K^*, as depicted in Fig. 2(a). Let us see if this production mechanism is apparent at the highest energy available in this experiment.

Looking at Table IV, the ratio Y_1^{*+}/Y_1^{*-} seems to change at about 1.5 BeV/c. The particles Y_1^{*-} are more numerous below that energy, whereas Y_1^{*+} are slightly more numerous at higher energies. On the other hand, both charge states become less populated relative to other final states (in the next section, it is determined that the absolute cross section is decreasing). Figure 34 shows the normal decay distribution of the Y_1^* for the momentum interval 1.60-1.75 BeV/c. A fit to $N[1 + a(\hat{\Lambda}\cdot\hat{n}) + b(\hat{\Lambda}\cdot\hat{n})^2]$ gives

$$a = -0.16 \pm 0.23, \quad b = 2.40 \pm 0.43. \tag{113}$$

We see that the Y_1^{*+} is strongly aligned; by contrast, the Y_1^{*-} distribution is quite flat at this energy. At 1.30-1.45 BeV/c the Y_1^{*-} is the more strongly aligned, and at 1.45-1.60 BeV/c the two states are about equally aligned. The indication is that peripheral production is appearing at the highest energy available to this experiment, but that some other mechanism which favors Y_1^{*-} and which presumably gave the observed charge ratio at lower energies is still operative to cancel some of the expected effects. However, a firm statement cannot be made until it is known what happens to the charge ratio and alignment at still higher energies.

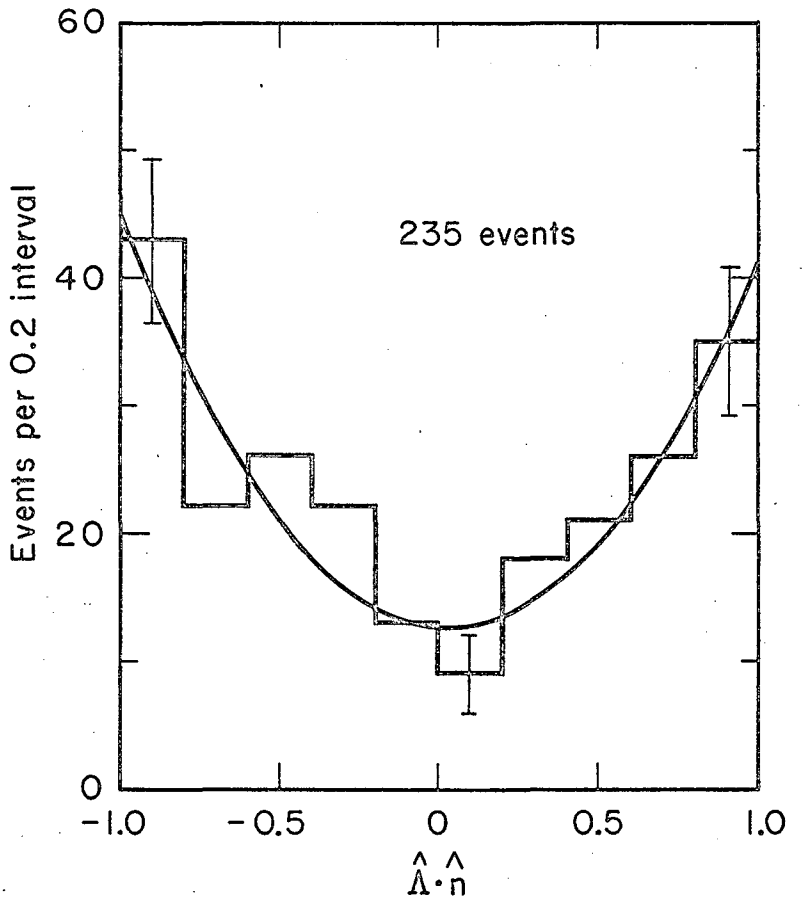

MU-34379

Fig. 34. Normal decay distribution of the Y_1^* from the reaction $K^-+p\rightarrow\Lambda+\pi^++\pi^-$ for P=1.60-1.75 BeV/c. The solid curve is a least-square fit of the data to $a+b(\hat{\Lambda}\cdot\hat{n})+c(\hat{\Lambda}\cdot\hat{n})^2$, with a=63±9, b=-10±14, and c=152±27. In addition to the general criteria described in the text, events must have 1340 MeV $< M_{\Lambda\pi^+} <$ 1430 MeV and $|\hat{Y}_1^{*+}\cdot\hat{K}^-| < 0.8$. The normal is defined by $\hat{n}=(\hat{K}^-\times\hat{Y}_1^*)/|\hat{K}^-\times\hat{Y}_1^*|$.

J. Cross Sections

The excitation function of reaction (1) was determined, subject to the difficulties inherent in measurement of cross sections from bubble chamber data. Other related reactions, also found in vee-two-prong events, were naturally studied at the same time.

1. Number of Events

The number of events for each reaction was determined by counting the number of vee-two-prong events found in the scan and the number of events fitting each reaction after measuring and subsequent analysis. These numbers must be corrected for certain biases and ambiguities.

a. Scanning efficiency. The basic numbers of events found in the scan for type-32 events are given in Table III. The sample used was reduced in two cases: (a) at 1.22 BeV/c, the first 21 rolls of film were badly obscured by recoil protons from a heavy neutron flux into the chamber, so that these rolls were not used in the cross-section determination; and (b) at 1.51 BeV/c, only 40% of the total sample was measured for this study, so that a smaller sample was also chosen from which to count the scan. The result showed 3356 events at 1.22 BeV/c and 12040 events at 1.5 BeV/c. These numbers must be corrected to compensate for the efficiency of the scanner in finding this event type.

The scan lists for the two scans were compared by computer, and those events for which the two lists did not agree were examined by a third scanner who resolved the conflict. For 1.22, 1.60, and 1.69 BeV.c, this conflict was performed for the total sample used, but at 1.32, 1.42, and 1.51 BeV/c, only about 20% of the sample was conflicted. The library system was designed so that the events from the second scan could be added to the main sample only after this conflicting procedure had been performed. The single-scan efficiencies determined from the conflicted samples varied from 94 to 98%. Very little correction was necessary in the completely conflicted samples, but the incompletely conflicted samples were corrected for the number

of events that would have been discovered had the conflict been completed. These corrections assume random failures to find events or misidentifications, but there possibly is a systematic bias from events that are very obscure and would not be found in an infinite number of regular scans.

b. Detection efficiency. Some events are lost because the vee particle leaves the chamber before it decays, and other events are lost because the vee travels such a short distance that the event is called a four-prong (see Fig. 4). For the latter effect, the mean length of Λ particles just distinguishable as separate vees was determined by examination of the distribution of lengths in the measured sample. There was a linear rise from zero at zero length, followed by a roughly exponential decline beyond 2.8-mm length. On the average, then, a Λ must be 1.4 mm or longer in order to be detected as a separate vee. The correction for the two effects was calculated by determining for each measured Λ the probability that this Λ would leave the chamber without decaying or that it would decay in less than 1.4 mm distance. The first effect is very small, 1/2 to 1%, because of the large size of the 72-inch chamber. The combination of the two effects is about 3-1/2% at all momentum settings. The correction was assumed to be the same for the much smaller number of $\overline{K}^0$ events, and the scan numbers were increased to correct for this loss.

A correction is also necessary because of neutral decay modes of the vee particles not detected. The standard correction factors of 3/2 for Λ events and 3 for $\overline{K}^0$ events were applied after the two species were separated. For additional information on $\overline{K}^0$ events, see reference 66.

c. Measurement and analysis efficiency. In Sec. III. C, it was explained that not all events are measured and that not all events that are measured succeed in reaching the KICK phase of the analysis program where fitting to hypotheses is done. Numbers of these categories are given in Table III under the headings Result 0 and Result 8, respectively. There is no choice but to assume that these events are distributed among the possible reactions in the same proportions as those

analyzed in the KICK program. So the entire scan sample is considered to be distributed among the possible reactions in the same proportion as those events processed by KICK.

Some events, listed under Result 11 in Table III, do not fit any hypothesis in the KICK analysis (a) because they are actually some reaction not covered in the set of hypotheses tried, (b) because a track or tracks suffered a large Coulomb scatter or similar accident that renders the event unfittable, or (c) the operator made large enough errors in the measurement to render the event unfittable. An estimate of category (c) can be determined by a second operator's remeasuring the failing events and determining the number that succeeds in fitting some hypothesis the second time. The results of this program are summarized in Table III. On the average, the number that pass the second time is 4.1% as large as the total number that pass either the first or the second time. A very small correction is needed if the whole sample of failures was remeasured, but the samples that were partially or not remeasured must be corrected for the events that would have been found upon remeasurement. As a check, the ratio of failures to good events among the events generated by the program FAKE (described in Sec. III. D) is 4.9%. The agreement seems satisfactory, since FAKE may generate some events that fall into category (b). It is not known how many events might be in category (b), and no correction was made for this bias.

d. Separation of hypotheses. Separation of Λ events from $\overline{K}^0$ events was the same as described in Sec. III. D, and the ambiguous events were assumed to have the same distribution between Λ and $\overline{K}^0$ hypotheses as the nonambiguous events had. So the two samples were increased to include their portions of the ambiguous events.

The numbers of events in reactions having $\Lambda \pi^+ \pi^-$ and $\Sigma^0 \pi^+ \pi^-$ final states were determined by means of the missing-mass distribution of all the neutrals as outlined in Sec. III. D and illustrated in Fig. 5. In this way the events ambiguous between these two final states are automatically taken care of (in this instance, there is no need to isolate a

a clean sample). Events with $\Lambda\pi^+\pi^-\pi^0$ in the final state were selected by confidence level as described in Sec. III.D. Then all these samples were increased so that their total number was the same as the number fitting any Λ hypothesis with a chi squared less than 10 times the number of constraints.

Another bias present but not corrected for affects primarily the $\Lambda\ \pi^+\ \pi^-\ \pi^0$ final state. In some instances, one piece of information, such as the curvature of a track, is lost because the program-estimated error on that quantity is too large. The fitting procedure is then done with one less constraint. The $\Lambda\ \pi^+\ \pi^-$ events can still be fit with three constraints; the $\Sigma^0\ \pi^+\ \pi^-$ events can be fit with zero constraint fits for the production followed by one-constraint fits for the Σ^0 decay; but $\Lambda\ \pi^+\ \pi^-\ \pi^0$ events were not searched for in this instance. Judging from the number of $\Lambda\ \pi^+\ \pi^-$ fits that had three constraints, 3 to 5% of the events might be included in this category. But there is a compensating bias. Events having $\Sigma^0\ \pi^+\ \pi^-\ \pi^0$ in the final state may fit $\Lambda\ \pi^+\ \pi^-\pi^0$ and be accepted as such. These effects will tend to cancel each other, and the net effect is not known.

2. Path Length

To complete a cross-section calculation, one must also know the flux of incoming particles. The total K^- path length at each momentum setting has been calculated by Richard Hubbard.[96] He employed two independent methods--comparison of an intensive scan with the reported K^--p total cross section at these energies, and use of the τ decay mode of the K^--meson.

a. Intensive Scan. A subsample of approximately 10 rolls of film at each momentum setting was intensively scanned for all incoming beam tracks, all beam tracks passing through without deflection, and all 0-prong, 1-prong, 2-prong, 3-prong, 4-prong, and 6-prong vertices occurring on the beam tracks (vees, secondary interactions, etc. were ignored). The even-prong vertices were considered to be interactions, and their number was extrapolated to the entire sample at each momentum. Hubbard estimated the π^- contamination by finding in each sample

the number of events fitting $\pi^- + p \rightarrow \Lambda + K^0$ and by counting the numbers of large δ rays on interacting tracks. This contamination ranges from 2 to 9%. The remaining interactions were considered to be K^- interactions. The flux of K^- particles was calculated for each sample by comparison as the total number of K^- interactions with the K^- total cross section at each energy.[97] The path length, expressed in terms of events/mb, is listed in Table XV.

Table XV. Best estimate of total path length.[a]

Momentum setting (BeV/c)	By interactions (events/mb)	By decays (events/mb)	Best estimate (events/mb)
1.22	1300	1160	1230± 60
1.32	1410	1470	1440± 70
1.42	850	795	825± 40
1.51	5100	5070	5085± 200
1.60	760	670	715± 35
1.69	1135	1060	1100± 55

[a] Richard Hubbard, K^- Path-Length Determination--K-72 Experiment, Alvarez Group Physics Note 496, 1964.

b. τ-Decay. The τ-decay mode of the K^-

$$K^- \rightarrow \pi^+ + \pi^- + \pi^- \qquad (114)$$

gives a distinctive three-prong topology, which was included in the regular scan. The number of three-prong events was recorded for each sample, and correction was made for scanning efficiency. The branching ratio of this decay mode was taken to be 5.7± 0.2%[73,98] but this number was corrected to 6.1± 0.2% because some other K^- decay modes have one or two π^0s that occasionally produce a Dalitz pair and hence a three-prong topology. The number of three-prong decays can then be used to find the total number of K^- entering the chamber at

each momentum setting. The total path length determined by this method, and a best estimate obtained by giving the two methods equal weight, are listed in Table XV.

3. Calculation of Cross Sections

When the number of events for each reaction at each momentum setting is known and the total path length is known at each momentum setting in terms of events/mb, the cross section in each case is calculated simply by dividing the former by the latter. The cross-section determinations are listed in Table XVI.

Turning our attention back to reaction (1) (the subject of this paper), we present a plot of the excitation function for this reaction in Figure 35, using this experiment and published data from other experiments from threshold to 2.24 BeV/c. The points from 1.1 to 1.7 BeV/c seem to follow quite closely a curve proportional to $\pi \lambda^2$, indicating once again that the various production amplitudes are changing slowly in this energy interval. The point at 2.24 BeV/c is considerably below this curve, but it was reported as a preliminary value and a lower limit (no error was given), so that no conclusion can be drawn from this apparent departure.

With Table IV, the cross section for each final state of reaction (1) can be deduced. Because the cross section for reaction (1) varies so smoothly in this interval, the values can be interpolated easily to give the average cross section over the intervals used in the analysis of final-state interactions. Results are given in Table XVII. The interesting features are the peaking of the $K^- + p \rightarrow \rho^0 + \Lambda$ cross section at about 1.5 BeV/c and the rapid drop-off of the $K^- + p \rightarrow Y_1^* + \pi^+$ cross section above this energy.

Table XVI. Vee-two-prong cross sections.

Momentum (BeV/c)	c.m. Energy (BeV/c)	$K^- + p \rightarrow \Lambda + \pi^+ + \pi^-$ (mb)	$K^- + p \rightarrow \Lambda + \pi^+ + \pi^- + \pi^0$ (mb)	$K^- + p \rightarrow \Sigma^0 + \pi^+ + \pi^-$ (mb)
1.22± 0.04	1.89± 0.02	2.78± 0.17	0.68± 0.05	0.76± 0.06
1.32± 0.05	1.94± 0.02	2.66± 0.16	1.51± 0.10	0.73± 0.05
1.42± 0.05	1.98± 0.02	2.44± 0.18	2.12± 0.16	0.76± 0.07
1.51± 0.05	2.02± 0.02	2.32± 0.12	2.47± 0.12	0.80± 0.05
1.60± 0.05	2.06± 0.02	2.09± 0.14	2.19± 0.15	0.68± 0.06
1.69± 0.05	2.10± 0.02	1.98± 0.12	2.83± 0.17	0.91± 0.06

Momentum (BeV/c)	c.m. Energy (BeV/c)	$K^- + p \rightarrow \begin{Bmatrix} \Lambda + \pi^+ + \pi^- + \pi^0 + \pi^0 \\ \Sigma^0 + \pi^+ + \pi^- + \pi^0 \end{Bmatrix}$ (mb)	$K^- + p \rightarrow \bar{K}^0$ - two prongs[a] (mb)
1.22± 0.04	1.89± 0.02	0.12± 0.02	1.33± 0.10
1.32± 0.05	1.94± 0.02	0.13± 0.01	1.33± 0.10
1.42± 0.05	1.98± 0.02	0.15± 0.02	1.68± 0.14
1.51± 0.05	2.02± 0.02	0.27± 0.02	2.00± 0.11
1.60± 0.05	2.06± 0.02	0.30± 0.03	1.58± 0.13
1.69± 0.05	2.10± 0.02	0.41± 0.03	1.87± 0.13

[a] See Reference 66.

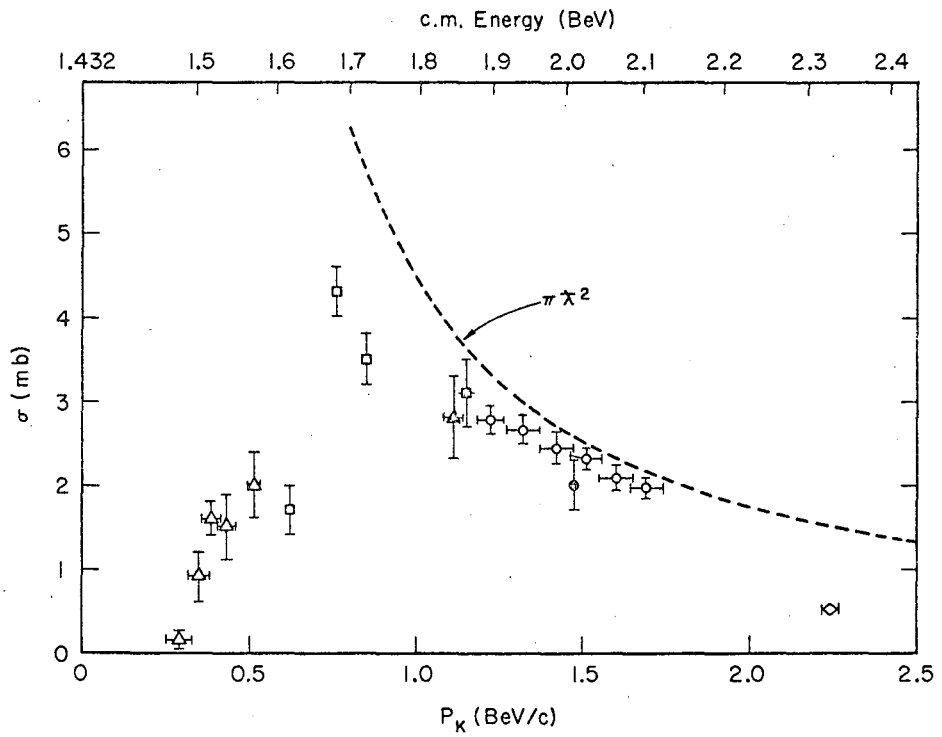

Fig. 35. Excitation curve for the reaction, $K^- + p \rightarrow \Lambda + \pi^+ + \pi^-$, from threshold to 2.24 BeV/c, using all known published data plus that from this experiment. The point at 2.24 BeV/c was published as a preliminary value and a lower limit, and no error was given for this point. The dashed curve gives the value of $\pi \lambda^2$ for the K^- in the K^--p center-of-mass system, which curve the excitation function would be proportional to if there were no change of production mechanism as a function of energy.

△ Ref. 99; □ Ref. 4; ▲ Ref. 5; ▣ Ref. 100;
○ this experiment; ◎ Ref. 6; ◇ Ref. 101.

Table XVII. $\Lambda \pi^+\pi^-$ cross sections.

Momentum (BeV/c	c.m. Energy (BeV/c)	$K^- + p \rightarrow \Lambda + \pi^+ + \pi^-$ nonresonant (mb)	$K^- + p \rightarrow Y^{*+} + \pi^-$ (mb)	$K^- + P \rightarrow Y^{*-} + \pi^+$ (mb)	$K^- + p \rightarrow \Lambda + \rho^0$ (mb)
1.15-1.30	1.864-1.932	0.24± 0.15	1.13± 0.08	1.43± 0.09	0.00± 0.07
1.30-1.45	1.932-1.999	0.05± 0.17	0.86± 0.06	1.33± 0.07	0.29± 0.09
1.45-1.60	1.999-2.065	0.35± 0.15	0.79± 0.05	0.68± 0.05	0.46± 0.09
1.60-1.75	2.065-2.130	0.87± 0.16	0.51± 0.07	0.48± 0.05	0.14± 0.09

IV. CONCLUSIONS

A. Spin and Parity of the $Y_1^*(1385)$

The spin of the Y_1^* is most certainly not $\frac{1}{2}$. Many experiments have determined anisotropies in the observed decay of this state that are inconsistent with $J = \frac{1}{2}$,[5, 7, 9, 11]. Other experiments are less conclusive, either being ambigious in conclusions or favoring $J = \frac{1}{2}$ with a low statistical confidence.[90, 92, 93, 94] In this experiment, the Adair analysis was inconclusive (no experiment has yet made a conclusive analysis of Y_1^* using this analysis), favoring $J = 3/2$ mildly. But the normal decay distribution of the Y_1^*, the distribution of the polarization relative to the normal and rotated directions, and the complete analysis covering all angular correlations all deny strongly the possibility that $J = \frac{1}{2}$. Only interference with background amplitudes can negate this argument, and behavior of the above distributions with mass of the Y_1^* are not consistent with the hypothesis that interference alone gives the observed anisotropies. The large range of energy over which significant anisotropy is observed, when other experiments are included, also argues against this source for the effect.

If the spin is 3/2, then the parity is positive. Large polarizations observed in pion experiments are inconsistent with negative parity.[93, 94] Earlier analyses with part of this same data definitely ruled out $D_{3/2}$.[9, 11] The analysis of this paper agrees strongly that a $D_{3/2}$ assignment is inconsistent with the data. In addition, one parity state is eliminated for each value of J; the permitted states are $P_{3/2}$, $D_{5/2}$, and $F_{7/2}$.

With somewhat less conclusiveness, the Y_1^* has spin and parity of $P_{3/2}$. An assignment of $F_{7/2}$ is made very unlikely by the results from the complete analysis at P = 1.00-1.15 BeV/c. Hypothesis $P_{3/2}$ is mildly favored over $D_{5/2}$ by all the complete analyses and by the Adair analysis. There may be 1 chance in 25 that the Y_1^* is $D_{5/2}$.

This analysis is based essentially on maximum-complexity arguments; so it is not surprising that, when one state fits the data well, the state of slightly greater complexity fits almost as well.

B. Classification of the $Y_1^*(1385)$

Let us proceed with the spin-parity assignment of $P_{3/2}$ for the Y_1^*. In Table I are listed a number of predictions from various theories for the properties of the Y_1^*. From this spin-parity assignment and from the other properties determined in this experiment, we can compare theory with experiment.

The $\bar{K}$-N bound-state theory is definitely excluded by the exclusion of $J = \frac{1}{2}$. Of the remaining theories, global symmetry and the eightfold way seem to describe the findings of this experiment most accurately. However, global symmetry predicts an $I = 2$ resonance, which has never been seen, and fails to take into account the large number of strange-particle resonances that have been found. For these reasons, historically, the eightfold way has replaced global symmetry as the higher symmetry scheme that shows the most promise of unifying the description of the strongly interacting particles. Accordingly, Table XVIII lists for convenience the experimental values and those predicted by the eightfold way. Some care must be used in comparing these numbers because (a) the experimental values possibly have systematic errors both from the detection and measurement system and from the use of simple models to fit the data; and (b) the theory is based upon group theory and dynamical calculations apparently have not yet been done accurately enough to compare with experiment. On the whole, the $Y_1^*(1385)$ does seem to fit into the eightfold way very well.

C. Branching Ratio of ω into $\pi^+\pi^-$

Table V shows the range of values of the branching ratio $R_\omega = \Gamma(\omega \to \pi^+\pi^-)/\Gamma(\omega \to \pi^+\pi^-\pi^0)$, which are admitted by this experiment if the net phase difference between the ω and the ρ^0 is allowed

Table XVIII. Comparison of experiment with the eightfold way for $Y_1^*(1385)$.

Property	Prediction	Experiment[a]
Spin-parity	3/2+	3/2+
Mass	Input[b]	(1383.5± 1.6) MeV
Width	64 MeV	(51.4± 4.2) MeV
Branching ratio	0.16	0.09± 0.04

[a] Errors given are statistical only. There may be unknown systematic errors from the detection and measurement system from the use of oversimplified models.

[b] Strongly corroborated by discovery of Ω^- particle with mass close to the predicted mass (Ref. 37).

to vary over its total range. The lower limit $R_\omega > (0.6 \pm 0.2)\%$ is significant and establishes the existence of this decay mode, if one bars a large statistical fluctuation. Combined with the upper limit of $R_\omega < 5\%$ from antiproton-annihilation data,[54] it gives the present experimental range of this quantity independent of π^--p experiments where the large background of ρ^0 meson produced by one-pion exchange is a serious problem. The value of 4.3% calculated by Gell-Mann, Sharp, and Wagner[53] for this ratio falls within the experimental range; but if coupling constants are adjusted to give the proper total width, their model predicts a branching ratio of only 0.0001%, a very poor agreement.

D. Production Mechanism

As has been said before, this paper is primarily concerned with final-state interactions and only secondarily concerned with production mechanism. However, some general statements based on outstanding features of this experiment can be made.

All indications show that there is only gradual change in the production process from 1.2 BeV/c to about 1.5 BeV/c. Angular distributions remain about the same, the excitation function for Y_1^* decreases smoothly, the Y_1^{*-} population remains higher than that of the Y_1^{*+} by about 20%, and the excitation function of ρ^0 production rises from threshold.

Above 1.5 BeV/c, there seems to be a different production situation. Production-angle distributions of the Y_1^* are more complicated and sometimes cannot be fit. The excitation function of the ρ^0 reaches a maximum and decreases. The Y_1^* becomes more numerous than the Y_1^{*-}, and there is some evidence that peripheral production of the Y_1^* by K^* exchange is initiated in this interval. Peripheral production is, however, not yet the dominant mechanism below 1.7 BeV/c.

E. Future Experiments

Study of reactions from $K^- + p$ at a wide range of energy contains fruitful possibilities for discovering all the properties of the strange-particle resonances and how they are produced. Exposures now underway or planned in the near future at Berkeley will provide film to fill the gaps remaining between threshold and about 2.7 BeV/c. Our findings based upon final-state interactions can be verified at other energies and can be extended to other resonant states, such as $Y_0^*(1405)$, $Y_1^*(1660)$, and $Y_1^*(1765)$. Then there is a need to make a unified study of all channels at higher energy comparable to that being done by Charles Wohl in the region $P = 1.00\text{-}1.15$ BeV/c.[64] It will be too bad if only the exciting and obvious features are reported, but other features that require diligent and organized research are not investigated.

ACKNOWLEDGMENTS

I wish to express sincere thanks to Dr. Joseph Murray for initiating me into the study of this reaction, to Dr. Janice Shafer and Prof. Arthur Rosenfeld for their continued advice and encouragement, to Dr. Stanley Wojcicki for having written many of the computer programs used, and finally to Prof. Luis Alvarez and the many other people in his group with whom I have had many fruitful consultations and without whom this work would not have been possible.

This work was performed under the auspices of the U. S. Atomic Energy Commission.

APPENDICES

A. Irreducible Tensors

Following are specific matrix forms of the irreducible tensors, T^M_L, for $J = 1/2$ and for $J = 3/2$.

1. $J = 1/2$

$$T^0_1 = \begin{pmatrix} 1 & 0 \\ 0 & 1 \end{pmatrix} \qquad T^0_1 = \begin{pmatrix} \sqrt{1/3} & 0 \\ 0 & -\sqrt{1/3} \end{pmatrix}$$

2. $J = 3/2$

$$T^0_1 = \begin{pmatrix} 1 & 0 & 0 & 0 \\ 0 & 1 & 0 & 0 \\ 0 & 0 & 1 & 0 \\ 0 & 0 & 0 & 1 \end{pmatrix}$$

$$T^0_1 = \begin{pmatrix} \sqrt{3/5} & 0 & 0 & 0 \\ 0 & \sqrt{1/15} & 0 & 0 \\ 0 & 0 & -\sqrt{1/15} & 0 \\ 0 & 0 & 0 & -\sqrt{3/5} \end{pmatrix}$$

$$T^0_2 = \begin{pmatrix} \sqrt{1/5} & 0 & 0 & 0 \\ 0 & -\sqrt{1/5} & 0 & 0 \\ 0 & 0 & -\sqrt{1/5} & 0 \\ 0 & 0 & 0 & \sqrt{1/5} \end{pmatrix}$$

$$T^0_3 = \begin{pmatrix} \sqrt{1/35} & 0 & 0 & 0 \\ 0 & -\sqrt{9/35} & 0 & 0 \\ 0 & 0 & \sqrt{9/35} & 0 \\ 0 & 0 & 0 & -\sqrt{1/35} \end{pmatrix}$$

$$T_2^2 = \begin{pmatrix} 0 & 0 & \sqrt{2/5} & 0 \\ 0 & 0 & 0 & \sqrt{2/5} \\ 0 & 0 & 0 & 0 \\ 0 & 0 & 0 & 0 \end{pmatrix}$$

$$T_2^{-2} = \begin{pmatrix} 0 & 0 & 0 & 0 \\ 0 & 0 & 0 & 0 \\ \sqrt{2/5} & 0 & 0 & 0 \\ 0 & \sqrt{2/5} & 0 & 0 \end{pmatrix}$$

$$T_3^2 = \begin{pmatrix} 0 & 0 & \sqrt{2/7} & 0 \\ 0 & 0 & 0 & -\sqrt{2/7} \\ 0 & 0 & 0 & 0 \\ 0 & 0 & 0 & 0 \end{pmatrix}$$

$$T_3^{-2} \begin{pmatrix} 0 & 0 & 0 & 0 \\ 0 & 0 & 0 & 0 \\ \sqrt{2/7} & 0 & 0 & 0 \\ 0 & -\sqrt{2/7} & 0 & 0 \end{pmatrix}$$

B. Solutions of Complete Analysis

Here are listed in tabular form the values of the t_L^M parameters (through $J = 3/2$) from the fitting program in the complete analysis of angular correlations, together with the theoretical maximum values of these parameters.[41] See Table B-I for the tabulated values.

C. Moments through $J = 7/2$

In Table C-I are listed the coefficients $A(L, M, \ell, m)$ [as defined in equation (104) of the text], which are pertinent for states through $J = 7/2$. They are listed in an arbitrary order and each is given an ordinal number. Where two ordinal numbers are listed, the coefficient is

Table B-I. Parameters from fit in complete analysis.

Hyp.	t_L^M	$\|t\|_{max}$	P = 1.00-1.15 (BeV/c	1.15-1.30 BeV/c	1.30-1.45 BeV/c
$S_{1/2}$	t_0^0	1.00000	1.00± 0.07	1.00± 0.04	1.00± 0.05
	t_1^0	0.57735	-0.17± 0.05	-0.03± 0.03	-0.01± 0.04
$P_{1/2}$	t_0^0	1.00000	1.00± 0.09	1.00± 0.06	1.00± 0.07
	t_1^0	0.57735	-0.05± 0.07	-0.04± 0.05	-0.04± 0.05
$P_{3/2}$	t_0^0	1.00000	1.00± 0.08	1.00± 0.06	1.00± 0.06
	t_1^0	0.77460	-0.23± 0.07	-0.07± 0.04	-0.05± 0.05
	t_2^0	0.47721	-0.22± 0.07	-0.10± 0.05	-0.08± 0.05
	t_3^0	0.50709	0.31± 0.05	0.29± 0.04	0.20± 0.04
	Re t_2^2	0.31623	-0.07± 0.04	-0.02± 0.03	-0.11± 0.03
	Im t_2^2	0.31623	0.03± 0.04	-0.02± 0.03	-0.02± 0.03
	Re t_3^2	0.26726	0.00± 0.04	-0.10± 0.02	-0.06± 0.03
	Im t_3^2	0.26726	-0.10± 0.04	-0.02± 0.02	0.08± 0.03
$D_{3/2}$	t_0^0	1.00000	1.00± 0.09	1.00± 0.07	1.00± 0.07
	t_1^0	0.77460	0.01± 0.08	-0.03± 0.05	-0.01± 0.06
	t_2^0	0.47721	-0.21± 0.07	-0.09± 0.05	-0.08± 0.05
	t_3^0	0.50709	0.01± 0.06	-0.03± 0.04	0.04± 0.05
	Re t_2^2	0.31623	-0.06± 0.06	-0.02± 0.04	-0.11± 0.04
	Im t_2^2	0.31623	0.03± 0.06	-0.03± 0.04	-0.03± 0.04
	Re t_3^2	0.26726	-0.02± 0.05	0.04± 0.04	-0.01± 0.04
	Im t_3^2	0.26726	0.13± 0.05	-0.06± 0.03	-0.02± 0.04

Table C-I. Pertinent $A(L, M, \ell, m)$ through $J = 7/2$.

Ordinal	$A(L, M, \ell, m)$	Ordinal	$A(L, M, \ell, m)$
1	A(0, 0, 0, 0)	37 & 38	A(6, 2, 1, 0)
2	A(0, 0, 1, 0)	39 & 40	A(6, 4, 1, 0)
3	A(2, 0, 0, 0)	41 & 42	A(6, 6, 1, 0)
4 & 5	A(2, 2, 0, 0)	43	A(6, 1, 1, -1)
6	A(2, 0, 1, 0)	44 & 45	A(6, 1, 1, 1)
7 & 8	A(2, 2, 1, 0)	46 & 47	A(6, 3, 1, -1)
9	A(2, 1, 1, -1)	48 & 49	A(6, 3, 1, 1)
10 & 11	A(2, 1, 1, 1)	50 & 51	A(6, 5, 1, -1)
12	A(4, 0, 0, 0)	52 & 53	A(6, 5, 1, 1)
13 & 14	A(4, 2, 0, 0)	54	A(8, 0, 1, 0)
15 & 16	A(4, 4, 0, 0)	55 & 56	A(8, 2, 1, 0)
17	A(4, 0, 1, 0)	57 & 58	A(8, 4, 1, 0)
18 & 19	A(4, 2, 1, 0)	59 & 60	A(8, 6, 1, 0)
20 & 21	A(4, 4, 1, 0)	61	A(8, 1, 1, -1)
22	A(4, 1, 1, -1)	62 & 63	A(8, 1, 1, 1)
23 & 24	A(4, 1, 1, 1)	64 & 65	A(8, 3, 1, -1)
25 & 26	A(4, 3, 1, -1	66 & 67	A(8, 3, 1, 1)
27 & 28	A(4, 3, 1, 1)	68 & 69	A(8, 5, 1, -1)
29	A(6, 0, 0, 0)	70 & 71	A(8, 5, 1, 1)
30 & 31	A(6, 2, 0, 0)	72 & 73	A(8, 7, 1, -1)
32 & 33	A(6, 4, 0, 0)		
34 & 35	A(6, 6, 0, 0)		
36	A(6, 0, 1, 0)		

complex and the two numbers refer to real and imaginary parts, respectively. In a few cases, the coefficient is complex in general, but only the real part is pertinent.

D. Discussion of Breit-Wigner Resonance Form

In the discussion of Watson's theorem in Sec. II of the text, we concluded that a Breit-Wigner resonance shape, equation (4), is appropriate for almost all final-state interactions encountered in high-energy particle reactions. This form is certainly well known, but a discussion of its validity and properties is perhaps useful.

This resonance form was first proposed by Breit and Wigner in a study of capture and scattering on neutrons.[102] Its general validity for use in describing intermediate states in primary interactions in cases for which long-range interactions can be ignored was established by means of formal scattering theory[103] and Heisenberg S-matrix theory.[104] As explained in the text, Watson[14] showed that the same form can be used in final-state interactions when certain conditions were satisfied. Jackson[105] has recently proposed a different form using first-order perturbation theory, but for energies near to the resonant energy it reduces to exactly the same shape as the Breit-Wigner form. The validity of the form for use in high-energy scattering experiments of strongly interacting particles seems to follow from all theories.

It is not always appreciated, however, that the width is also a function of the energy. It is reasonable to express the width as a product of three factors,[106]

$$\Gamma = \gamma B_{\ell}(p)\,(p/E). \qquad (D1)$$

In this formula, γ is the reduced width, which contains the coupling constant and other constant factors, $B_{\ell}(p)$ is the barrier-penetration factor, and p/E is proportional to the two-body phase space of the pair of particles. Also, p is the momentum of either of the particles in the center-of-mass frame of the pair, and E is the total energy of both particles in that frame. It is convenient to introduce some characteristic mass, M, giving the approximate range of the interaction, and define the dimensionless quantity $x = p/M$. In terms of this variable,

the barrier-penetration factor was worked out by Wigner and Eisenbud[103] and is listed also in Blatt and Weisskopf.[107] The first few $B_\ell(x)$ are

$$\begin{aligned} B_0(x) &= 1, \\ B_1(x) &= x^2 (1 + x^2)^{-1}, \\ B_2(x) &= x^4(9 + 3x^2 + x^4)^{-1}, \\ B_3(x) &= x^6(225 + 45x^2 + 6x^4 + x^6)^{-1}. \end{aligned} \tag{D2}$$

Note that as $x \to 0$, $B_\ell(x) \to x^{2\ell} ((2\ell + 1)!!)^{-2}$, and as $x \to \infty$, $B_\ell(x) \to 1$.

Gell-Mann and Watson used essentially this form, with $\ell = 1$, in order to fit the asymmetric shape of the $\Delta(1238)$.[72] The same form has been used more recently to fit to all available pion-proton total-cross-section data with reasonable success.[108] In these cases, the resonance is an intermediate state in the primary reaction, so that the relevant formula is

$$\left(\frac{d\sigma}{dE}\right)_{ab} = \frac{4\pi}{p^2} \frac{2J + 1}{\prod_i (2s_i+1)} \frac{\Gamma_a \Gamma_b}{(E-E_J)^2 + \frac{1}{4}\Gamma_J^2}. \tag{D3}$$

The notation is similar to that for equation (4), except that all variables refer to the primary reaction, Γ_a is the width of the incoming channel, and Γ_b is the width of the outgoing channel. Note that the $1/p^2$ factor in equation (D3) will distort the resonance shape, whereas the $1/K^2$ factor in equation (4) will not affect the shape of a resonance produced in the final state because K is not a function of the energy of the resonant particles. Note also that the width of the resonance appears twice as a factor in the numerator of equation (D3) but only once in that of equation (4), so that a different energy dependence between the two situations will also result from this source.

In order to study the effect of having neglected this energy dependence in the study of the $Y_1^*(1385)$, a special computer program was written to incorporate the energy dependence of the width into the resonance formula. Results from this program for various values of orbital angular momentum ℓ are plotted in Fig. 36. A value of

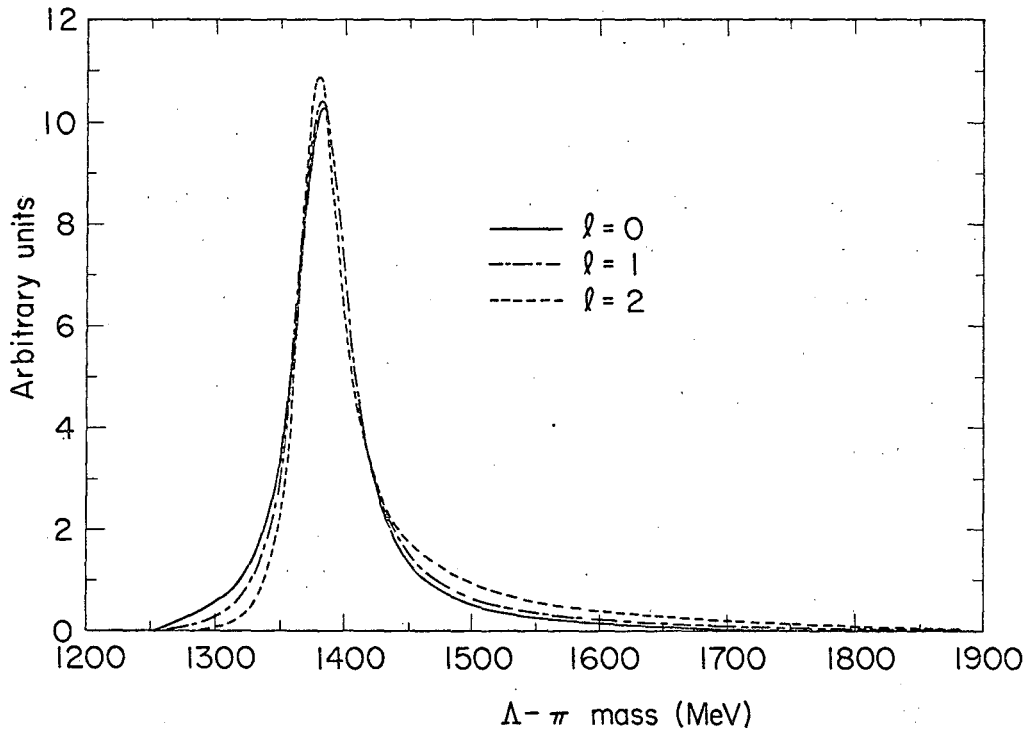

Fig. 36. Breit-Wigner function for a Λ-π resonance with central energy 1385 MeV, width 50 MeV, and orbital angular momentum ℓ=0, 1, and 2 respectively. The resonance is formed in final-state interactions in the reaction $K^- + p \rightarrow \Lambda + \pi + \pi$ at P = 1.51 BeV/c. The curve appropriate to each value of ℓ may be identified by reference to the box on the graph.

200 MeV was used for the mass M characteristic of the range of the interaction, but the shape of the curves is insensitive to reasonable changes in this parameter. The peak of the curve shifts to lower values of invariant mass, the low-energy tail is depleted, and the high-energy tail is enhanced slightly as ℓ is increased. The magnitude of these changes, however, is not significant compared with the statistical errors of the experimental distribution and the expected magnitude of other distortions. The use of the $\ell = 0$ form of the Breit-Wigner formula, currently employed in program ATHOS, seems to be justified in the study of this resonance.

FOOTNOTES AND REFERENCES

1. M. H. Alston, L. W. Alvarez, P. Eberhard, M. L. Good, W. Graziano, H. K. Ticho, and S. G. Wojcicki, Resonance in the $\Lambda\pi$ System, Phys. Rev. Letters 5, 520 (1960).
2. R. H. Dalitz, Strange Particle Resonant States, Ann. Rev. Nucl. Sci. 13, 339 (1963).
3. J. P. Berge, P. Bastien, O. Dahl, M. Ferro-Luzzi, J. Kirz, D. H. Miller, J. J. Murray, Jr., A. H. Rosenfeld, R. D. Tripp, and M. B. Watson, Pion-Lambda Resonance (Y_1^*), Phys. Rev. Letters 6, 557 (1961).
4. P. L. Bastien and J. P. Berge, K^--p Interactions near 760 MeV/c, Phys. Rev. Letters 10, 188 (1963).
5. R. P. Ely, S. Fung, G. Gidal, Y. Pan, W. M. Powell, and H. S. White, Spin of Y_1^*, Phys. Rev. Letters 7, 461 (1961).
6. W. A. Cooper, H. Courant, H. Filthuth, E. I. Malamud, A. Minguzzi-Ranzi, H. Schneider, A. M. Segar, G. A. Snow, W. Willis, E. S. Gelsema, J. C. Kluyver, A. G. Tenner, K. Browning, I. S. Hughes, and R. Turnbull, Proceedings of the 1962 International Conference on High-Energy Physics at CERN, (CERN, Geneva, 1962), p. 298.
7. L. Bertanza, V. Brisson, P. L. Connolly, E. L. Hart, I. S. Mittra, G. C. Moneti, R. R. Rau, N. P. Samios, I. O. Skillicorn, S. S. Yamamoto, M. Goldberg, J. Leitner, S. Lichtman, and J. Westgard, Spin of the Y_1^*, Phys. Rev. Letters 10, 176 (1963).
8. J. Button-Shafer, D. O. Huwe, and J. J. Murray, Jr., Proceedings of the 1962 International Conference on High-Energy Physics at CERN (CERN, Geneva, 1962), p. 303.
9. J. B. Shafer, J. J. Murray, Jr., and D. O. Huwe, Spin and Parity of the 1385-MeV Y_1^* Resonance, Phys. Rev. Letters 10, 179 (1963).

10. L. W. Alvarez, M. H. Alston, M. Ferro-Luzzi, D. O. Huwe, G. R. Kalbfleisch, D. H. Miller, J. J. Murray, Jr., A. H. Rosenfeld, J. B. Shafer, F. T. Solmitz, and S. G. Wojcicki, 1660-MeV Y_1^* Hyperon, Phys. Rev. Letters 10, 184 (1963).

11. J. B. Shafer and D. O. Huwe, $Y_1^*(1385)$: Study of Spin and Parity by Moment Analysis for J = 5/2, 3/2, and 1/2, Phys. Rev. 134, B1372 (1964).

12. J. J. Murray, Jr., M. Ferro-Luzzi, D. O. Huwe, J. B. Shafer, F. T. Solmitz, and M. L. Stevenson, Properties of the ω Meson from $K^- + p \rightarrow \Lambda + \omega$. Phys. Letters 7, 358 (1963).

13. M. H. Alston and M. Ferro-Luzzi, Pion-Hyperon Resonances, Rev. Mod. Phys. 33, 416 (1961).

14. K. M. Watson, The Effect of Final State Interactions on Reaction Cross Sections, Phys. Rev. 88, 1163 (1952).

15. R. H. Dalitz and D. H. Miller, Bose Statistics and Y^* Production and Decay in K^--p Collisions, Phys. Rev. Letters 6, 562 (1961).

16. M. Gell-Mann, Model of the Strong Couplings, Phys. Rev. 106, 1296 (1957).

17. D. Amati, B. Vitale, and A. Stanghellini, Some Considerations on the Recently Found Evidence for a πΛ Resonance, Phys. Rev. Letters 5, 524 (1960).

18. G. Morpurgo, Strong Interactions and Reactions of Hyperons and Heavy Mesons, Ann. Rev. Nucl. Sci. 11, 41 (1961).

19. M. H. Alston, A. Barbaro-Galtieri, A. H. Rosenfeld, and S. G. Wojcicki, A Search for Y_2^* Resonances, Phys. Rev. 134, B1289 (1964).

20. R. H. Dalitz and S. F. Tuan, Possible Resonant State in Pion-Hyperon Scattering, Phys. Rev. Letters 2, 425 (1959)

21. R. H. Dalitz, $\bar{K}$ - Nucleon Bound-State Interpretation of the 1385 MeV π-Λ Resonance, Phys. Rev. Letters 6, 239 (1961).

22. W. E. Humphrey and R. R. Ross, Low-Energy Interactions of K^- Mesons in Hydrogen, Phys. Rev. 127, 1305 (1962).

23. R. H. Dalitz, On the Strong Interactions of the Strange Particles, Rev. Mod. Phys. 33, 471 (1961).

24. T. L. Trueman, Influence of $\bar{K}$-Nucleon Interactions on Pion-Hyperon Scattering, Phys. Rev. 127, 2240 (1962).

25. R. Chand, $\bar{K}$-Nucleon Interactions and Y_1^*-Resonance, Nuovo Cimento 30, 1445 (1963).

26. S. Sakata, On a Composite Model for the New Particles, Progr. Theoret. Phys. (Kyoto) 16, 686 (1956).

27. M. Ikeda, S. Ogawa, and Y. Ohnuki, A Possible Symmetry in Sakata's Model for Bosons-Baryons System, Progr. Theoret. Phys. (Kyoto) 22, 715 (1959).

28. J. J. Sakurai, Proceedings of the International School of Physics "Enrico Fermi," Course 26, Elementary Particles (Academic Press, New York, to be published).

29. D. D. Carmony, G. M. Pjerrou, P. E. Schlein, W. E. Slater, D. H. Stork, and H. K. Ticho, Properties of Ξ Hyperons, Phys. Rev. Letters 12, 482 (1964).

30. R. Armenteros, L. Montanet, D. R. O. Morrison, S. Nilsson, A. Shapira, J. Vandermeulen, Ch. d' Andlau, A. Astier, J. Ballam, C. Ghesquière, B. P. Gregory, D. Rahm, P. Rivet, and F. Solmitz, Proceedings of the 1962 International Conference on High-Energy Physics at CERN (CERN, Geneva, 1962), p. 351.

31. M. Gell-Mann, Symmetries of Baryons and Mesons, Phys. Rev. 125, 1067 (1962).

32. Y. Ne'eman, Derivation of Strong Interactions from a Gauge Invariance, Nucl. Phys. 26, 222 (1961).

33. R. E. Behrends, J. Dreitlein, C. Fronsdahl, and W. Lee, Simple Groups and Strong Interaction Symmetries, Rev. Mod. Phys. 34, 1 (1962).

34. S. Okubo, Note on Unitary Symmetry in Strong Interactions, Progr. Theoret. Phys. (Kyoto) 27, 949 (1962).

35. G. M. Pjerrou, D. J. Prowse, P. E. Schlein, W. E. Slater, D. H. Stork, and H. K. Ticho, Resonance in the ($\Xi\pi$) System at 1.53 GeV, Phys. Rev. Letters 9, 114 (1962); and L. Bertanza, V. Brisson, P. L. Connolly, E. L. Hart, I. S. Mittra,

G. C. Moneti, R. R. Rau, N. P. Samios, I. O. Skillicorn, S. S. Yamamoto, M. Goldberg, L. Gray, J. Leitner, S. Lichtman, and J. Westgard, Possible Resonances in the $\Xi\pi$ and $K\bar{K}$ Systems, Phys. Rev. Letters 9, 180 (1962).

36. P. E. Schlein, D. D. Carmony, G. M. Pjerrou, W. E. Slater, D. H. Stork, and H. K. Ticho, Spin-Parity Determination of the $\Xi\pi$ Resonance (1.530 GeV), Phys. Rev. Letters 11, 167 (1963).

37. V. E. Barnes, P. L. Connolly, D. J. Crennell, B. B. Culwick, W. C. Delaney, W. B. Fowler, P. E. Hagerty, E. L. Hart, N. Horwitz, P. V. C. Hough, J. E. Jensen, J. K. Kopp, K. W. Lai, J. Leitner, J. L. Lloyd, G. W. London, T. W. Morris, Y. Oren, R. B. Palmer, A. G. Prodell, D. Radojičić, D. C. Rahm, C. R. Richardson, N. P. Samios, J. R. Sanford, R. P. Shutt, J. R. Smith, D. L. Stonehill, R. C. Strand, A. M. Thorndike, M. S. Webster, W. J. Willis, and S. S. Yamamoto, Observation of a Hyperon with Strangeness Minus Three, Phys. Rev. Letters 12, 204 (1964).

38. S. L. Glashow and A. H. Rosenfeld, Eightfold-Way Assignments for $Y_1^*(1660)$ and other Baryons, Phys. Rev. Letters 10, 192 (1963).

39. A. H. Rosenfeld, Proceedings of the 1962 International Conference on High-Energy Physics at CERN (CERN, Geneva, 1962), p. 325.

40. M. Taher-Zadeh, D. J. Prowse, P. E. Schlein, W. E. Slater, D. H. Stork, and H. K. Ticho, Parity of the $Y_1^*(1660)$ Resonance, Phys. Rev. Letters 11, 470 (1963).

41. Following standard practice, the algebraic sign following the numerical value of the spin is the sign of the parity of the resonance relative to that of the daughter baryon. For example, if the Y_1^* decays through the reaction $Y_1^* \rightarrow \Lambda+\pi$ with an orbital angular momentum $\ell = 1$ (P wave) (the π is known to be pseudoscalar, and the Λ is commonly assigned a parity of +1), then the sign following the numerical value of J would be $-(-)^1=+$.

42. A. W. Martin and K. C. Wali, Coupled Channel Approach to J = 3/2+ Resonances in Unitary Symmetry Model, Phys. Rev. 130, 2455 (1963).

43. For a description of the density matrix in quantum mechanics, see P. A. M. Dirac, The Principles of Quantum Mechanics (Clarendon Press, Oxford, 1958), pp. 130-135.

44. R. Gatto and H. P. Stapp, Spin and Parity Analysis from Production and Decay of Hyperon Resonant States, Phys. Rev. 121, 1553 (1961).

45. R. H. Capps, Method of Determining the Spin and Parity of a Pion-Hyperon Resonance, Phys. Rev. 122, 929 (1961).

46. N. Byers and S. Fenster, Determination of Spin and Decay Parameters of Fermion States, Phys. Rev. Letters 11, 52 (1963).

47. M. E. Rose, Elementary Theory of Angular Momentum (John Wiley and Sons, New York, 1957), pp. 76-106.

48. J. W. Cronin and O. E. Overseth, Measurement of the Decay Parameters of the Λ^0 Particle, Phys. Rev. 129, 1795 (1963).

49. See references 11 and 36 for use of the latter method.

50. R. K. Adair, Some Considerations Concerning Final-State Interactions and the Reaction $K_2^0 + p \rightarrow \text{Lambda}^0 + \text{Pi}^+ + \text{Pi}^-$, Rev. Mod. Phys. 33, 406 (1961).

51. R. K. Adair, Angular Distribution of Λ^0 and θ^0 Decays, Phys. Rev. 100, 1540 (1955).

52. S. L. Glashow, Is Isotopic Spin a Good Quantum Number for the New Isobars?, Phys. Rev. Letters 7, 469 (1961).

53. M. Gell-Mann, D. Sharp, and W. G. Wagner, Decay Rates of Neutral Mesons, Phys. Rev. Letters 8, 261 (1962).

54. R. Armenteros, D. N. Edwards, T. Jacobsen, A. Shapira, J. Vandermeulen, Ch. d' Andlau, A. Astier, P. Baillon, H. Briand, J. Cohen-Ganouna, C. Defoix, J. Siaud, C. Ghesquière, and P. Rivet, Proceedings of the Sienna International Conference on Elementary Particles, Vol. 1

(Società Italiana di Fisica, Bologna, 1963), p. 2961 and N. Glefand, D. Miller, M. Nussbaum, J. Ratau, J. Schultz, J. Steinberger, T. H. Tan, L. Kirsch, and R. Plano, Lifetime of the ω Meson, Phys. Rev. Letters 11, 436 (1963).

55. J. Bernstein and G. Feinberg, Electromagnetic Mixing Effects in Elementary-Particle Physics, Nuovo Cimento 25, 1343 (1962).

56. G. Feinberg, Decay Products of Vector Mesons, Phys. Rev. Letters 8, 151 (1962).

57. S. Fubini, Vector Mesons and Possible Violations of Charge Symmetry in Strong Interactions, Phys. Rev. Letters 7, 466 (1961).

58. Y. Nambu and J. Sakurai, Rare Decay Modws of the ω(η) Meson, Phys. Rev. Letters 8, 79 (1962).

59. J. C. Taylor, Elctromagnetic Transitions Between Vector Mesons, Phys. Rev. Letters 8, 219 (1962).

60. L. Stodolsky and J. J. Sakurai, Vector Meson Exchange Model for Isobar Production, Phys. Rev. Letters 11, 90 (1963).

61. R. W. Huff, Pseudoscalar and Vector Exchanges in the Production of Vector Mesons, Phys. Rev. 133, B1078 (1964).

62. S. M. Flatté, R. W. Huff, D. O. Huwe, F. T. Solmitz, and M. L. Stevenson, Investigation of Exchange Mechanisms in $K^-p \to \Lambda\omega$, Bull. Am. Phys. Soc. 8, 603 (1963).

63. R. Hubbard, D. O. Huwe, G. R. Kalbfleisch, J. Kirz, D. H. Miller, J. B. Shafer, D. H. Stork, H. K. Ticho, and C. Wohl, A Variable Momentum, Separated K^- Beam, UCRL-10690 (in preparation).

64. C. Wohl, K^--p Interactions at 1.0-1.1 BeV/c, (Ph. D. thesis), UCRL-11528 (1964).

65. A. H. Rosenfeld and W. E. Humphrey, Analysis of Bubble Chamber Data, Ann. Rev. Nucl. Sci. 13, 103 (1963).

66. S. G. Wojcicki, The $K^-p \to \bar{K}^0\pi^-p$ Reaction from 1.0 to 1.7 BeV/c, Phys. Rev. 135, B484 (1964), and S. G. Wojcicki, M. H. Alston, and G. R. Kalbfleisch, Study of the Reactions $K^-p \to \bar{K}2\pi N$ from 1.2 to 1.7 BeV/c, Phys. Rev. 135, B495 (1964).

67. H. D. Brunk, An Introduction to Mathematical Statistics (Ginn and Company, Boston, 1960), p. 380.

68. J. Button and A. Rosenfeld, Probability Paper for Testing Chi-Squared Distributions, Alvarez Group Physics Note 240 (1960).

69. G. R. Lynch, Program FAKE: Monte Carlo Simulation of Bubble Chamber Events, UCRL-10355 (1962).

70. M. Gell-Mann and A. H. Rosenfeld, Hyperons and Heavy Mesons (Systematics and Decay), Ann. Rev. Nucl. Sci. 7, 407 (1957).

71. W. A. Cooper, H. Filthuth, A. Fridman, E. Malamud, E. S. Gelsema, J. C. Kluyver, and A. G. Tenner, Difference in Mass Between the Y_1^{*-} and Y_1^{*+} Isobars, Phys. Letters 8, 365 (1964).

72. M. Gell-Mann and K. M. Watson, The Interactions between π-Mesons and Nucleons, Ann. Rev. Nucl. Sci. 4, 219 (1954).

73. W. H. Barkas and A. H. Rosenfeld, Data for Elementary Particles, UCRL-8030 Rev. (1963).

74. A. Abashian, N. E. Booth, and K. M. Crowe, Possible Anomaly in Meson Production in p+d Collisions, Phys. Rev. Letters 5, 258 (1960).

75. N. E. Booth, A. Abashian, and K. M. Crowe, Anomaly in Meson Production in p+d Collisions, Phys. Rev. Letters 7, 35 (1961).

76. N. E. Booth and A. Abashian, Meson Production in p+d Collisions, and the I = 0 π-π Interaction. IV. Double-Pion Production and Pion-Pion Scattering, Phys. Rev. 132, 2314 (1963).

77. J. Button, G. R. Kalbfleisch, G. R. Lynch, B. C. Maglić, A. H. Rosenfeld, and M. L. Stevenson, Phys. Rev. 126, 1858 (1962).

78. C. Alff, D. Berley, D. Colley, N. Gelfand, U. Nauenberg, D. Miller, J. Schultz, J. Steinberger, T. H. Tan, H. Brugger, P. Kramer, and R. Plano, Decays of the ω and η Mesons, Phys. Rev. Letters 9, 325 (1962).

79. E. Pickup, D. K. Robinson, and E. O. Salant, Departures from One-Pion Exchange in 1.25-BeV π^--p Interactions, Phys. Rev. Letters 9, 170 (1962).

80. W. J. Fickinger, D. K. Robinson, and E. O. Salant, Evidence for a Two-Pion Decay Mode of the ω Meson, Phys. Rev. Letters 10, 457 (1963).

81. W. D. Walker, E. West, A. R. Erwin, and R. H. March, Proceedings of the 1962 International Conference on High-Energy Physics at CERN (CERN, Geneva, 1962), p. 42

82. W. D. Walker, J. Boyd, A. R. Erwin, P. H. Satterblom, M. A. Thompson, and E. West, Improved Branching Ratio for $\omega^0 \to \pi^+\pi^-/\pi^+\pi^-\pi^0$, Phys. Letters 8, 208 (1964).

83. G. Lütjens and J. Steinberger, Compilation of Results on the Two-Pion Decay of the ω, Phys. Rev. Letters 12, 517 (1964).

84. A. R. Erwin, R. March, W. D. Walker, and E. West, Evidence for a π-π Resonance in the I = 1, J = 1 State, Phys. Rev. Letters 6, 628 (1961).

85. R. Barlotaud, J. Heughebaert, A. Leveque, J. Meyer, and R. Omnes, Evidence for a T = 1 Pion-Pion Resonance at 575 MeV, Phys. Rev. Letters 8, 32 (1962).

86. Velocity transformation is the name given by E. Wichmann to those homogeneous Lorentz transformations that are parameterized by a velocity $\vec{v}$, to distinguish them from rotations, parameterized by an axis $\hat{n}$ and an angle θ, which are also homogeneous Lorentz transformations. Every homogeneous Lorentz transformation can be written as the product of a velocity transformation and a rotation.

87. H. P. Stapp, Relativistic Transformations of Spin Directions, UCRL-8096 (1957). By private communication, the series of transformations discussed therein for production followed by decay may be continued in the same fashion for any number of subsequent decays.

88. M. M. Block, E. B. Brucker, R. Gessaroli, T. Kikuchi, A. Kovacs, C. M. Meltzer, R. Kraemer, M. Nussbaum, A. Pevsner, P. Schlein, R. Strand, H. O. Cohn, E. M. Harth, J. Leitner, L. Lendinara, L. Monari, and G. Puppi, K^- Absorption in ^4He, Nuovo Cimento 20, 724 (1961).

89. T. B. Day and G. A. Snow, Capture of K^- Mesons from High S Orbitals in Helium, Phys. Rev. Letters 5, 112 (1960).

90. J. Auman, M. M. Block, R. Gessaroli, J. Kopelman, S. Ratti, L. Grimellini, T. Kikuchi, L. Lendinara, L. Monari, and E. Harth, Proceedings of the 1962 International Conference on High-Energy Physics at CERN (CERN, Geneva, 1962), p. 330.

91. C. T. Coffin, L. J. Curtis, D. I. Meyer, and K. M. Terwilliger, Proceedings of the 1962 International Conference on High-Energy Physics at CERN (CERN, Geneva, 1962), p. 327.

92. L. J. Curtis, C. T. Coffin, D. J. Meyer, and K. M. Terwilliger, Production of the 1385-MeV $(Y_1^*)^0$ in 1.5 BeV/c π^--p Interactions (to be submitted to Phys. Rev.).

93. D. Colley, N. Gelfand, U. Nauenberg, J. Steinberger, S. Wolf, H. R. Brugger, P. R. Kramer, and R. J. Plano, Resonances in Strange-Particle Production, Phys. Rev. 128, 1930 (1962).

94. A. R. Erwin, R. H. March, and W. D. Walker, Preliminary Results on Y_1^* and K^* Production in π-p Collisions, Nuovo Cimento 24, 237 (1962).

95. R. K. Adair, Background Amplitude and Spin of the Y_1^* (in preparation).

96. R. Hubbard, K^- Path Length Determination--K-72 Experiment, Alvarez Group Physics Note 496 (1964).

97. V. Cook. B. Cork, T. F. Hoang, D. Keefe, L. T. Kerth, W. A. Wenzel, and T. F. Zipf, K^--p and K^--n Cross Sections in the Momentum Range 1-4 BeV/c, Phys. Rev. 123, 320 (1961).

98. W. Becker, M. Goldberg, E. Harth, J. Leitner, and S. Lichtman, K^--Decay Branching Fractions, Nuovo Cimento 31, 1 (1964).

99. M. Ferro-Luzzi, R. D. Tripp, and M. B. Watson, Excited Hyperon of Mass 1520 MeV, Phys. Rev. Letters 8, 28 (1962).

100. Wm. Graziano and S. Wojcicki, K^-p Interactions at 1.15 BeV/c, Phys. Rev. 128, 1868 (1962).

101. L. Bertanza, V. Brisson, P. L. Connolly, E. L. Hart, I. S. Mittra, G. C. Moneti, R. R. Rau, N. P. Samios, I. O. Skillicorn, S. S. Yamamoto, M. Goldberg, L. Gray, J. Leitner, S. Lichtman, and J. Westgard, Proceedings of the 1962 International Conference on High-Energy Physics at CERN (CERN, Geneva, 1962), p. 284.

102. G. Breit and E. P. Wigner, Capture of Slow Neutrons, Phys. Rev. 49, 519 (1936).

103. E. P. Wigner and L. Eisenbud, Higher Angular Momenta and Long Range Interaction in Resonance Reactions, Phys. Rev. 72, 29 (1947).

104. Ning Hu, On the Application of Heisenberg's Theory of S-Matrix to the Problems of Resonance Scattering and Reactions in Nuclear Physics, Phys. Rev. 74, 131 (1948).

105. J. D. Jackson, Remarks on the Phenomenological Analysis of Resonances (in preparation).

106. A. H. Rosenfeld, private communication.

107. J. M. Blatt and V. F. Weisskopf, Theoretical Nuclear Physics (John Wiley and Sons, New York, 1952), p. 361.

108. N. P. Klepikov, V. A. Meshcheryakov, and S. N. Sokolov, Analysis of Experimental Data on the Total Cross Sections for Pion-Proton Interaction (in preparation). David Cheng of this laboratory is repeating the analysis using some later data and some refinements in technique.